STELLINGEN

1. De "internationalisering" van het onderwijs aan de Nederlandse universiteiten leidt tot een verarming van dat onderwijs.

2. De term universitair (hoofd)*docent* is misleidend.

3. Ondubbelzinnigheid in natuurwetenschappelijke publikaties kan bereikt worden door, in navolging van de wiskunde en de muziek, een eigen taal te ontwikkelen.

4. Onderzoekscholen en topinstituten leggen beslag op onderzoekskapaciteit zonder dat deze voor onderzoek benut wordt.

5. Het beleid dat de landbouwuniversiteit voert ten aanzien van buitenlandse post-docs is asociaal en is in strijd met de Grondwet.
   — Grondwet voor het Koninkrijk der Nederlanden, Artikel 1.

6. Het streven van de raad van bestuur van het Kenniscentrum Wageningen alleen de in de kern van de KCW-missie passende delen van de exakte basiswetenschappen te behouden of uit te breiden, gaat voorbij aan het feit dat basiswetenschappen niet aan bepaalde toepassingsgebieden gebonden zijn.
   — Raad van bestuur KCW, *Strategische visie Kenniscentrum Wageningen; eerste aanzet*, Wageningen, 1997.

7. De orde van een bevochtigingsovergang in polymere systemen hangt af van de ketenlengte.
   — Dit proefschrift, hoofdstuk 2.

8. De wijze waarop Bajpai en Bajpai de adsorptiekinetiek van polymeren bestuderen en bediskussiëren duidt op onvoldoende kennis van het onderwerp.
   — U. D. N. Bajpai en A. K. Bajpai. *Polym Int*, 32:43, 1993.

9. De door de politiek veel gebruikte uitspraak "het gaat goed met de natuur in Nederland" is een teken van onkunde of van volksverlakkerij.

10. Het sociaal stelsel in Nederland is zowel in ekonomisch als in sociaal opzicht een mislukking.
    — Piet van Elswijk. *De markteconomie sociaal ingevuld*, Van Gorcum, Assen, 1996.

Stellingen behorende bij het proefschrift "Semi-flexible polymers near interfaces; equilibrium aspects and adsorption kinetics" van Marcel van Eijk, Wageningen 1998.

Semi-flexible polymers near interfaces

equilibrium aspects and adsorption kinetics

promotoren: dr. M. A. Cohen Stuart,
hoogleraar fysische chemie, met bijzondere aandacht voor de kolloïdchemie

dr. G. J. Fleer,
hoogleraar op persoonlijke gronden werkzaam bij het departement Biomolekulaire Wetenschappen

Semi-flexible polymers near interfaces

equilibrium aspects and adsorption kinetics

Marcel van Eijk

Proefschrift
ter verkrijging van de graad van doktor
op gezag van de rector magnificus
van de Landbouwuniversiteit Wageningen,
dr. C. M. Karssen,
in het openbaar te verdedigen
op dinsdag 16 juni 1998
des namiddags te vier uur in de Aula.

Nederlandse titel: Semi-flexibele polymeren aan grensvlakken; evenwichtsaspekten en adsorptiekinetiek

ISBN 90-5485-854-0
Subject headings: semi-flexible polymer/adsorption kinetics/wetting.

Dit proefschrift is tot stand gekomen met steun van de Stichting Scheikundig Onderzoek in Nederland (SON) met een subsidie van de Nederlandse Organisatie voor Wetenschappelijk Onderzoek (NWO).

Die Bäume

Denn wir sind wie Baumstämme im Schnee. Scheinbar liegen sie glatt auf, und mit kleinem anstoß sollte man sie wegschieben können. Nein, das kann man nicht, denn sie sind fest mit dem Boden verbunden. Aber sieh, sogar das ist nur scheinbar.

Franz Kafka

This thesis is based on the following papers:

- Chapter 1
  M. C. P. van Eijk and F. A. M. Leermakers. Semi-flexible polymers at a liquid–liquid interface: self-consistent-field calculations. Submitted to *J Chem Phys*, 1998.
- Chapter 2
  M. C. P. van Eijk and F. A. M. Leermakers. Wetting by polymers of a liquid–liquid interface: effects of short-range interactions and of chain stiffness. To be submitted, 1998.
- Chapter 3
  M. C. P. van Eijk, M. A. Cohen Stuart, and G. J. Fleer. Adsorption kinetics of a semi-flexible polymer. *Progr Colloid Polym Sci*, 105:31–37, 1997.
- Chapter 4
  M. C. P. van Eijk and M. A. Cohen Stuart. Polymer adsorption kinetics: effects of supply rate. *Langmuir*, 13:5447–5450, 1997.
- Chapter 5
  M. C. P. van Eijk, M. A. Cohen Stuart, S. Rovillard, and J. De Coninck. Adsorption and spreading of polymers at plane interfaces; theory and molecular dynamics simulations. *Eur Phys J B*, 1:233–244, 1998.

Voorwoord

Een voor- of nawoord bij een proefschrift is meestal niet veel meer dan een opsomming van klichés. De strekking is dat je een promotieonderzoek niet alleen doet en daarna volgt een opsomming van mensen die in meer of mindere mate hebben bijgedragen aan de totstandkoming van het proefschrift (vaak oneerbiedig aangeduid met "boekje"). Hoe gerechtvaardigd een dergelijke reflektie op de voorafgaande vier jaar ook mag zijn, het lezen ervan is als het kijken naar een hollywoodfilm: je weet van begin tot eind waar het naar toe gaat. Dat moet anders kunnen. Deze boude uitspraken geven de lezer het volste recht om in dit voorwoord niet overspoeld te worden met klichés.

Dat dit proefschrift er nu ligt is terug te voeren op het feit dat ik me de afgelopen jaren onder andere heb bezig gehouden met het bedrijven van wetenschap. Terwijl ik daarmee bezig was, vroeg ik mezelf ook af, en doe dat nog steeds, in welke positie de wetenschap zich in de Nederlandse samenleving bevindt en hoe deze zich ontwikkelt. Ik zal proberen de lezer aan het denken te zetten over de recente veranderingen op het gebied van wetenschapsbeleid. Uiteraard zal ik hierbij voorbeelden uit de Wageningse hoek gebruiken om een en ander tastbaarder te maken.

Waar begint wetenschap? Het antwoord op deze vraag zou moeten zijn: bij het wetenschappelijk onderwijs, aan de universiteiten dus. Beleidsmakers in Zoetermeer denken

Representatie van de wetenschap in de Nederlandse samenleving: brug in de Schotse Hooglanden.

daar echter iets anders over. Zij kwamen eind 1997 met het advies de universitaire studies meer te laten aansluiten op het bedrijfsleven en de opleiding tot wetenschapper naar de achtergrond te schuiven. Met andere woorden: de universiteiten moeten een deel van de taken van het hoger beroepsonderwijs overnemen. Dat Wageningen daarmee voorop loopt blijkt bijvoorbeeld uit de doelstelling van de opleiding Bodem, Water en Atmosfeer in de studiegids 1997–1998:

> "De opleiding leidt op voor beroepen op het vlak van bodemkunde, hydrologie en meteorologie."

Zelfs bij een van de meest fundamentele studierichting Molekulaire Wetenschappen is dit beleid al zichtbaar:

> "Het doel van het onderwijs in de eerste fase van de opleiding Moleculaire Wetenschappen is het geven van kennis van en inzicht in de fundamentele fysische, chemische en biologische disciplines en de betekenis daarvan voor het meer op de praktijk gerichte landbouwkundig en milieukundig onderzoek."

Een van de pogingen om het universitair onderzoek te structureren was de instelling van zogenaamde onderzoekscholen. De achterliggende gedachte is dat door samenwerking tussen verschillende onderzoekgroepen de kwaliteit van het onderzoek verhoogd wordt. Om deze onderzoekscholen leven in te blazen worden promovendi erbij ingedeeld. Tot zover lijkt een en ander inderdaad tot kwaliteitsverbetering te kunnen leiden. In de praktijk zie je iets heel anders gebeuren: de bestaande onderzoekgroepen blijven hun eigen onderzoekslijn uitzetten en uitvoeren en deze wordt slechts op papier gekoppeld aan de onderzoekschool. Gevolg is dat er op bestuurlijk vlak meer taken te verrichten zijn, terwijl op onderzoeksvlak niet meer samenwerking plaatsvindt dan voor de oprichting van de onderzoekscholen. De bestuurstaken worden door wetenschappelijk personeel uitgevoerd wat leidt tot vermindering van onderzoekskapaciteit, zodat er sprake is van burokratisering zonder kwaliteitsverbetering.

Op Europees nivo vindt een vergelijkbare burokratisering van het wetenschappelijk onderzoek plaats. Daar worden universiteiten gemotiveerd gezamenlijk onderzoek uit te voeren door het voorhouden van een geldbuidel; publikaties met auteurs van verschillende groepen leveren geld op. Deze politiek heeft zeker geleid tot meer gezamenlijke publikaties, maar of dit ook meer samenwerking betekent is de vraag. Een voorbeeld hiervan is hoofdstuk 5 in dit proefschrift.

Een blijvend probleem voor universiteiten is de financiering van hun onderzoek. Momenteel hebben de universiteiten de mogelijkheid de financiën uit de eerste geldstroom te besteden aan vrij te kiezen onderzoeksonderwerpen. Daar moet volgens de overheid verandering in komen: een vijfde van deze financiering zal besteed moeten worden aan onderzoek binnen nader op te stellen industrieel relevante thema's. Hierin schuilt het gevaar dat wetenschappelijk onderzoek zal moeten passen binnen een, door de industrie al gehanteerd, korte-termijnbeleid, zodat in ieder geval langlopende onderzoekprojekten steeds minder voor zullen komen. In hetzelfde straatje past de oprichting van raden van toezicht voor de universiteiten. Je zou verwachten dat een raad van toezicht wordt

samengesteld uit vertegenwoordigers van verschillende maatschappelijke groeperingen. Niets is echter minder waar, ze bestaat uitsluitend uit industriëlen, waardoor ekonomische motieven zonder twijfel de bovenhand zullen voeren.

Een universiteit heeft bij eerste-geldstroomonderzoek nog een onafhankelijke positie, maar dat wordt anders wanneer er sprake is van derde-geldstroomonderzoek. Bedrijven kiezen er voor om een deel van hun, vaak fundamentele, onderzoek uit te laten voeren aan een universiteit. Hiermee besparen ze niet alleen geld, maar hebben ook toegang tot experts op het betreffende vakgebied. Doordat veel bedrijven bezuinigen op onderzoek, zullen ze vaker met universiteiten samenwerken. Tot zover hoeft er geen probleem te zijn, maar daar komt verandering in zodra het profijtbeginsel en de openbaarheid van akademische kennis botsen. Het is al meer dan eens voorgekomen dat een universitaire onderzoeker (lees aio) zijn werk niet, of pas jaren later, kon publiceren, omdat er een mogelijk oktrooi in het geding was. Hier ligt een taak voor de universiteiten om daar paal en perk aan te stellen.

Bovengenoemde punten vertegenwoordigen een grote skepsis ten aanzien van het wetenschappelijk onderzoek in Nederland. Voorlopig lijkt het erop dat het onderzoek de kant opgaat waar het meeste geld is te krijgen. Waarom? Geen rugge(n)graat.

Contents

Voorwoord vii

Chapter 0. Introduction 1
0.1. Polymers and their semi-flexibility 1
0.2. Polymers near interfaces 3
0.2.1. Semi-flexible polymers and adsorption experiments 4
0.2.2. Theoretical approach 4
0.3. Outline of this thesis 6
References 7

Chapter 1. Semi-flexible polymers at a liquid–liquid interface: self-consistent-field calculations 9
1.1. Introduction 9
1.2. Theory 10
1.2.1. General formulation of the model 10
1.2.2. Analytical mean-field approach 10
1.2.3. Numerical self-consistent-field theory 11
1.2.4. Chain dimensions 14
1.3. Results and discussion 15
1.3.1. Adsorbed amount 16
1.3.2. Density profiles 19
1.4. Conclusions 21
Appendix 1.A. Mean-field Ising model 22
Appendix 1.B. Chain dimensions within the rotational isomeric state model 25
References 28

Chapter 2. Wetting by polymers of a liquid–liquid interface: effects of short-range interactions and of chain stiffness 29
2.1. Introduction 29
2.1.1. Contact angles and surface tension 29
2.1.2. The wetting transition 30
2.1.3. Wetting in the presence of polymer chains 31
2.2. Theory and methods 31
2.3. Results and discussion 36
2.3.1. Flexible polymer 36
2.3.2. Semi-flexible polymer 44
2.4. Conclusions 47
References 47

Chapter 3. Adsorption kinetics of the polysaccharide xanthan on ZrO_2 49
3.1. Introduction 49
3.2. Experimental 51
3.3. Results and discussion 52
3.3.1. Transport-limited regime 54
3.3.2. Long-term adsorption kinetics 56
3.4. Conclusions 59
References 59

Chapter 4. Competition between transport and spreading in protein adsorption kinetics 61
4.1. Introduction 61
4.2. Experimental 62
4.2.1. Materials 62
4.2.2. Reflectometry 62
4.3. Results and discussion 63
4.4. Analytical model 66
Acknowledgements 69
References 69

Chapter 5. Adsorption and spreading of polymers at plane interfaces; theory and molecular dynamics simulations 71
5.1. Introduction 71
5.2. Transport and spreading 72
5.2.1. Transport to the interface 73
5.2.2. Spreading models 77
5.2.3. Molecular dynamics 77
5.3. Analytical expressions for adsorption kinetics 81
5.3.1. Adsorption at immobile interfaces 82
5.3.2. Adsorption at expanding interfaces 85
5.4. Discussion and conclusion 86
5.4.1. Immobile interface 87
5.4.2. Expanding interface 88
5.4.3. Final remarks 89
Acknowledgements 90
Appendix 5.A. Differential equations in adsorption kinetics 91
5.A.1. Growing disk 91
5.A.2. n-Step model 91
References 92

Samenvatting 95

Levensloop 99

CHAPTER 0

Introduction

ABSTRACT

In this chapter I supply the reader with background information on the contents of this thesis. In the first part, the different length scales in polymers are introduced and a criterion for semi-flexibility is given. I discuss some basic aspects of polymers near an interface where both experimental and theoretical techniques are discussed. Finally, an outline of this thesis is given.

0.1. POLYMERS AND THEIR SEMI-FLEXIBILITY

In both chemistry and physics polymers are viewed upon in numerous ways. The reason for this is at least twofold. Depending on the academic background of the individual researcher, he or she has a bias towards the use of a certain model. An organic chemist is likely to look at a polymer on an atomic level, defining it as a collection of atoms, linked by different types of bonds to form a chain. On the other hand, a condensed-matter physicist will view it as a line in D-dimensional space, where its properties are defined in a more global way. These are, of course, only two examples of the wide variety of different researchers, and their models, who look at polymers in a certain way. A second reason for the existence of the different views is the way one uses a certain polymeric system. It is of little use to describe a polymer quantum-mechanically if one is interested in the adsorption of a polymer to a liquid–liquid interface, although, in principle, it would be possible. The title of this section already implies the use of a certain model, and I will try to describe this model in somewhat more detail.

Basically, a polymer molecule is a chain consisting of a large number of repeating units (monomers). I will restrict myself to homopolymers, containing only one type of repeating unit. Furthermore, as long as no atomic detail is required, it is sufficient to consider a polymer chain as a number of bonded segments, where one should note that such a segment is not necessarily an atom. It should be clear that a segment contains no atomic detail, whereas a monomer does. When studying polymer adsorption, one has to consider at least the conformation and size of the polymer molecules. These important features are determined by the interactions of the polymer with its environment, and by intramolecular interactions. A widely used approach to describe the interactions with the environment, not only in polymeric systems, is the so-called Bragg-Williams approximation, where the actual surrounding of a segment is replaced by a time-averaged (or space-averaged) one. In polymer science this mean-field approach is generally known as the Flory-Huggins theory [1, 2]. A homopolymer chain can be characterised by the number of bonds L, the bond length b, its radius of gyration R_g, and the persistence length q (see fig. 0.1). The first two quantities require no further explanation, whereas I will briefly introduce the latter two.

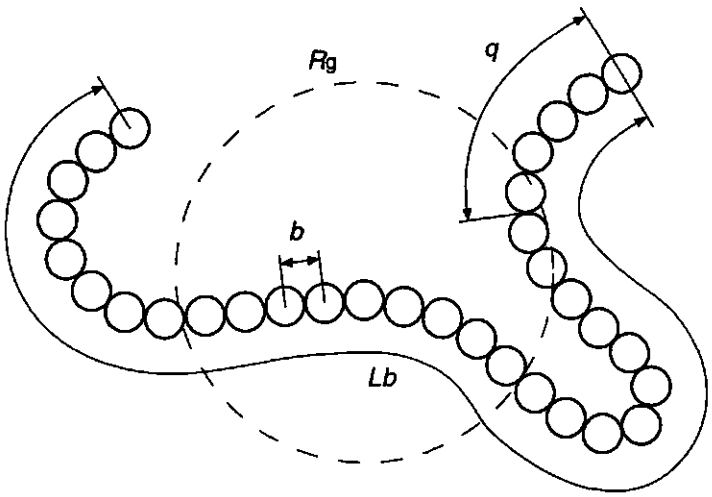

FIGURE 0.1. Schematic representation of a homopolymer with its characteristic lengths.

In the presented picture of a polymer chain, one can describe its conformation by L bond vectors $\{\mathbf{r}_L\} = (\mathbf{r}_1, \mathbf{r}_2, \ldots, \mathbf{r}_L)$. I am not interested in the conformation of a single chain at a given moment, but mainly in its average properties. A measure for the average size of a polymer coil is its mean-square radius of gyration, R_g^2, which is defined as

$$R_g^2 = \langle S^2 \rangle = \frac{1}{L} \sum_j \langle \mathbf{S}_j^2 \rangle, \tag{0.1.1}$$

where $\mathbf{S}_j$ denotes the distance of the centre of mass to segment j at a given moment, and the angular brackets denote a time-average. For a random-flight chain the radius of gyration is related to the frequently used end-to-end distance $\langle R^2 \rangle^{1/2}$ by

$$\langle S^2 \rangle = \frac{1}{6} \langle R^2 \rangle. \tag{0.1.2}$$

The stiffness of a polymer chain, originating from the orientational correlations between bonds, is usually characterised by the persistence length. It can be viewed upon as the distance along the chain to the point where the directional correlation with the starting bond is only just noticeable. A more quantitative definition is the averaged sum of the projections of all bond vectors $\mathbf{r}_i$ on the direction of the first bond vector:

$$q = \frac{1}{b} \sum_i \langle \mathbf{r}_1 \cdot \mathbf{r}_i \rangle. \tag{0.1.3}$$

With these definitions in mind, a polymer is denoted as *semi-flexible* if $b \ll q \ll Lb$. There exists a large number of polymers that can be considered to be semi-flexible. This is related to the fact that, from a molecular point of view, there are numerous ways to introduce semi-flexibility into a polymer. Not only the primary structure of a

macromolecule, but also a more global one, or even secondary structures (e.g. helices), can give rise to the formation of semi-flexible objects.

0.2. POLYMERS NEAR INTERFACES

The process of either accumulation or depletion of a substance near an interface is called adsorption (depletion is usually referred to as negative adsorption). This accumulation can eventually lead to the formation of a new macroscopic phase; this process is then referred to as wetting. That the adsorption of polymers has many applications in every day life, should be no surprise. I shall not attempt to give an exhaustive overview of these applications, but restrict myself to list some examples based on products and processes of the top-3 companies in the Dutch stock market in table 0.1. This table just gives an idea about the wide variety of systems where polymer adsorption plays a role. At Shell one adds poly(ethylene oxide) to Otto-fuel to prevent carbon deposition on valves and pistons. The same polymer is used by Unilever in shampoo to prevent "jumpy" hair due to electrostatic repulsion by adsorbing it on keratin in hair. In magnetic media, a polymer film is used to stabilise the magnetisable particles.

TABLE 0.1. Examples of products and processes in which polymer adsorption plays a key role of the top-3 (based on turnover in 1995) Dutch companies with an Amsterdam Stock-Exchange quotation.

company	turnover 1995 in mln DFL	product or process
Koninklijke/Shell	175379	drilling, gas and oil recovery, composites, blends, fuel additives, lubricants
Unilever	79703	detergents, shampoo, food stabilisers, fat replacers
Philips	64462	integrated circuits, television tubes, magnetic media

This widespread "use" of polymer adsorption in industrial processes and products makes it a popular object of both fundamental and applied study. An extensive overview of both experimental and theoretical approaches is given by Fleer et al. [3]. In this monograph the emphasis is on equilibrium properties. The *kinetics* of polymer adsorption are only slowly gaining the attention they deserve. One could say that the study of the adsorption kinetics of polymers is still in its hobbledehoyhood. This means that there is, as yet, no established way of tackling problems concerned with these kinetics. Even worse, kinetic aspects are sometimes overlooked. Especially polymers which are not flexible are of interest when studying adsorption kinetics. The stiffness of these molecules gives rise to, e.g. slow reorientation processes which could play a role in their behaviour near an interface.

0.2.1. Semi-flexible polymers and adsorption experiments

A large group of semi-flexible polymers is formed by helix-forming macromolecules. It is obvious that here not the molecular chain itself, but the helix structure has a certain rigidity. A large number of biological molecules belongs to this class of semi-flexible polymers. DNA, xanthan, schizophyllan, poly(γ-benzyl-L-glutamate), and scleroglucan are just some examples.

Other macromolecules with "local" stiffness are proteins. Their strong internal structure with high energy barriers makes reorientation and reconformation processes slow. Proteins are rather complex polymers because they consist of segments of a large number of different types. However, numerous properties are comparable to that of simpler polymers. Especially denaturation of such proteins can strongly influence the kinetics of their adsorption, leading to nonequilibrium adsorbed layers.

There exist numerous experimental techniques to study polymer adsorption, but when it comes to its kinetics the range to choose from becomes limited. The reason for this lies in the fact that one has to control the processes that could influence the adsorption behaviour. It is therefore necessary to use well-defined transport conditions, which leaves only a few methods. One of the remaining techniques to study adsorption kinetics at a solid–liquid interface is reflectometry in a stagnation-point flow setup, which was extensively described by Dijt et al. [4, 5]. The basic idea behind this technique is that an adsorbing polymer changes the optical properties of the interfacial region. This effect causes the reflectivity of the system to change, from which the adsorbed amount can be determined. Because the transport of polymer from solution to the stagnation point (at the interface) is exactly known, at least for an empty interface, kinetic data can be gathered from the experiment.

0.2.2. Theoretical approach

Equilibrium. As mentioned before, for polymeric systems often the Bragg-Williams approximation is used. This implies the use of the so-called mean-field assumption. In the case of adsorption, the polymeric system of interest is inhomogeneous in at least one direction, i.e. perpendicular to the interface. The densities of the different components are now a function of position, which is not the case in the Flory-Huggins theory. Calculating thermodynamic properties of such interfacial systems can be done in several ways. The two theoretical approaches that I will discuss are both lattice-based models, in which every segment is of the same size and a polymer molecule is represented by a chain of connected segments. In the following I define a monomer to consist of one segment.

The first type of model is the so-called density-functional theory, where a local free energy density is introduced which, integrated over the total system, gives the total free energy. For a simple binary monomeric system this free energy density has the following continuous form

$$\frac{f(\rho, \nabla\rho)b^3}{k_B T} = \rho \ln \rho + (1-\rho)\ln(1-\rho) + \chi\rho(1-\rho) + \lambda\chi b^2(\nabla\rho)^2, \tag{0.2.1}$$

where ρ denotes the local reduced density (or volume fraction) of one of the components, b is the step length of the underlying lattice, and λ is a lattice parameter; e.g. in a simple cubic lattice $\lambda = 1/6$. The Flory-Huggins interaction parameter χ is a measure for the energy difference between a monomer of a certain type surrounded by monomers of its own type, and that of the same monomer surrounded by those of a different type. Equation 0.2.1 can be derived starting from an Ising model (see, e.g. ref. 6 or chapter 1). Although the latter is a lattice theory, one can rewrite the equations to obtain a continuous form of the free energy density function as given in eq. (0.2.1). The total free energy can then be written in a functional form $F[\rho(\mathbf{r}), \nabla\rho(\mathbf{r})] = \int_V \mathrm{d}V f(\rho, \nabla\rho)$. Minimisation of this functional with respect to $\rho(\mathbf{r})$ yields an equilibrium reduced density profile and the corresponding total free energy. However, this minimisation can only be carried out analytically if an approximation for the free energy density is used. To this end an order parameter, $\Psi = \rho - \rho_c$, is introduced. Here ρ_c denotes the critical reduced density for phase separation, which is $1/2$ for a binary monomeric system. The free energy density, $f(\rho, \nabla\rho)$, is expanded with respect to this Ψ, which is known as the Ginzburg-Landau expansion. The use of this expansion also implies that only systems in the neighbourhood of the critical point can be studied this way. This approach can also be used for polymeric systems, and can in principle be extended to multi-component systems. One of the complicating factors when describing polymer systems with such a density-functional theory is the way chain connectivity has to be introduced. A fraction of $(1-1/N)$ segments per chain can not be placed independently on the lattice, which implies a non-local contribution to the conformational entropy of the polymer. For a multi-component mixture of molecules with different chain lengths N_α eq. (0.2.1) should be rewritten, and becomes

$$\frac{fb^3}{k_B T} = \sum_\alpha \left(\frac{\rho_\alpha}{N_\alpha} \ln \rho_\alpha - \left(1 - \frac{1}{N_\alpha}\right) \rho_\alpha \ln \left(1 + \frac{\lambda b^2 \nabla^2 \rho_\alpha}{\rho_\alpha}\right)\right) + \sum_{\alpha\beta} \left(\chi_{\alpha\beta}\rho_\alpha\rho_\beta - \lambda b^2 \chi_{\alpha\beta}\rho_\alpha \nabla^2 \rho_\beta\right) \tag{0.2.2}$$

where α and β denote molecules constituted of α- or β-segments, and $\sum_{\alpha\beta}$ denotes a sum over all pairs of different segments. The Laplacians in this equation, except the one in the logarithmic term, can in principle be rewritten as square gradients by applying the divergence theorem, and by choosing a proper boundary of integration. It is clear that both the expansion and the minimisation of eq. (0.2.2) are complex problems. An analytical solution is in this case impossible, and even a numerical approach is difficult.

Another way to tackle polymer adsorption is the use of Markoff statistics [7] to create all possible conformations of a test chain in an external field, generated by the rest of the system of interest. In this method the external mean field is a functional of the densities of all constituting components, which are in their turn functionals of the external field. This interdependency between mean field and densities gives this approach its name: self-consistent field (SCF) theory. The fixed point of a system can

be found numerically and is denoted as the SCF solution. An SCF theory for polymer adsorption was introduced by Scheutjens and Fleer [8, 9].

Kinetics. Both theoretical approaches discussed above are equilibrium theories, which do not reveal any information about the adsorption kinetics. For the kinetics, no theoretical treatments of the same level are available. Most theoretical approaches for polymer adsorption kinetics, focus on the processes near the interface, and do not consider the limitations due to material transport to (or from) the interface (see e.g. ref. 10). To include these transport properties a phenomenological approach is more feasible. At least three different timescales are important in the kinetics: transport to the interface, attachment, and spreading. The processes that occur near the interface can be modelled by empirically "derived" equations. One of the ways to describe the spreading of a polymer near an interface is by the "growing disk" model. Here, one assumes that a polymer occupies a certain area a_0 at the interface on arrival ($t = t'$), and subsequently grows according to $a(t;t') = a_0 + \alpha\,(1 - \exp(-(t-t')/\tau_s))$, where τ_s is a characteristic time, and α the final area increase. This model can then be combined with the transport equations to lead to expressions for the adsorption kinetics (see chapters 4 and 5).

0.3. OUTLINE OF THIS THESIS

In this thesis I employ both theoretical models and experiments to gain more insight in the adsorption of semi-flexible and rodlike molecules. I start in chapter 1 to explore some consequences of chain flexibility for interfacial behaviour, with the emphasis on the equilibrium adsorption of semi-flexible polymers at a liquid–liquid interface. An SCF approach is applied to a system consisting of two phase-separating monomeric liquids and a small amount of semi-flexible polymer chains, and systematically investigate the influence of chain stiffness, chain length, and interfacial width on the adsorption behaviour. In chapter 1 I continue to study the equilibrium interfacial behaviour of semi-flexible chains. The basis of this study is laid in the preceding chapter, but now I extend the system to a 3-phase system, for which wetting phenomena are discussed. Again, stiffness and intermolecular interactions play an important role. After these "equilibrium" chapters I continue with kinetic experiments in chapter 3, which deals with a systems where semi-flexibility of homopolymers influences the adsorption kinetics. I consider the helix-forming polysaccharide xanthan adsorbing onto zirconium(IV)oxide, where both pH and ionic strength are varied to control the flexibility of the polymer. In this case a decrease of the ionic strength induces a helix–coil transition, which gives rise to a coil conformation of the polymer. When xanthan adsorbs in its helical conformation, equilibration of the adsorbed layer is shown to be slow, and no plateau in the kinetic adsorption curve is found, in contrast to the adsorption experiments with the coiled molecule. Chapters 4 and 5 are mainly devoted to kinetic effects resulting from the process of polymer spreading near an interface. As examples the adsorption kinetics of two proteins, immunoglobulin and savinase, onto silicon(IV)oxide are presented. These proteins are believed to denaturate, at least partly, near the surface which gives

rise to a spreading of the molecule. The time constant of this denaturation process is relevant for the adsorption kinetics. I also introduce a phenomenological model to describe these adsorption kinetics. This model is generalised in chapter 5 and supplemented with some molecular dynamics calculations to justify the use of a "growing disk" model.

REFERENCES

[1] P. J. Flory. *Principles of polymer chemistry.* Cornell University Press, Ithaca, 1953.

[2] M. L. Huggins. Some properties of solutions of long-chain compounds. *J Phys Chem*, 46:151–158, 1942.

[3] G. J. Fleer, M. A. Cohen Stuart, J. M. H. M. Scheutjens, T. Cosgrove, and B. Vincent. *Polymers at interfaces.* Chapman & Hall, London, 1993.

[4] J. C. Dijt, M. A. Cohen Stuart, J. E. Hofman, and G. J. Fleer. Kinetics of polymer adsorption in stagnation point flow. *Colloids Surfaces*, 51:141–158, 1990.

[5] J. C. Dijt, M. A. Cohen Stuart, and G. J. Fleer. Reflectometry as a tool for adsorption studies. *Adv Colloid Interface Sci*, 50:79–101, 1994.

[6] S. A. Safran. *Statistical thermodynamics of surfaces, interfaces, and membranes.* Addison-Wesley, Reading, 1994.

[7] A. A. Markoff. *Wahrscheinlichkeitsrechnung.* Teubner, Leipzig, 1912. Secs. 16 and 33.

[8] J. M. H. M. Scheutjens and G. J. Fleer. Statistical theory of the adsorption of interacting chain molecules. I. Partition function, segment density distribution and adsorption isotherms. *J Phys Chem*, 83:1619–1635, 1979.

[9] J. M. H. M. Scheutjens and G. J. Fleer. Statistical theory of the adsorption of interacting chain molecules. II. Train, loop, and tail size distribution. *J Phys Chem*, 84:178–190, 1980.

[10] A. N. Semenov and J.-F. Joanny. Kinetics of adsorption of linear homopolymers onto flat surfaces: Rouse dynamics. *J Phys II France*, 5:859–876, 1995.

CHAPTER 1

Semi-flexible polymers at a liquid–liquid interface: self-consistent-field calculations

ABSTRACT

The adsorption of semi-flexible polymers at a liquid-liquid interface largely differs from that at a solid surface. The width of the interface is an additional length scale in the problem, making the system behaviour particularly rich. We consider two phase-separating monomeric liquids, C and D, and a polymer A_N which dissolves equally well in both liquids. We study this system in a self-consistent-field model in the dilute regime. The stiffness of the polymer is controlled by the use of a rotational isomeric state approach. We show that the interfacial width ξ (determined by the interaction parameter between the two solvents), the persistence length q, and the chain length N are relevant parameters in the adsorption behaviour. A key observation is that, while keeping $N^{1/2}/\xi$ constant, the adsorbed amount goes through a minimum with increasing q/ξ. An initial increase of q/ξ ($q/\xi \lesssim 1$) effectively leads to a larger coil size, leading to a decrease of the adsorbed amount. However, when $q/\xi \gg 1$, alignment of parts of the polymer within the interfacial region occurs due to the lack of entropic penalties. This alignment process induces an increase of the adsorbed amount. These observations also have implications for the ongoing discussion about the preferential adsorption in a mixture of flexible and stiff polymers. In this discussion one should consider the effects of the finite size of the interfacial region.

1.1. INTRODUCTION

The adsorption of macromolecules at liquid–liquid interfaces is of major importance in a wide variety of relevant systems, ranging from food products to oil recovery. The flexibility of a polymer should have an effect on its adsorption behaviour, but an a priori statement about the precise nature of these effects can not be given from simple considerations. Most theoretical adsorption studies on semi-flexible polymers consider a solid surface, where the problems associated with the boundary condition usually do not receive much attention. Monte Carlo simulations on a mixture of flexible and stiff short chains show that the stiff chains near a Fresnel (i.e. infinitely sharp) interface are most surface active [1, 2]. On the other hand, using an analytical self-consistent-field (SCF) theory, Wu et al. [3] report the opposite. The apparent conflict in these results probably has its origin in the choice of the definition of the solid surface. In the former an infinitely sharp interface is used, whereas in the latter case a fairly sharp but smooth density profile is assumed.

In the present paper we like to take an alternative route to by-pass the problems associated with a solid–liquid interface. By using a liquid–liquid interface, we not only

circumvent the problem of an ad-hoc choice of the boundary condition, but are also able to control the width of the interfacial region. We will use a numerical SCF theory to study the behaviour of a polymer A_N near an interface formed by the phase boundary of two monomeric liquids. By varying the Flory-Huggins interaction parameter between the two solvents, we are able to control the interfacial width. We apply a rotational isomeric state (RIS) model to vary the stiffness of the polymer chain, and study its influence on the adsorption behaviour. Other parameters in our calculations are chosen such that the analysis of the adsorption process is relatively easy. We will show that the interfacial width (to be defined below) is a relevant parameter, even when this width is small. In particular we will concentrate on the interplay between this parameter and the persistence length of the polymer. Obviously, the length of the polymer and the solvent quality (effective adsorption energy) are additional parameters in the system.

1.2. THEORY

1.2.1. General formulation of the model

We consider a lattice model of a three-component system, containing two monomeric components, denoted by C and D, and one polymer A_N, where N denotes the number of constituting units. We choose the interaction parameters such that the two monomeric components phase separate, creating a liquid–liquid interface at which polymer adsorption can occur. We examine the system not too far from its critical point, using the interfacial width as a tuning parameter. However, we have to keep in mind that this width must be substantially smaller than the system size to avoid finite-size effects. In line with this, we will keep the overall polymer concentration low in order to minimise the effect of added polymer on the interfacial width and on the location of the Gibbs dividing plane. Adsorption from dilute solution will be limited to the Henry regime, i.e. polymer overlap does not play a decisive role. Starting from the lattice model, there are several ways to evaluate the properties of the system. We will discuss two possible approaches: an analytical and a numerical mean-field theory. We will use the analytical approach to describe the system without polymer, and the numerical one to account for the presence of the polymer.

1.2.2. Analytical mean-field approach

As long as the polymer concentration is low, some characteristics of the system can already be deduced from the properties of the binary mixture of the monomeric components. These characteristics can be used to determine which parameters should be varied to access interesting regions of the ternary system. We are interested in the behaviour of this system beyond its critical point, i.e. it consists of a C-rich and a D-rich phase. We consider the system to be described by the exact Hamiltonian $\mathcal{H}$, leading to the probability distribution function

$$P \propto \exp\left(-\frac{\mathcal{H}}{k_{\mathrm{B}}T}\right). \tag{1.2.1}$$

The total Helmholtz energy (or free energy) of our system, expressed in terms of P is given by

$$\mathcal{F} = k_B T \int \mathrm{d}\Lambda P \ln P + \int \mathrm{d}\Lambda P \mathcal{H}, \tag{1.2.2}$$

where Λ represents the phase space of the system. Minimisation of this exact free energy is not possible, but requires a variational approximation to the Boltzmann weight. We consider a model system, described by a Hamiltonian $\mathcal{H}_0$, and minimise eq. (1.2.2) with respect to the constituting parameters of the model system. The free energy is now approximated by

$$F = k_B T \int \mathrm{d}\Lambda P_0 \ln P_0 + \int \mathrm{d}\Lambda P_0 \mathcal{H}, \tag{1.2.3}$$

where $P_0 \propto \exp(-\mathcal{H}_0/k_B T)$. The exact free energy $\mathcal{F}$ is bound by the inequality [4]

$$\mathcal{F} < F = F_0 + \langle \mathcal{H} - \mathcal{H}_0 \rangle_0. \tag{1.2.4}$$

Here, F_0 denotes the free energy of the model system and averaging is carried out with respect to $\exp(-\mathcal{H}_0/k_B T)$.

An easy way to access the properties of a binary mixture is the use of an Ising model (see, e.g. ref. 5). In appendix 1.A a mean-field approximation of this model is discussed and the relevant equations within this approach are given. For a system, not too far from its critical point, the reduced density ρ of component D as a function of the distance z from the interface is given by substitution of eq. into eq. (1.A.19), which leads to

$$\rho(z) = \frac{1}{2} + \sqrt{\frac{3(\chi - 2)}{8}} \tanh \frac{z}{\xi}, \tag{1.2.5}$$

where the interfacial width, or bulk correlation length, is given by

$$\xi = b \sqrt{\frac{2\lambda_1 \chi}{\chi - 2}}. \tag{1.2.6}$$

In these equations b denotes the nearest-neighbour distance, χ is the Flory-Huggins interaction parameter, and λ_1 accounts for the relative number of nearest neighbours of a segment in the direction of the reduced density gradient.

We will use the interfacial width from eq. (1.2.6) as a tuning parameter for the self-consistent-field calculations, where polymer is incorporated into the system. In doing this, we take special care that the addition of a small amount of polymer to the system does not change the interfacial width significantly. One should also bear in mind that eq. (1.2.6) is only valid rather close to the critical point, i.e. $\chi - 2 \ll 1$.

1.2.3. Numerical self-consistent-field theory

We used the self-consistent-field (SCF) formalism developed by Scheutjens and Fleer (SF) [6, 7], which was originally set up to study polymer adsorption from dilute or semi-dilute solution onto solid surfaces. We will only discuss some basic aspects of the theory, and touch upon the assumptions made in it. Finally, we will mention some

extensions to this theory, which make it suitable for the liquid–liquid interface system in the presence of semi-flexible polymer.

The SF SCF approach is a mean-field lattice theory, where only one of the three spatial coordinates remains as a variable, whereas in the other directions density gradients are averaged out. One should bear in mind that this theory starts from the same assumptions as the aforementioned mean-field approximation to the Ising model. However, no Taylor expansion of the free energy density is needed. Therefore, the theory is especially valuable away from the critical point, but it can also be used in the neighbourhood of the critical point as long as the correlation length does not exceed the system size. In this SCF model a test molecule is situated in a one-dimensional potential field, set up by the other components in the system. All the possible conformations of the test molecule are generated using Markoff statistics, and these are weighted with the local potential field. Appropriate normalisation leads to the composition profile of the system. The potential field is a functional of the reduced density profile and this profile is, in turn, itself a functional of the potential field. The goal of the SF SCF approach is to find a unique solution to this problem, which involves the choice of proper boundary conditions and constraints.

In the SF SCF theory all molecules are built up from equally sized segments and are placed on a lattice. The lattice is composed of m parallel layers of thickness b, where the layers are numbered $i = 1, 2, \ldots, m$. The lattice is furthermore characterised by so-called *a priori* step probabilities λ_{ij}, which give the relative number of contacts of a segment in layer i with those in layer j. Obviously, $\lambda_{ij} = 0$ if $|j - i| > 1$, and $\sum_{j=1}^{m} \lambda_{ij} = 1$. We will use the notation λ_0 for $i = j$, and λ_1 for $|j - i| = 1$. For the calculation of the composition profile we define the local reduced density (in layer i) for segment type x as $\rho_x(i) = n_x(i)/l$, where $n_x(i)$ denotes the number of segments of type x in layer i, and l is the number of sites in every layer. We denote molecule related quantities by an index α. The segments constituting molecule α are numbered $s = 1, 2, \ldots, N_\alpha$. The local reduced density of a segment type can also be expressed in terms of the local reduced density $\rho_\alpha(i, s)$ of segment s of molecule α:

$$\rho_x(i) = \sum_{\alpha} \sum_{s=1}^{N_\alpha} \rho_\alpha(i, s) \delta_\alpha(s, x), \tag{1.2.7}$$

where $\delta_\alpha(s, x)$ is defined as being unity if segment s of molecule α is of type x and zero otherwise.

We only take into account nearest-neighbour interactions, which are accounted for by the Flory-Huggins interaction parameter χ_{xy} between segments x and y. The imposed mean-field approximation causes the interactions within one layer to be smeared out. The potential energy $u_x(i)$ of a segment in layer i with respect to the bulk (in our case the C-rich phase) is then by

$$u_x(i) = u'(i) + k_B T \sum_{y} \chi_{xy} \left(\langle \rho_y(i) \rangle - \rho_y^b \right), \tag{1.2.8}$$

where the angular brackets indicate the weighted average over layers $i-1$, i, and $i+1$, which is needed to account for the nearest-neighbour interactions. The first term in eq. (1.2.8), u', is a Lagrange field to ensure that the total reduced density is constant, i.e.

$$\sum_x \rho_x(i) = 1 \quad \forall i. \tag{1.2.9}$$

Next, we define the segment weighting factor $G_x(i) = \exp(-u_x(i)/k_BT)$, which is just a Boltzmann factor of the field for segment x. In order to account for chain connectivity the end-segment distributions $G_\alpha(i,s|1)$ and $G_\alpha(i,s|N_\alpha)$ are introduced, defined as the average statistical weight of all conformations with segment s in layer i and the first or last segment, respectively, located anywhere in the system. They can be calculated by a propagator scheme

$$G_\alpha(i,s|1) = G_\alpha(i,s)\langle G_\alpha(i,s-1|1)\rangle, \tag{1.2.10a}$$

$$G_\alpha(i,s|N_\alpha) = G_\alpha(i,s)\langle G_\alpha(i,s+1|N_\alpha)\rangle, \tag{1.2.10b}$$

where the angular brackets again indicate the weighted average over layers $i-1$, i, and $i+1$. This averaging ensures the chain connectivity.

In the original SF SCF approach a first-order Markoff approximation is used, which is characterised by the so-called connectivity law

$$\rho_\alpha(i,s) = C_\alpha \frac{G_\alpha(i,s|1)G_\alpha(i,s|N_\alpha)}{G_\alpha(i,s)}, \tag{1.2.11}$$

where C_α is a normalisation constant which, in an open system, is most conveniently written as $C_\alpha = \rho_\alpha^b/N_\alpha$. The free segment weighting factor for segment s in molecule α is given by $G_\alpha(i,s) = \sum_x G_x(i)\delta_x(i,s)$. It is needed in the numerator of eq. (1.2.11) to correct for double counting of the statistical weight of segment s.

The fundamental equations of the SF SCF approach, given above, set the stage for our system. The presence of a liquid–liquid interface implies the following boundary conditions

$$\rho_x(0) = \rho_x(1), \quad \rho_x(m+1) = \rho_x(m), \tag{1.2.12}$$

i.e. the system has reflecting boundaries on either side. One of the features which is not described by the above equations is the chain stiffness. Introduction of this property involves a change in the connectivity law from eq. (1.2.11) and requires another propagator scheme (eq. (1.2.10)). In modelling association colloids, Leermakers et al. implemented a rotational isomeric state (RIS) approach in the SCF theory to include chain stiffness [8]. In this way local self-avoidance of the chains is accounted for, and chain rigidity can be controlled by changing the energy difference Δu_{tg} between the *trans* and the *gauche* states. Because no fundamental change in the theory occurs, we will not give a full description of the implementation here but refer to the literature [8]. Basically, the RIS approach implies the use of third-order Markoff statistics in the SCF theory. The exact implications of this approach to the chain stiffness will be discussed in the next section.

Our system consists of $m = 300$ lattice layers and the number of sites per layer is conveniently chosen as $l = 1$. In planar systems, however, this latter choice is irrelevant, because all quantities are calculated using densities and energies per site. Because of the RIS model, it is convenient to use a tetrahedral lattice, which ensures that the connectivity constraints are based on the same lattice as the nearest-neighbour interactions [8]. The tetrahedral lattice is characterised by $\lambda_1 = 1/4$. The monomeric component C is used as solvent and the total amount of D in the system is $\Theta_D = 150$. The bulk concentration of polymer A_N is chosen to be $\rho_A^b = 10^{-5}$, which, in our case, is in the dilute regime. The interaction parameters of the A-segments with both liquids are $\chi_{AC} = \chi_{AD} = 0$ throughout the paper. This choice makes the system symmetric for the polymer. The parameter χ_{CD}, simply denoted as χ, should be chosen such as to ensure a phase separation, and thus the presence of an interface. The critical point of phase separation $(\rho_{A,c}, \chi_c)$ is found by solving

$$\left(\frac{\partial^2 f}{\partial \rho_C^2}\right)_{\rho_{C,c}} = 0, \tag{1.2.13}$$

where f is the Helmholtz free energy per site for a homogeneous system, which in the random mixing approximation is for the ternary system given by (see eq. (1.A.11))

$$\frac{f}{k_B T} = \rho_C \ln \rho_C + (1 - \rho_C - \rho_A) \ln(1 - \rho_C - \rho_A) + \frac{\rho_A}{N} \ln \rho_A + \chi \rho_C (1 - \rho_C - \rho_A). \tag{1.2.14}$$

At the critical point $\rho_{C,c} = \rho_{D,c}$, so the solution of eq. (1.2.13) is

$$\chi_c = \frac{2}{1 - \rho_A}, \qquad \rho_{C,c} = \frac{1 - \rho_A}{2}. \tag{1.2.15}$$

Because the polymer concentration is low, the total amount of solvent C is given by $\Theta_C = 150 - \mathcal{O}(m\rho_C^b)$, The exact value of Θ_C is such that the Gibbs dividing plane is located on the boundary of layers 150 and 151, which prevents lattice artifacts to play a role. We define the distance from the interface as $z = (i - 150.5)b$.

1.2.4. Chain dimensions

The adsorption of a polymer at a liquid–liquid interface will depend on the dimensions of the polymer. Within a homopolymer at least two different length scales can be distinguished. We will consider the end-to-end distance $\langle R^2 \rangle^{1/2}$ and the persistence length q as the relevant length scales. These quantities are defined in terms of the bond vectors $\mathbf{r}_i$ and the number of bonds L as follows

$$\langle R^2 \rangle \equiv \sum_{i=1}^{L} \sum_{j=1}^{L} \langle \mathbf{r}_i \cdot \mathbf{r}_j \rangle, \tag{1.2.16}$$

$$q \equiv \frac{1}{|\mathbf{r}_1|} \sum_{i=1}^{L} \langle \mathbf{r}_1 \cdot \mathbf{r}_i \rangle. \tag{1.2.17}$$

In appendix 1.B we follow the same lines of argument as Yamakawa [9] to arrive at the required expressions for the calculation of those length scales.

We view a homopolymer as a chain of L bonds with identical bond lengths b and bond angles θ between bond vectors $\mathbf{r}_i$ and $\mathbf{r}_{i+1}$. The rotational angles are described within a rotational isomeric state model, where the energy difference between the *trans* and the *gauche* state is denoted by Δu_{tg}. For sufficiently long polymer chains the end-to-end distance and the persistence length are then given by

$$\langle R^2 \rangle_\infty = Lb^2 \frac{2\omega + 4}{3\omega}, \tag{1.2.18}$$

$$q_\infty = b \frac{5\omega + 4}{6\omega}, \tag{1.2.19}$$

where $\omega = \exp(-\Delta u_{\mathrm{tg}}/k_{\mathrm{B}}T)$. When calculating the two discussed length parameters, we will use the number of segments N instead of L, which implies that $N \approx N - 1$.

1.3. RESULTS AND DISCUSSION

The main goal of our analysis of semi-flexible polymers near a liquid–liquid interface is to relate adsorption behaviour to the three relevant length scales in the system, ξ, q, and $\langle R^2 \rangle^{1/2}$. To make the discussion more transparent all variables are made dimensionless in the following way

$$\xi/b \to \xi, \quad z/b \to z, \quad q_\infty/b \to q_\infty, \quad \frac{\Delta u_{tg}}{k_{\mathrm{B}}T} \to \Delta u_{tg}. \tag{1.3.1}$$

The stiffness of the polymer A_N is reflected in the persistence length q, which in the RIS scheme is determined by the the energy difference Δu_{tg}. For large N this length scale is given by eq. (1.2.19) and is plotted in fig. 1.1. It should be noted that the persistence length determined in this way may only be used as long as $q_\infty < N$.

The interfacial width ξ is mainly determined by the interaction between components C and D, which, in the SCF approach, is reflected in the Flory-Huggins parameter χ. From the SCF calculations for a 2-component system, ξ is calculated from the slope of the reduced density profile at $z = 0$ (between layers $m/2$ and $m/2 + 1$) as follows

$$2(\rho(m/2 + 1) - \rho_{\mathrm{c}})\xi = \rho(m) - \rho_{\mathrm{c}}, \tag{1.3.2}$$

where ρ_{c} is the reduced density at the critical point. To show that ξ_{GL}, as given by eq. (1.2.6), does not deviate much from that determined from numerical SCF calculations, we plot both quantities in fig. 1.2. The fact that $\xi_{\mathrm{SCF}} < \xi_{\mathrm{GL}}$, even near the critical point, is caused by two effects. The first is that the slope $\mathrm{d}\rho/\mathrm{d}z$ at $z = 0$ is slightly underestimated due to the finite width of a lattice layer. The second is that for large ξ, i.e. close to the critical point, the number of lattice layers m should be increased to ensure that $\rho(m) = \rho^{\mathrm{b}}$. Bearing these limitations in mind, the agreement between the two quantities is quite satisfactory. Hence, we can vary the value of χ to obtain the desired ξ.

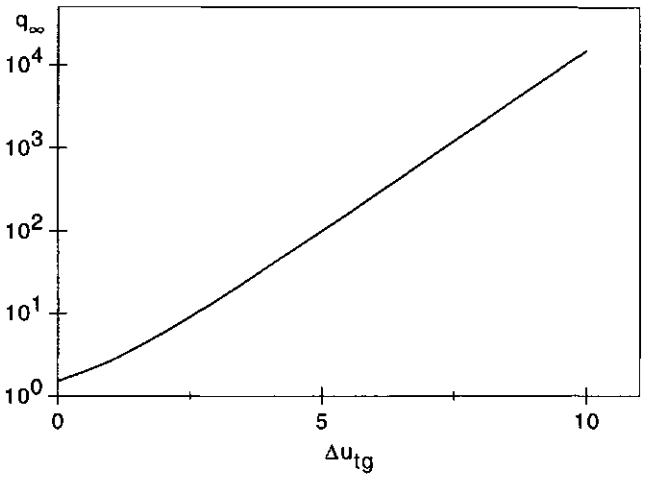

FIGURE 1.1. Persistence length for large N calculated with the rotational isomeric state model using eq. (1.2.19).

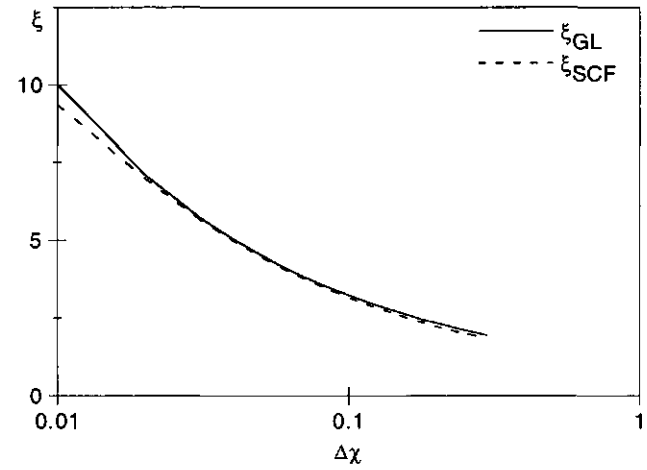

FIGURE 1.2. Interfacial width as a function of $\chi - \chi_c$, calculated with the Ginzburg-Landau approximation (eq. (1.2.6)) and with the SF SCF model ($m = 300$).

1.3.1. Adsorbed amount

From the composition profiles as calculated with the SF SCF theory, we can determine the excess amount of polymer A_N, which we shall call the adsorbed amount

$$\Theta_A^{exc} = -\rho_A^b m + \sum_{i=1}^{m} \rho_A(i) \tag{1.3.3}$$

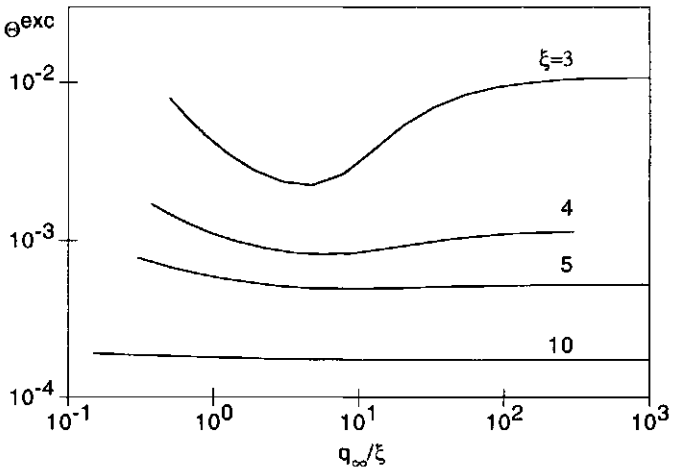

FIGURE 1.3. Adsorbed amount as a function of the ratio between the persistence length and the interfacial width for different values of ξ at $N = 100$.

Note that the term $\rho_A^b m$ can only be used in a symmetrical system, and should be replaced by two terms if the bulk densities are unequal in both phases. We will use this adsorbed amount to compare the behaviour of our system for different values of the length parameters.

Figure 1.3 depicts the adsorption of A_{100} for given values of ξ as a function of the ratio q_∞/ξ. The most remarkable feature extracted from these curves is the minimum in Θ_A^{exc}, which is located at q_∞ of order (but higher than) ξ. The occurrence of this minimum can be understood in the following way. If q_∞/ξ is small, the polymer behaves (more or less) as a flexible coil, and adsorbs at the interface to reduce the unfavourable C–D contacts. An increase of the persistence length causes the polymer dimension to increase. This causes the exclusion of other polymer chains from the interface, which leads to a decrease of the adsorbed amount. A further increase of q_∞ effectively changes the polymer chains into stiff objects in comparison to the interfacial width, for which the entropy loss upon adsorption becomes less, and they will align both to each other and to the interface. This alignment causes the adsorbed amount to increase. The levelling off of the curves at even higher q_∞ is due to the fact that there $q_\infty \gg N$, which means that the chains are effectively rods.

The fact that the shape of the curves in fig. 1.3 changes with increasing interfacial width is caused by our choice of parameters for the calculation. Here, we neglected the effect of the third length scale, $\langle R^2 \rangle^{1/2}$, on the adsorption behaviour. Instead of changing ξ, whilst keeping N constant, one could vary N in such a way that $N^{1/2}/\xi$ remains constant. The factor $N^{1/2}$ stems from eq. (1.B.16), which states that $\langle R^2 \rangle \propto N$. So, in this way we effectively keep the ratio of the end-to-end distance to the interfacial width constant. One should bear in mind that this scheme is only valid for long (semi-)flexible chains or, in other words, $1 \ll q_\infty \ll N$.

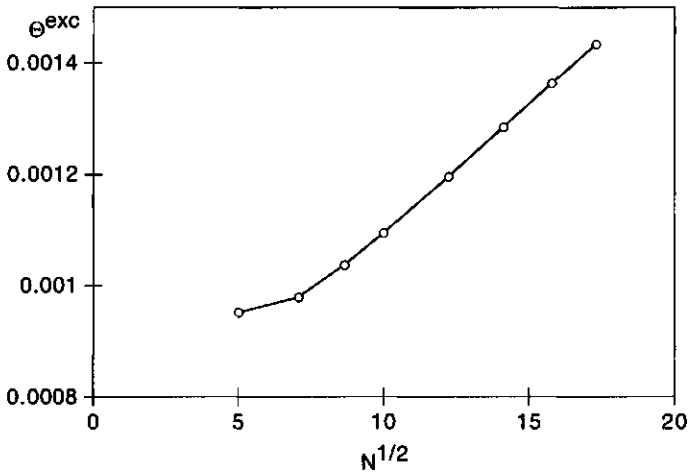

FIGURE 1.4. Chain length dependence of the adsorbed amount for $q_\infty/\xi = 1$ and $N^{1/2}/\xi = 5/2$.

Figure 1.4 shows the adsorbed amount as a function of chain length N, where we kept q_∞/ξ and $N^{1/2}/\xi$ constant. Two important observations can be made. First, the adsorbed amount remains positive for all N. This can be easily understood by the fact that any third component in our system for which both C and D are good solvents, will decrease the number of unfavourable contacts between the monomeric solvents when adsorbed. In other words, there is an effective adsorption energy. Secondly (and more importantly), the additional adsorbed amount scales with $N^{1/2}$ (for large N), which indicates that N is indeed the only remaining relevant parameter for the shape of the adsorption curve if q_∞/ξ and $N^{1/2}/\xi$ are fixed.

Having made these observations, we expect that, when plotting Θ_A^{exc} as a function of q_∞/ξ for different values of N whilst keeping $N^{1/2}/\xi$ constant, these curves should have the same shape. That this is indeed the case is seen in fig. 1.5, where $N^{1/2}/\xi = 5/2$. This is even more clear when Θ_A^{exc} is related to its value at the minimum of the curve (or to any other point where $q_\infty \gtrsim 1$ and $q_\infty < N$). The latter procedure is equivalent to comparing the q_∞-dependent adsorbed amount from fig. 1.5 to the N-dependent one plotted in fig. 1.4. For large N it is possible to rescale the adsorption curves as $\Theta_A^{exc}/\left(\Theta_0^{exc} + \nu N^{1/2}\right)$, where $\nu = d\Theta_A^{exc}/dN$ for large N, and Θ_0^{exc} is the extrapolation of the adsorbed amount $N \to 0$ from large N (see fig. 1.4). Figure 1.6 shows that there is an almost perfect collapse of the curves on a "mastercurve" for the different chain lengths as long as $q_\infty/\xi < 20$. The deviation of the curves beyond this point is obvious, if one realises that the chain length is the limiting factor. The deviation occurs when $q_\infty \gtrsim N$, so the "real" shape of the adsorption curve can only be found for very large N. This observation can also be understood in terms of the fact that the adsorbed amount for rods will be proportional to N, which is not the case for the semi-flexible

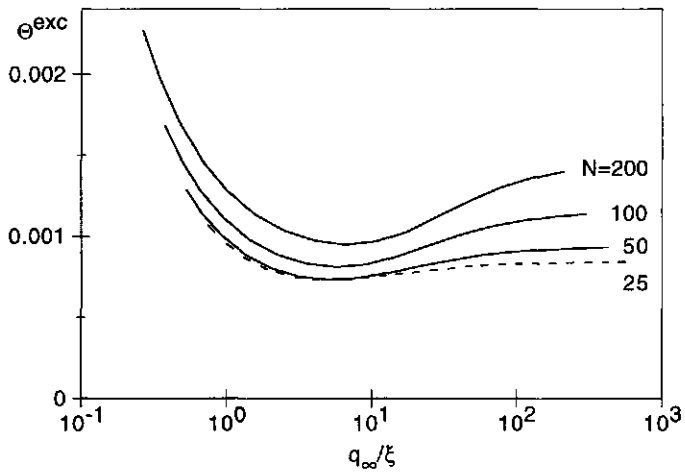

FIGURE 1.5. Adsorbed amount for different chain lengths N with $N^{1/2}/\xi = 5/2$, again as function of q_∞/ξ.

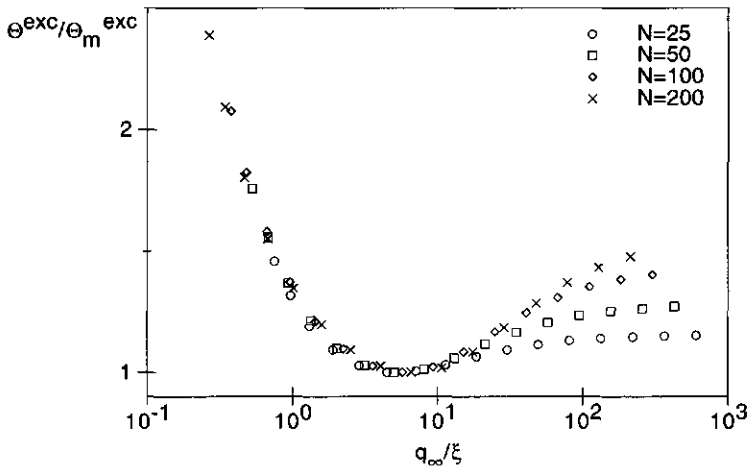

FIGURE 1.6. Relative adsorbed amount related to $\Gamma_{\min}$ at the minimum of the curve. All data is taken from fig. 1.5.

objects as was concluded from fig. 1.4. In other words, we kept $N^{1/2}/\xi$ fixed instead of $\langle R^2 \rangle^{1/2}$.

1.3.2. Density profiles

The observations for the adsorbed amounts of A_N can be further illustrated by taking a closer look at the composition profiles. Figure 1.7 gives the reduced density profiles of systems corresponding to points on the curve in fig. 1.5 for $N = 100$. Due to

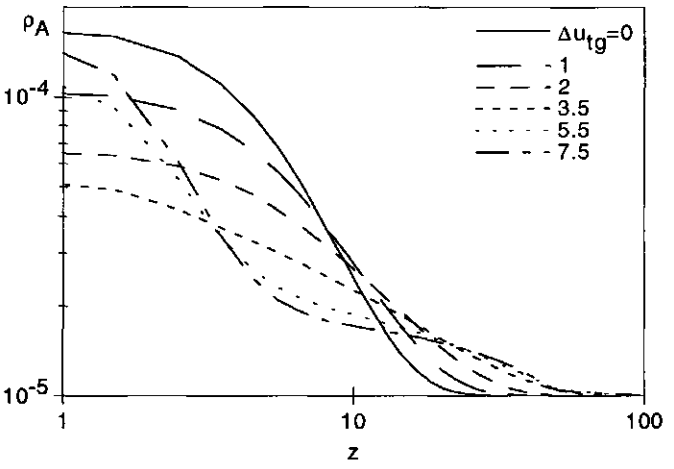

FIGURE 1.7. Reduced density profiles of A_{100} for $\xi = 4$ at different values of Δu_{tg}, corresponding to $q_\infty = 1.5, 2.6, 5.8, 23, 160, 1200$.

the symmetry of the system, it is sufficient to show only the positive part of the z-axis. Clearly, the transition from a semi-flexible to rodlike conformation of the polymer chain is reflected in these profiles. One observes that by increasing the chain stiffness, the polymer initially penetrates more into the solution, whereas ρ_A decreases near the interface. However, when the chains become rodlike, the density at $z = 0$ increases again, indicating alignment with the interface. The small fraction of rodlike chains that extend into the solution must do so over their full length. The decreases of the density at intermediate distance from the interface for rodlike chains also implies alignment.

To visualise the penetration of the polymer into the solution, $\rho_A - \rho_A^b$ is plotted in fig. 1.8 as a function of z^2. Both flexible and semi-flexible objects show a more or less exponential decrease of the excess reduced density with the square of the distance from the interface. This indicates a Gaussian distribution of the polymer around the C–D phase boundary. Clearly, the reduced density profiles for the stiffer polymers ($\Delta u_{tg} = 5.5$ and $\Delta u_{tg} = 7.5$) differ only slightly from each other, which indicates that the conformation of the molecules must be similar. This is what we expected, because in both cases $q_\infty > N$, which means we are dealing with stiff polymers, where the one characterised by $\Delta u_{tg} = 7.5$ (i.e. $q_\infty = 1200$) can be regarded as a rod. The kink in the reduced density profile for these two stiff polymers at $z \approx 50$ originates from the fact that modelling rodlike molecules on a lattice introduces artifacts. In this case, the use of a RIS scheme on a tetrahedral lattice allows six orientations for a rod: one parallel to the interface, one perpendicular to it, and four making an angle $\Phi = (\pi - \theta)/2$, where θ is the tetrahedral bond angle. The kink presumably originates from the latter four possible orientations. This conjecture is confirmed by similar calculations (not shown) carried out on a cubic lattice and using second-order Markoff statistics. In

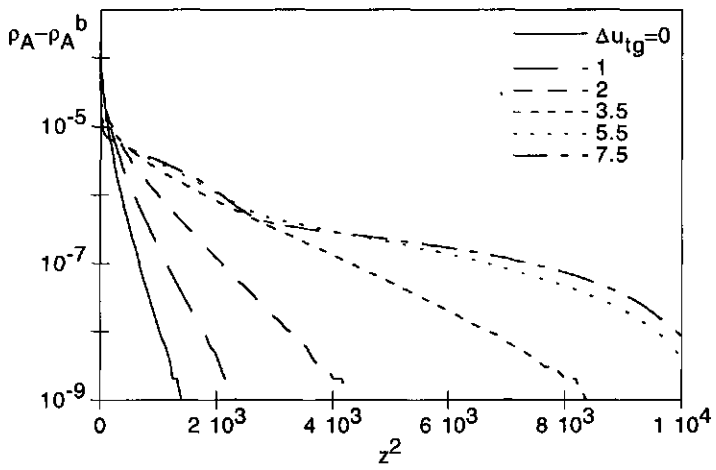

FIGURE 1.8. Reduced density profiles of A_{100} compared to the bulk reduced density. Data as in fig. 1.7.

that case such a kink does not show up due to the absence of orientations other than perpendicular and parallel to the interface.

The impact of the observed phenomena on the ongoing discussion about the question which molecule is more surface active in a mixture of flexible and stiff polymers [1–3] should be clear. In the Henry regime, as studied here, the adsorption in a mixture of two types of polymer, differing in stiffness only, is an additive property. From fig. 1.3 we conclude that decreasing the interfacial width will eventually favour the adsorption of the stiff polymer over a flexible one. However, figs. 1.3–1.6 make clear that the chain-length dependence on this preferential adsorption behaviour plays an important role. It is evident that only rodlike polymers of sufficient length at a given interfacial width will show higher adsorbed amounts than their flexible counterpart. So, one can imagine that in a system where several types of polymer (only differing in chain stiffness) are present, the precise associated length scales will be of major importance. This is the primary reason that the observations made in literature about preferential adsorption in such systems are sometimes contradicting [1–3]. We expect that preferential adsorption of sufficiently long rodlike polymer chains will occur at both sharp and smooth interfaces. Short rodlike polymers will only adsorb preferentially at sharp interfaces.

1.4. CONCLUSIONS

We have shown that the adsorption of semi-flexible polymers onto a liquid–liquid interface is strongly influenced by the competition between the different length scales in the system. Increasing the stiffness of a polymer chain gives rise to a minimum in the adsorbed amount at a certain persistence length. This phenomenon originates from the transition of the polymer from flexible to rodlike, but also depends on the width of the interfacial region and the chain length. This observation is also of importance for

preferential adsorption problems, where one is interested in whether a stiff or a flexible polymer is more likely to adsorb. We showed that if only one type of polymer is present, the adsorbed amount is very sensitive to different length parameters. This leads to the key conclusion that especially the interfacial width should be taken into account when studying adsorption of polymers with variable flexibility (or stiffness).

APPENDIX 1.A. MEAN-FIELD ISING MODEL

To access the properties of a binary mixture we start from an Ising model. We choose the local composition variable $s_i = 0, 1$ for a site occupied by either C or D, respectively. A composition profile is determined by averaging over this variable, thus the local reduced density of D is given by

$$\rho_i = \langle s_i \rangle. \tag{1.A.1}$$

If we only consider two-body interactions between the components, the exact Hamiltonian can be written as a function of the local composition variable s_i:

$$\mathcal{H} = \frac{1}{2} \sum_{ij} J_{ij} s_i (1 - s_j), \tag{1.A.2}$$

where J_{ij} is the net interaction between the C and D component. Due to the coupling between the sites, the partition function of this Hamiltonian is difficult to evaluate. As a model system we choose one which only depends on single-site variables. The model Hamiltonian can then be written in terms of the model parameters β_i

$$\mathcal{H}_0 = k_B T \sum_i \beta_i s_i. \tag{1.A.3}$$

The least upper bound to the exact free energy $\mathcal{F}$ is found by minimising F from eq. (1.2.4) with respect to the parameters β_i. This upper bound is also the best estimate in the variational approach. The integration over phase space, $\int \mathrm{d}\Lambda$, is now given by $\prod_i \sum_{\{s_i\}}$, where $\{s_i\}$ denotes the set of possible values for s_i. Because of boundary conditions, the locally average compositions and, hence, β_i may vary in space. We are interested in a binary system beyond its critical point, where an interface exists, so that such a spatial variation does indeed occur.

For the free energy and for the partition function of the model system we may write

$$F_0 = -k_B T \ln Z_0, \qquad Z_0 = \prod_i \sum_{\{s_i\}} e^{-\beta_i s_i} = \prod_i \frac{1}{1 - \rho_i}, \tag{1.A.4}$$

with $\rho_i = (1 + e^{\beta_i})^{-1}$. Averaging s_i with respect to P_0 results in

$$\langle s_i \rangle_0 = \frac{\sum_{\{s_i\}} s_i e^{-\beta_i s_i}}{\sum_{\{s_i\}} e^{-\beta_i s_i}} = \rho_i. \tag{1.A.5}$$

The variable ρ will be used to describe the reduced density profile of our system. It is easily shown that

$$\langle \mathcal{H} - \mathcal{H}_0 \rangle = \frac{1}{2} \sum_{ij} J_{ij} \rho_i (1 - \rho_j) - \sum_i \beta_i \rho_i. \tag{1.A.6}$$

Substituting eqs. (1.A.4) and (1.A.6) in eq. (1.2.4) gives us the upper bound of the free energy of the system

$$F = k_B T \sum_i \left((1 - \rho_i) \ln(1 - \rho_i) + \rho_i \ln \rho_i \right) + \frac{1}{2} \sum_{ij} J_{ij} \rho_i (1 - \rho_i). \tag{1.A.7}$$

This equation is the generalisation of the free energy of a homogeneous system in the random mixing approximation, i.e. the composition variable can vary in space. The composition variables ρ_i can now be regarded as the variational parameters to minimise F with fixed overall composition. In fact one minimises $G = F - \sum_i \mu \rho_i$. In our system an interface is present, which implies that ρ_i varies in space. Minimisation is most effectively done in the continuum limit since this will lead to differential equations instead of finite difference equations.

Taking the continuum limit of eq. (1.A.7) is done by noting that

$$J_{ij} \rho_i (1 - \rho_j) = \frac{1}{2} J_{ij} \left((\rho_i - \rho_j)^2 - \rho_i^2 - \rho_j^2 + 2\rho_i \right). \tag{1.A.8}$$

We will change to a notation for a free energy per unit volume, which allows us to convert $\rho_i - \rho_j$ to a gradient. We only take into account nearest-neighbour interactions, i.e. J_{ij} is only non-zero if site i and j are adjacent. Doing this, we may write

$$(\rho_i - \rho_j) \mapsto b \nabla \rho, \tag{1.A.9}$$

where b is the nearest-neighbour distance. Obviously, $\rho_i \mapsto \rho(\mathbf{r})$, which gives the continuum version of eq. (1.A.7)

$$F = \int \mathrm{d}\mathbf{r} \left(f_0(\rho(\mathbf{r})) + \frac{1}{2} B |\nabla \rho(\mathbf{r})|^2 \right), \tag{1.A.10}$$

where $f_0(\rho)$ is defined in eq. (1.A.11) and $B = 2\lambda_1 \chi k_B T / b$. We choose to use the Flory-Huggins interaction parameter, here defined as $\chi = \frac{1}{2k_B T} \sum_j J_{ij}$, $\forall i$. The parameter λ_1 originates from the type of underlying lattice, and also appears in the self-consistent-field approach. It accounts for the relative number of nearest neighbours of a segment in the direction of the reduced density gradient. For a tetrahedral lattice $\lambda_1 = 1/4$. Equation (1.A.10) is also known as the square gradient approach, which was already used by Van der Waals to describe the liquid–vapour interface [10]. However, it were Cahn and Hilliard [11] who made this method "popular". The local part of the free energy density is given by

$$f_0(\rho) = \frac{k_B T}{b^3} \left(\rho \ln \rho + (1 - \rho) \ln(1 - \rho) + \chi \rho (1 - \rho) \right). \tag{1.A.11}$$

We now have the free energy as a functional of the local, average composition. We can find the spatial variation in this by minimising F with respect to $\rho(\mathbf{r})$ with the

appropriate boundary conditions. Unfortunately, using eq. (1.A.11) there is no analytical solution. However, near the critical point ($\rho = 1/2$), one can expand f_0 about $\Psi = \rho - 1/2$, which gives

$$f_0 \approx \frac{k_B T}{b^3}\left(2\Psi^2 + \frac{4\Psi^4}{3} - \ln 2 + \chi\left(\frac{1}{4} - \Psi^2\right)\right). \tag{1.A.12}$$

This approach is known as the Ginzburg-Landau expansion of the free energy. Using this approximation, we can write for the Helmholtz free energy

$$F = \int \mathrm{d}\mathbf{r}\left(-\frac{\epsilon}{2}\Psi^2 + \frac{c}{4}\Psi^4 + \frac{B}{2}|\nabla\Psi|^2\right), \tag{1.A.13}$$

where constant terms in the integral are dropped, because they are irrelevant in finding the minimum of F. Furthermore, we apply the constraint that the total composition remains unchanged (i.e. $\int \rho(\mathbf{r})$ is fixed). The coefficients in eq. (1.A.13) are given by $\epsilon = (2\chi - 4)k_B T/b^3$ and $c = 16 k_B T/(3b^3)$.

We look for the minimisation of F for a system with an interface, such that

$$\Psi \to \pm\Psi_0 \quad \text{if } z \to \pm\infty. \tag{1.A.14}$$

To this end, we apply calculus of variations [12] that minimises the functional

$$F = \int \mathrm{d}\mathbf{r} f(\Psi, \nabla\Psi) \tag{1.A.15}$$

with respect to all possible variations of $\Psi(\mathbf{r})$. The function f which minimises F is given in Einstein notation by

$$\frac{\partial F}{\partial \Psi(\mathbf{r})} = \frac{\partial f}{\partial \Psi} - \frac{\partial}{\partial r_i}\frac{\partial f}{\partial \Psi_{r_i}} = 0, \tag{1.A.16}$$

where $\Psi_{r_i} = \partial\Psi/\partial r_i$. This results in

$$-\epsilon\Psi + c\Psi^3 - B\nabla^2\Psi = 0 \tag{1.A.17}$$

with the appropriate boundary conditions. Assuming the system to have its equilibrium bulk values far away from the interface, it is easily seen that these composition values are given by

$$\Psi \to \pm\Psi_0 = \pm\sqrt{\frac{\epsilon}{c}}. \tag{1.A.18}$$

In the present system, a one-dimensional concentration variation $\Psi(z)$ is likely, and $\mathrm{d}\Psi/\mathrm{d}z = 0$ at $z \to \pm\infty$. The solution of eq. (1.A.17) is then given by

$$\Psi(z) = \sqrt{\frac{\epsilon}{c}}\tanh\frac{z}{\xi}, \tag{1.A.19}$$

where the interfacial width, or bulk correlation length, is given by

$$\xi = \sqrt{\frac{2B}{\epsilon}} = b\sqrt{\frac{2\lambda_1\chi}{\chi - 2}}. \tag{1.A.20}$$

APPENDIX 1.B. CHAIN DIMENSIONS WITHIN THE ROTATIONAL ISOMERIC STATE MODEL

We depict a homopolymer as a chain of L bonds with identical bond lengths b and bond angles θ between bond vectors $\mathbf{r}_i$ and $\mathbf{r}_{i+1}$. We take the rotation angles ϕ_i as internal coordinates, where we we denote $\{\phi_L\} = \phi_1, \phi_2, \ldots, \phi_L$. The configurational partition function is written as

$$Z = \int \mathrm{d}\{\phi_L\} \exp\left(-\frac{U(\{\phi_L\})}{k_\mathrm{B}T}\right), \tag{1.B.1}$$

where U is the energy, strictly the potential of mean force, of internal rotation. The crux of the problem is to express $\mathbf{r}_i \cdot \mathbf{r}_j$ in terms of $\{\phi_L\}$. The matrix formalism, first suggested by Eyring [13, 14], can be used for this purpose.

Every bond vector is linked to a Cartesian coordinate system, where the positive direction of the x_j axis coincides with $\mathbf{r}_j$. The positive direction of the y_j axis makes an acute angle with $\mathbf{r}_{j-1}$ and is in the same plane as $\mathbf{r}_j$ and $\mathbf{r}_{j-1}$. The z_j axis is chosen such that it forms a right-handed coordinate system with the x_j and y_j axes. The rotation angle ϕ_j about $\mathbf{r}_{j-1}$ is defined by the angle between the two planes containing $\mathbf{r}_{j-2}$ and $\mathbf{r}_{j-1}$, and $\mathbf{r}_{j-1}$ and $\mathbf{r}_j$, respectively. When $\mathbf{r}_{j-2}$ and $\mathbf{r}_j$ are in the *trans* position with respect to each other, $\phi_j = 0$, and it takes positive values when $\mathbf{r}_j$ lies in the positive range of the z_{j-1} axis. To transform the jth coordinate system into the $(j-1)$th one, one uses the orthogonal matrix

$$\mathbf{A}_j = \begin{pmatrix} -\cos\theta & \sin\theta & 0 \\ \sin\theta\cos\phi_j & \cos\theta\cos\phi_j & \sin\phi_j \\ \sin\theta\sin\phi_j & \cos\theta\sin\phi_j & -\cos\phi_j \end{pmatrix}. \tag{1.B.2}$$

The bond vector $\mathbf{r}_j$ is represented in the $(j-1)$th coordinate system by $\mathbf{A}_j\mathbf{b}$, where $\mathbf{b}$ denotes the column vector $(b\,0\,0)$ representing $\mathbf{r}_j$ in its own coordinate system. This procedure can be repeated to arrive at a representation in the ith coordinate system. The average of the scalar product of two bond vectors can be written as

$$\langle \mathbf{r}_i \cdot \mathbf{r}_j \rangle = \mathbf{b}^\mathrm{T} \left\langle \prod_{k=1+i}^{j} \mathbf{A}_k \right\rangle \mathbf{b}. \tag{1.B.3}$$

With the aid of eq. (1.B.1) the average on the right-hand side is given by

$$\left\langle \prod_{k=1+i}^{j} \mathbf{A}_k \right\rangle = Z^{-1} \int \mathrm{d}\{\phi_L\} \left(\exp\left(-\frac{U(\{\phi_L\})}{k_\mathrm{B}T}\right) \prod_{k=1+i}^{j} \mathbf{A}_k \right). \tag{1.B.4}$$

The problem now reduces to finding a suitable form for the energy U. It should enables us to introduce chain stiffness and should also be useful in the self-consistent-field calculations.

A realistic model includes first and second neighbour interactions. This is achieved by writing the energy as

$$U(\{\phi_L\}) = \sum_{i=1}^{L} u_{1i}(\phi_i) + \sum_{i=1}^{L} u_{2i}(\phi_i, \phi_{i+1}). \tag{1.B.5}$$

It is convenient to discretise the energy in order to simplify calculations. A suitable approximation for this purpose is the rotational-isomeric state model, where ϕ_i can only take a discrete number of fixed values, which we will denote as $\phi_i^{(k)}$ $(k = 1, 2, \ldots, \kappa)$. These rotational angles correspond to the local minima of U. Keeping in mind the lattice theory which we use, a 3-state model is obvious. We will consider three available states, T (*trans*, $\phi^{(1)} = 0$), G (*gauche*, $\phi^{(2)} = 2\pi/3$), and G' (another *gauche*, $\phi^{(3)} = -2\pi/3$). With this approximation we can rewrite the partition function of eq. (1.B.1) as

$$Z = \sum_{\{\phi_L\}} \prod_{i=1}^{L} p(\phi_i, \phi_{i+1}) \tag{1.B.6}$$

where

$$p(\phi_i, \phi_{i+1}) = \exp\left(-\frac{u_1(\phi_i) + u_2(\phi_i, \phi_{i+1})}{k_B T}\right). \tag{1.B.7}$$

This approach requires a value for ϕ_{L+1}, which we will assume to be ϕ_1. To tackle the present problem elegantly we introduce a 3×3 matrix $\mathbf{p}$ which is represented by

$$p_{kl} = p(\phi_i^{(k)}, \phi_{i+1}^{(l)}), \tag{1.B.8}$$

where p_{kl} is independent of i. Diagonalisation of $\mathbf{p}$ is done by $\mathbf{\Lambda}(\lambda_i) = \mathbf{Q}^{-1}\mathbf{p}\mathbf{Q}$, where λ_i are the eigenvalues of $\mathbf{p}$. Equation (1.B.6) simplifies to

$$\begin{aligned} Z &= \operatorname{trace} \mathbf{p}^L = \sum_{i=1}^{3} \lambda_i^L \\ &\approx \lambda^L \qquad \text{(for large } L\text{)}, \end{aligned} \tag{1.B.9}$$

where λ is the largest eigenvalue. Along the same lines we can express the average of a product of functions $g_i(\phi_i)$ as follows

$$\begin{aligned} \left\langle \prod_{k=i+1}^{j} g_k(\phi_k) \right\rangle &= Z^{-1} \sum_{\{\phi_L\}} \left(\prod_{k=i+1}^{j} g_k(\phi_k) \right) \left(\prod_{i=1}^{L} p(\phi_i, \phi_{i+1}) \right) \\ &= Z^{-1} \operatorname{trace} \mathbf{g}_{i+1} \left(\prod_{k=i+2}^{j} \mathbf{p}\mathbf{g}_k \right) \mathbf{p}^{L-(j-i-1)} \\ &\approx \mathbf{y}\mathbf{g}_{i+1} \left(\prod_{k=i+2}^{j} \lambda^{-1}\mathbf{p}\mathbf{g}_k \right) \mathbf{x} \qquad \text{(for large } L\text{)}, \end{aligned} \tag{1.B.10}$$

where $\mathbf{g}_i$ is the diagonal matrix with elements $g_i(\phi^{(k)})$, and $\mathbf{x}$ and $\mathbf{y}$ are normalised right-hand and left-hand eigenvectors of $\mathbf{p}$, respectively, i.e.

$$\mathbf{p}\mathbf{x} = \lambda\mathbf{x}, \qquad \mathbf{y}\mathbf{p} = \lambda\mathbf{y}, \qquad \mathbf{y}\mathbf{x} = 1. \tag{1.B.11}$$

We are interested in the element A_{rs} of the product of transformation matrices $\mathbf{A}_k$, which is of the form $g_{i+1} \dots g_j$. Using eq. (1.B.10) we obtain

$$\langle A_{rs} \rangle = \mathbf{y} \sum_t \cdots \sum_v \mathbf{a}_{rt}(\lambda^{-1}\mathbf{pa}_{tu}) \dots (\lambda^{-1}\mathbf{pa}_{vs})\mathbf{x}, \tag{1.B.12}$$

where $\mathbf{a}_{ij}$ represents the diagonal matrix with diagonal elements $a_{ij}(\phi^{(k)})$ with $a_{ij}(\phi)$ being the elements of $\mathbf{A}$. In short-hand notation eq. (1.B.12) reads

$$\left\langle \prod_{k=i+1}^{j} \mathbf{A}_k \right\rangle = \mathbf{YTS}^{j-i-1}\mathbf{X} \tag{1.B.13}$$

with

$$\mathbf{S} = \lambda^{-1}\mathbf{PT}, \tag{1.B.14}$$

where the "elements" $\mathbf{a}_{ij}$ constitute the matrix $\mathbf{T}$, resulting in a 9×9 matrix. The matrices $\mathbf{P}$, $\mathbf{X}$, and $\mathbf{Y}$ are defined as the direct products

$$\mathbf{P} = \mathbf{p} \times \mathbf{I}_3, \qquad \mathbf{X} = \mathbf{x} \times \mathbf{I}_3, \qquad \mathbf{Y} = \mathbf{y} \times \mathbf{I}_3, \tag{1.B.15}$$

where $\mathbf{I}_s$ denotes a $s \times s$ unit matrix. Combination of eqs. (1.B.13), (1.B.3), and (1.2.16) leads to the following expression for the end-to-end distance

$$\langle R^2 \rangle = Lb^2 \left(1 + 2\mathbf{e}^{\mathrm{T}}\mathbf{YT}(\mathbf{I}_9 - \mathbf{S})^{-1}\mathbf{Xe}\right) \qquad \text{(for large } L\text{)} \tag{1.B.16}$$

with $\mathbf{e} = (1\,0\,0)$ the unit bond vector. This expression was first derived by Lifson [15] and Nagai [16], independently. Along the same lines, using eq. (1.2.17), the expression for the persistence length reads

$$q = b\left(1 + \mathbf{e}^{\mathrm{T}}\mathbf{YT}(\mathbf{I}_9 - \mathbf{S})^{-1}\mathbf{Xe}\right) \qquad \text{(for large } L\text{)}. \tag{1.B.17}$$

The last step before we can calculate q and $\langle R^2 \rangle$ is to write $\mathbf{p}$ from eq. (1.B.8) in explicit form and take a value for the bond angle θ. The latter is conveniently chosen as the tetrahedral angle, for which $\cos\theta = -1/3$. We choose the potential $u_1(\phi^{(1)})$ in the *trans* state as the zero of energy, and assume the following statistical weights for the different conformations: 1 (T), ω (G, G'), and 1 $(TT, TG, TG', GT, G'T, GG, G'G', GG', G'G)$. With these definitions the matrix can be written as

$$\mathbf{p} = \begin{pmatrix} 1 & 1 & 1 \\ \omega & \omega & \omega \\ \omega & \omega & \omega \end{pmatrix}, \tag{1.B.18}$$

with $\omega = \exp(-\Delta u_{\mathrm{tg}}/k_{\mathrm{B}}T)$, where the energy difference Δu_{tg} between the *trans* and the *gauche* state is the same as the one introduced in section 1.2.3. It should be noted that these assumptions neglect the so-called pentane effect [17, 18], which is in accordance with the present implementation of the RIS model in the SF SCF theory. Substitution of this explicit form of $\mathbf{p}$ into eqs. (1.B.16) and (1.B.17) leads to surprisingly simple equations for the end-to-end distance and the persistence length of relatively long

polymers:

$$\langle R^2 \rangle_\infty = Lb^2 \frac{2\omega + 4}{3\omega}, \tag{1.B.19}$$

$$q_\infty = b \frac{5\omega + 4}{6\omega}. \tag{1.B.20}$$

REFERENCES

[1] A. Yethiraj, S. Kumar, A. Hariharan, and K. S. Schweizer. Surface segregation in polymer blends due to stiffness disparity. *J Chem Phys*, 100:4691–4694, 1994.

[2] S. K. Kumar, A. Yethiraj, K. S. Schweizer, and F. A. M. Leermakers. The effects of local stiffness disparity on the surface segregation from binary polymer blends. *J Chem Phys*, 103:10332–10346, 1995.

[3] D. T. Wu, G. H. Fredrickson, and J. P. Carton. Surface segregation in conformationally asymmetric polymer blends: incompressibility and boundary conditions. *J Chem Phys*, 104:6387–6397, 1996.

[4] J. P. Hansen and I. R. McDonald. *Theory of simple liquids*. Academic Press, New York, 1985.

[5] S. A. Safran. *Statistical thermodynamics of surfaces, interfaces, and membranes*. Addison-Wesley, Reading, 1994.

[6] J. M. H. M. Scheutjens and G. J. Fleer. Statistical theory of the adsorption of interacting chain molecules. I. Partition function, segment density distribution and adsorption isotherms. *J Phys Chem*, 83:1619–1635, 1979.

[7] J. M. H. M. Scheutjens and G. J. Fleer. Statistical theory of the adsorption of interacting chain molecules. II. Train, loop, and tail size distribution. *J Phys Chem*, 84:178–190, 1980.

[8] F. A. M. Leermakers and J. M. H. M. Scheutjens. Statistical thermodynamics of associated colloids. I. Lipid bilayer membranes. *J Chem Phys*, 89:3264–3274, 1988.

[9] H. Yamakawa. *Modern theory of polymer solutions*. Harper & Row, New York, 1971.

[10] J. D. van der Waals. Thermodynamische theorie der capillariteit in de onderstelling van continue dichtheidsverandering. *Verhand Kon Akad v Wetensch (1e Sectie)*, 1(8):1–56, 1893.

[11] J. W. Cahn and J. E. Hilliard. Free energy of a nonuniform system. I. Interfacial free energy. *J Chem Phys*, 28:258–267, 1958.

[12] G. Arfken. *Mathematical methods for physicists*. Academic Press, New York, 1985.

[13] H. Eyring. The resultant electric moment of complex molecules. *Phys Rev*, 39:746–748, 1932.

[14] F. T. Wall. Statistical lengths of rubber-like hydrocarbon molecules. *J Chem Phys*, 11:67–71, 1943.

[15] S. Lifson. Neighbor interactions and internal rotations in polymer molecules. III. Statistics of interdependent rotations and their application to the polyethylene molecule. *J Chem Phys*, 30:964–967, 1959.

[16] K. Nagai. Local steric hindrances and configurations of linear macromolecules in solutions. I. Formulation. *J Chem Phys*, 31:1169–1174, 1959.

[17] K. S. Pitzer. The vibration frequencies and thermodynamic functions of long chain hydrocarbons. *J Chem Phys*, 8:711–720, 1940.

[18] W. J. Taylor. Average length and radius of normal paraffin hydrocarbon molecules. *J Chem Phys*, 16:257–267, 1948.

CHAPTER 2

Wetting by polymers of a liquid–liquid interface: effects of short-range interactions and of chain stiffness

ABSTRACT

The behaviour of both flexible and semi-flexible polymers near a liquid–liquid interface is investigated with the aid of the self-consistent-field theory as developed by Scheutjens and Fleer. A ternary system ($A/B_N/C$) is studied near the wetting transition. In a symmetric system, i.e. $\chi_{AB} = \chi_{BC} = \chi$, a change in the interaction parameter χ introduces a wetting transition. The ratio of the interfacial width ξ of the binary A/C system and the coil size of the polymer determines the order of this transition. Beyond a certain chain length N_c (at fixed ξ) the wetting transition is of first order, whereas it is of second order for $N < N_c$. The characteristics of the prewetting line, including the prewetting critical point, are discussed in some detail. The non-trivial N-dependence of the position of this critical point is analysed in terms of a crude thermodynamic model. For a semi-flexible polymer an increase of the chain stiffness at a certain value of χ is sufficient to introduce a wetting transition.

2.1. INTRODUCTION

In the preceding chapter we have discussed the adsorption of a semi-flexible polymer at a liquid–liquid interface. There, we restricted ourselves to a situation where the polymer was soluble in both liquid phases, and we only considered small amounts of polymer in the system (Gibbs layers). However, good solvents for polymers are not common, and most frequently the polymer is only marginally soluble. As a consequence, the amounts of polymer, e.g. in industrially relevant multi-phase systems, often exceed the solubility limit in one or both of the constituting phases. It is therefore worthwhile to investigate the behaviour of semi-flexible polymers in a multi-phase system at less ideal conditions. If one adds polymer to a two-phase system of monomeric components, one can expect to arrive at a point where a third, polymer-rich, phase emerges. This phase will preferably appear at the interface between the two liquids (see chapter 1). This phenomenon is generally denoted as *wetting*. Before considering the polymeric system, it is worth while to review some basic features of wetting. We choose to do this from a physical adsorption perspective. We base this introduction on a number of excellent reviews on this subject [1–3].

2.1.1. Contact angles and surface tension

Consider a small liquid droplet at the interface of two other liquid phases. The droplet will adopt a lenslike shape as depicted in fig. 2.1. We distinguish two different

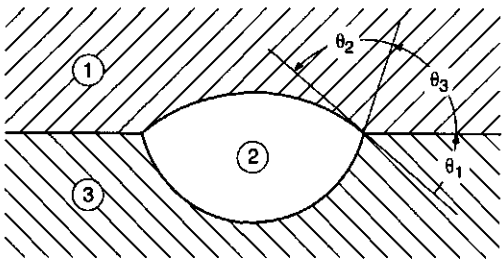

FIGURE 2.1. A three-phase system where phase 2 partially wets the interface between the two other phases. The lens-shaped drop is characterised by the three contact angles as indicated, with $\theta_1 + \theta_2 + \theta_3 = \pi$.

equilibrium states: partial wetting with $\theta_1 + \theta_3 > 0$, and complete wetting for $\theta_1 + \theta_3 = 0$. The contact angles can be fully defined in terms of thermodynamic parameters. The Young equation, originally derived from mechanical arguments for wetting in the presence of a solid surface, is replaced by a set of three equations for a drop at a liquid–liquid interface:

$$\gamma_{13} = \gamma_{12}\cos\theta_1 + \gamma_{23}\cos\theta_3, \tag{2.1.1a}$$

$$\gamma_{12} = \gamma_{13}\cos\theta_1 + \gamma_{23}\cos\theta_2, \tag{2.1.1b}$$

$$\gamma_{23} = \gamma_{12}\cos\theta_2 + \gamma_{13}\cos\theta_3, \tag{2.1.1c}$$

where γ_{ij} is the interfacial free energy per unit area (or interfacial tension) between phase i and j. From this set of equations one easily arrives at explicit expressions for the contact angles as a function of the interfacial free energies:

$$\cos\theta_1 = \frac{\gamma_{12}^2 + \gamma_{13}^2 - \gamma_{23}^2}{2\gamma_{12}\gamma_{13}}, \tag{2.1.2a}$$

$$\cos\theta_2 = \frac{\gamma_{12}^2 + \gamma_{23}^2 - \gamma_{13}^2}{2\gamma_{12}\gamma_{23}}, \tag{2.1.2b}$$

$$\cos\theta_3 = \frac{\gamma_{13}^2 + \gamma_{23}^2 - \gamma_{12}^2}{2\gamma_{13}\gamma_{23}}. \tag{2.1.2c}$$

2.1.2. The wetting transition

In a system of three fluid phases as depicted in fig. 2.1 one phase sits between the two others either as a lens-shaped drop (*partial wetting*) or as a macroscopically thick film (*complete wetting*). There may exist a certain temperature T_w at which the system switches from one regime to the other. This is the so-called wetting transition temperature. Similar observations can be made for systems where a solid surface is present. To grasp some basic ideas of wetting we first consider a binary system near a solid wall. Below, however, we will apply these ideas also to a system with a liquid–liquid interface. The system will phase separate below a certain critical temperature T_c. We

denote the chemical potential of a component at the coexistence line by μ_0. An appropriate quantity to gain insight into the wetting phenomenon is the excess amount or surface coverage, which in the presence of a solid surface can be defined as

$$\Theta^{\mathrm{exc}}(\mu,T) = \int_0^\infty \mathrm{d}z\,[\rho(z;\mu,T) - \rho(\infty;\mu,T)]\,, \tag{2.1.3}$$

where the solid surface is located at $z = 0$ and ρ is the number density of a component.

A first question that arises, is how the excess amount changes with μ and T near various phase boundaries. Furthermore, one wishes to know what would happen if the interactions within the system are altered. In figs. 2.2(a)–(d) we visualise how $\Theta^{\mathrm{exc}}(\mu,T)$ may vary along typical cuts in the phase diagram. Comparing figs. 2.2(a)–(d) with 2.2(e)–(h) shows the structural change of $\Theta^{\mathrm{exc}}(\mu,T)$ which might occur when changing the interaction potentials. Figure 2.2(a) shows how the coexistence line is approached from the low-density side along two different paths. In both cases Θ^{exc} increases (see fig. 2.2(b)). However, $\Theta^{\mathrm{exc}}(\mu_0^-, T < T_{\mathrm{w}})$ remains finite, whereas $\Theta^{\mathrm{exc}}(\mu_0^-, T \geq T_{\mathrm{w}})$ diverges for $\mu \uparrow \mu_0$. The latter case is usually referred to as *complete wetting*. The former case is called *partial wetting*, i.e. a microscopic phase is in equilibrium with a macroscopic phase (droplet). The question now arises how $\Theta^{\mathrm{exc}}(\mu_0^-, T < T_{\mathrm{w}})$ develops if the temperature is increased. To this end we consider the paths at μ_0^- in figs. 2.2(c) and (e). The *second*-order wetting transition is characterised by a smooth divergence of $\Theta^{\mathrm{exc}}(\mu_0^-, T)$ for $T \to T_{\mathrm{w}}$, as in fig. 2.2(d). The order of the wetting transition depends delicately on the interactions in the system. The wetting transition is of *first* order if $\Theta^{\mathrm{exc}}(\mu_0^-, T)$ jumps from a finite value at T_{w}^- to a macroscopic value at T_{w}^+. This infinite jump at coexistence develops smoothly from finite jumps in the one-phase region (see fig. 2.2(e)–(h)). A finite jump in the one-phase region is usually referred to as prewetting.

2.1.3. Wetting in the presence of polymer chains

In this study we focuss on the wetting behaviour of flexible and semi-flexible polymers in a binary monomeric system within a mean-field approach. We will show that not only the interaction parameters, but also the chain stiffness and chain length have a significant influence on the wetting process. The theoretical approach of this problem is comparable to that applied in the previous chapter on adsorption of semi-flexible polymer chains at a liquid–liquid interface. We apply a theory based on a self-consistent-field approximation by Scheutjens and Fleer [4, 5] and elaborated by Leermakers and Scheutjens [6].

2.2. THEORY AND METHODS

The self-consistent-field theory of Scheutjens and Fleer (SF SCF) was originally developed to describe the equilibrium properties of adsorbing flexible polymer chains at a solid surface. The implementation of the presence of a liquid-liquid interface into this theory is rather straightforward; it simply requires the proper boundary conditions (reflecting at both ends) with a sufficient effective repulsion between the molecular

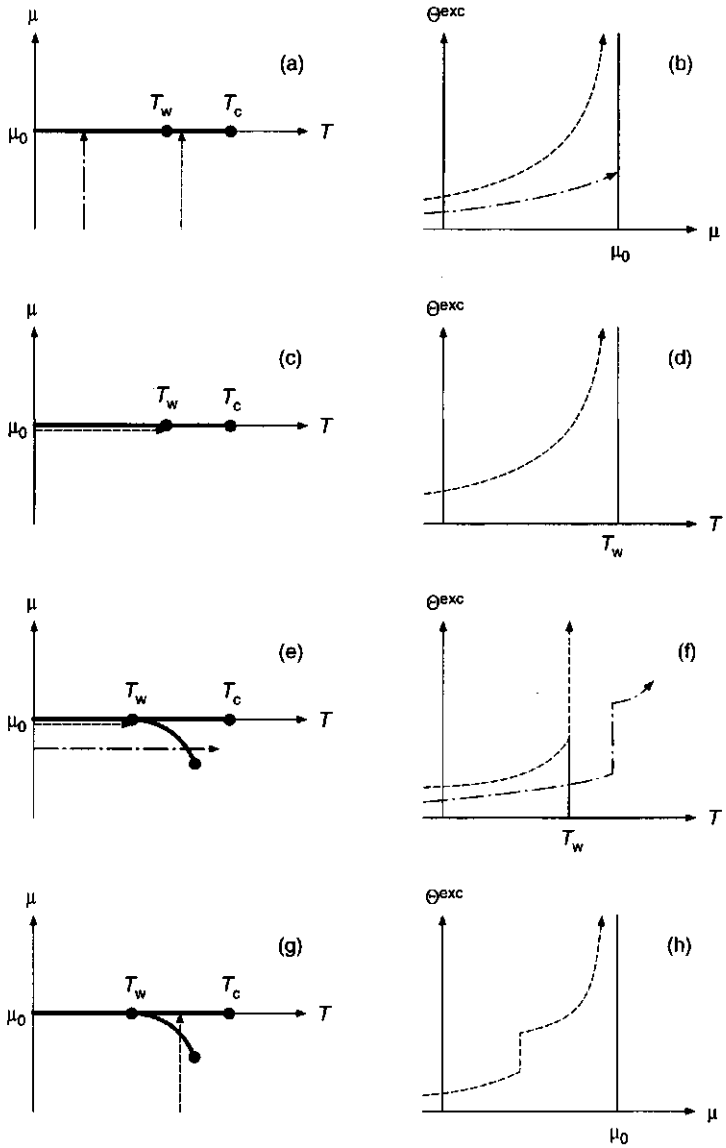

FIGURE 2.2. Excess amount (right panels) along several paths in the bulk phase diagram (left panels) for a binary mixture near a solid wall. The coexistence line ($\mu = \mu_0$, $T \leq T_c$) separating the two phases is the locus of singularities in the bulk free energy. The interfacial free energy has singularities at T_w and along the so-called prewetting line sticking out into the one-phase region as in (e) and (g). The difference between (a)–(d) and (e)–(h) lies in this example solely in the interaction with the solid surface.

components. The implementation of chain stiffness is more involving and requires a higher-order Markoff formalism for the chain statistics. Leermakers and Scheutjens [6] did the latter for the case of associated colloids. A short introduction into the SF SCF theory and into the implementation of chain stiffness is given in chapter 1. For the present study it is important to note that the nearest-neighbour interactions between segments of type x and y are represented by Flory-Huggins interaction parameters χ_{xy}, and that a controllable chain stiffness is achieved by the use of third-order Markoff statistics to describe the chain conformation. The latter means that a rotational isomeric state (RIS) model is used, characterised by an energy difference Δu_{tg} between the *gauche* and the *trans* state, where the *trans* state is chosen as the reference state. With this energy difference one is able to calculate the persistence length of the polymer chain as (see chapter 1)

$$q = b\frac{5\omega + 4}{6\omega} \qquad \text{for large } N, \tag{2.2.1}$$

where b denotes the bond length, N the number of bonds, and $\omega = \exp(-\Delta u_{\mathrm{tg}}/k_{\mathrm{B}}T)$.

The systems under consideration in this study all consist of two monomeric components, A and C, and of a homopolymer B_N. To keep the system characteristics transparent we restrict ourselves to a, from a polymer perspective, symmetric system, i.e. $\chi \equiv \chi_{\mathrm{AB}} = \chi_{\mathrm{BC}}$.

Before discussing the process of wetting, we first consider the bulk phase diagram. To calculate this diagram, we do not need the SF SCF theory for inhomogeneous systems; it suffices to use the classical Flory-Huggins theory. For the three components we can write the Helmholtz (or free) energy per lattice site for a bulk phase as

$$\begin{aligned}\frac{f}{k_{\mathrm{B}}T} = {} & \rho_{\mathrm{A}}\ln\rho_{\mathrm{A}} + \frac{\rho_{\mathrm{B}}}{N}\ln\rho_{\mathrm{B}} + (1-\rho_{\mathrm{A}}-\rho_{\mathrm{B}})\ln(1-\rho_{\mathrm{A}}-\rho_{\mathrm{B}}) \\ & + \chi_{\mathrm{AC}}\rho_{\mathrm{A}}(1-\rho_{\mathrm{A}}-\rho_{\mathrm{B}}) + \chi\rho_{\mathrm{B}}(1-\rho_{\mathrm{B}}).\end{aligned} \tag{2.2.2}$$

For convenience, and to stay in line with chapter 1, we switched to reduced densities, i.e. $\rho b^3 \mapsto \rho$, where b is the size of a lattice site. If we consider a phase-separated system where the volumes of the three phases are large, we can neglect the contribution of the interfaces to the free energy. In that case we may write for the total free energy

$$F = \sum_{j=1}^{3} \frac{V^{(j)}}{b^3} f(\rho_{\mathrm{A}}^{(j)}, \rho_{\mathrm{B}}^{(j)}), \tag{2.2.3}$$

where V is the volume and the superscript (j) identifies the phase. To obtain the composition and volumes of the three phases in equilibrium, one has to minimise the total free energy with the boundary conditions that the total volume remains constant, and that the number of molecules of every type is conserved. This optimisation can be

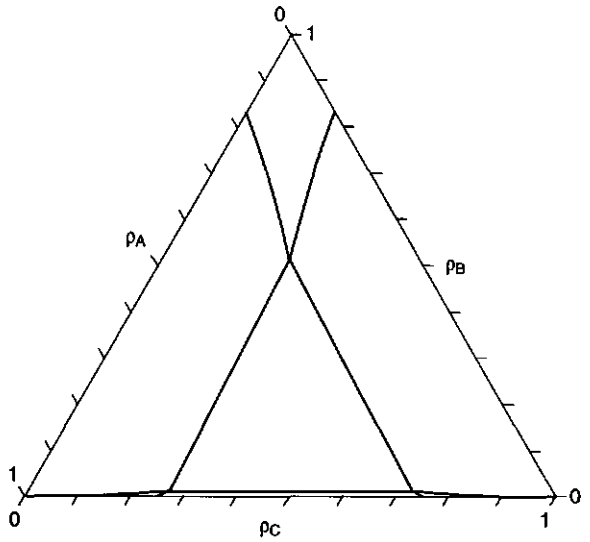

FIGURE 2.3. Ternary phase diagram for a system containing the components A, B_{10}, and C as calculated with the Flory-Huggins lattice theory. The interaction parameters are chosen such that a three-phase region (the central triangle) exists: $\chi_{AC} = 2.2$ and $\chi_{AB} = \chi_{BC} = 1.5$.

carried out using a Lagrange method by introducing the following function

$$g = \sum_{j=1}^{3} \frac{V^{(j)}}{b^3} f(\rho_A^{(j)}, \rho_B^{(j)}) - \mu_A \left(\sum_{j=1}^{3} \frac{V^j}{b^3} \rho_A^{(j)} - n_A \right) - \mu_B \left(\sum_{j=1}^{3} \frac{V^{(j)}}{b^3} \rho_A^{(j)} - n_B \right) + \Pi \left(\sum_{j=1}^{3} V^{(j)} - V \right), \tag{2.2.4}$$

where n_x is the total number of segments of type x. The chemical potentials of component A and B are reflected in the Lagrange parameters μ_A and μ_B, respectively. The parameter coupled to the constant-volume constraint is the osmotic pressure Π. Minimisation can only be carried out numerically. To this end we used a programme developed by Linse [7].

To give an idea about the nature of the ternary phase diagram of the systems under study we calculated the phase-equilibria for the $A/B_{10}/C$ system. Figure 2.3 depicts the phase diagram with $\chi_{AC} = 2.2$ and $\chi = 1.5$. The central triangle corresponds to the three-phase region, necessary for wetting. In fig. 2.4 the effect of lowering χ on the size of the three-phase region is shown. The critical interaction parameter χ_c, below which no three-phase region exists, is approximately equal to (but larger than) that in a two-phase system, which is given by

$$\chi_c = \frac{1}{2}(1 + N^{-1/2})^2, \tag{2.2.5}$$

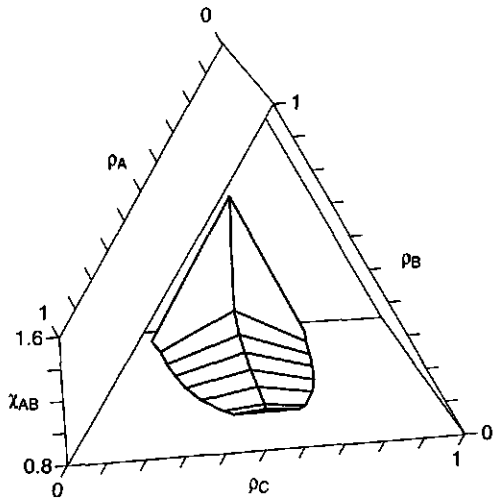

FIGURE 2.4. Change of the three-phase region in the $A/B_{10}/C$ system as a function of the interaction parameter χ_{AB}, with $\chi_{AC} = 2.2$ and $\chi_{BC} = \chi_{AB}$.

which is approximately 0.866 for $N = 10$. This is indeed in correspondence with the numerical calculations visualised in fig. 2.4. It should be noted that when the chain length N is increased the base of the triangle will be much closer to the ρ_C axis in the phase diagram.

The calculations for the inhomogeneous systems, i.e. where interfacial effects are relevant, are performed using the SF SCF theory. The system containing the flexible polymer is situated on a simple cubic lattice with an a priori step probability $\lambda_1 = 1/6$. The chain conformations are generated using first-order Markoff statistics. The conformations of the semi-flexible polymer are created by third-order Markoff statistics, i.e. a RIS model is used. This model implies a tetrahedral lattice for the bond correlations. Therefore, we also used a tetrahedral lattice for the interactions. The one-dimensional gradient has its direction perpendicular to the interface, and thus, there is a mean field in two directions parallel to the interface.

In the systems under study here it is most convenient to work in the canonical (nVT) ensemble. One should bear in mind that if in an SCF model there may exist values of Θ_B^{exc} (or Θ_B) which do not correspond to an equilibrium situation (see figs. 2.2(b) and (h)). This is fully comparable to the so-called Van der Waals loop in liquid–vapour systems. This means that when the number of different molecules in the generated system is fixed, the system will correspond to a point along this loop (or adsorption isotherm).

The systems in this study consist of m parallel lattice layers, and the number of sites per layer is chosen as $l = 1$, so the total number of sites, or reduced volume, is m. The number of layers is chosen large enough, so that no significant finite-size effects occur. The dimensionless excess amount ($\Theta_x^{exc} lb^2 \mapsto \Theta_x^{exc}$) is calculated from the

SF SCF solution by

$$\Theta_x^{\rm exc} = \int_0^{z_{\rm G}} {\rm d}z' \left(\rho_x(z') - \rho_x^{(1)}\right) + \int_{z_{\rm G}}^{m} {\rm d}z' \left(\rho_x(z') - \rho_x^{(3)}\right), \tag{2.2.6}$$

where $\rho_x^{(j)}$ denotes the bulk reduced density of component x in phase j (see fig. 2.1). The reduced distance is defined as $z' \equiv i - 1/2$, where i is the layer number. The Gibbs dividing plane, located at $z_{\rm G}$, is defined by $\Theta_{\rm A}^{\rm exc} = \Theta_{\rm C}^{\rm exc}$. Taking equal amounts of A and C ($\Theta_{\rm A} = \Theta_{\rm C}$) this choice leads to $z_{\rm G} = (m+1)/2$ for the symmetric case studied here. With this in mind we define the reduced distance from the "interface" as $z \equiv i - z_{\rm G}$. Phase separation between the A- and the B-rich phase is ensured by setting the Flory-Huggins parameter $\chi_{\rm AC} = 2.2$, i.e. substantially beyond the critical point.

An important quantity in wetting studies is the excess free energy, i.e. that part of the free energy that can not be attributed to the bulk phases in the system. This part is thus is a further characteristic of the wetting behaviour. As long as no third macroscopic phase is formed, the interfacial tension is simply defined as $\gamma = F^{\rm exc}/(b^2 l)$. When a third phase emerges, i.e. when two interfaces exist, the two interfacial tensions are equal in the symmetric system, and hence may be defined by $\gamma = F^{\rm exc}/(2b^2 l)$. A final useful quantity in this study is the chemical potential, which in the Flory-Huggins theory and within our restrictions to the system is given by

$$\frac{\mu_{\rm B}}{k_{\rm B}T} = \ln \rho_{\rm B} - N \ln(1 - \rho_{\rm A} - \rho_{\rm B}) - N + 1 + \chi(1 - 2\rho_{\rm B}) + N\chi_{\rm AC}\rho_{\rm A} \tag{2.2.7}$$

for component B. For interpreting the wetting phenomena, we need the difference between the chemical potential of a component in a system and that of the same component at the coexistence line, i.e. one is interested in $\mu - \mu_0$. This difference is, for component B, approximated by

$$\mu - \mu_0 = k_{\rm B}T \ln \frac{\rho}{\rho_0}, \tag{2.2.8}$$

where, for convenience, we already omitted the subscript referring to component B. We shall omit this subscript in all molecular properties. In this chapter we only use dimensionless quantities. To this end we introduce the following rescaling

$$\frac{F^{\rm exc}}{l k_{\rm B}T} \mapsto F^{\rm exc}, \quad \frac{\gamma b^2}{k_{\rm B}T} \mapsto \gamma, \quad \frac{\Delta u_{\rm tg}}{k_{\rm B}T} \mapsto \Delta u_{\rm tg}, \quad \frac{\mu}{k_{\rm B}T} \mapsto \mu, \quad \frac{q}{b} \mapsto q. \tag{2.2.9}$$

2.3. RESULTS AND DISCUSSION

2.3.1. Flexible polymer

Polymer–solvent interaction. We start with the wetting behaviour of a flexible polymer B_{100} at a liquid–liquid interface as found by the SF SCF theory, using first-order Markoff statistics. An adsorption isotherm is determined by increasing the total amount Θ of B, , whilst keeping the total volume and the $\Theta_{\rm A}/\Theta_{\rm C}$ ratio constant. Instead of the temperature, we use the interaction parameter $\chi_{\rm AB}$ to scan through the wetting phase diagram. Every point along the isotherm corresponds to an SF SCF solution. This

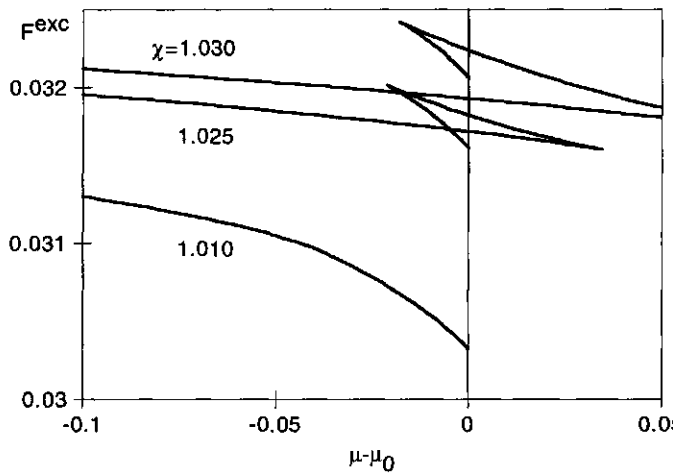

FIGURE 2.5. Excess free energy for the $A/B_{100}/C$ system where B_{100} is a flexible polymer. The curves represent the change in F^{exc} along three adsorption isotherms with $\chi_{AC} = 2.2$. From bottom to top we distinguish typical curves for: complete wetting ($\chi = 1.01$), prewetting ($\chi = 1.025$), and partial wetting ($\chi = 1.03$).

leads to an isotherm which, when in the prewetting or partial-wetting regime, contains a loop as discussed in section 2.2.

Suppose the interaction parameters of a system are such that a prewetting step exists in the adsorption isotherm, i.e, there is a finite jump in the excess amount Θ^{exc} at a certain μ. The chemical potential at which this jump occurs can be deduced from the fact that the two different adsorption layers (1 and 2) are subject to the equilibrium conditions: $\mu^{(1)} = \mu^{(2)}$ and $\gamma^{(1)} = \gamma^{(2)}$. This means that plotting the excess free energy as a function of the chemical potential reveals, from the intersection point, the conditions for the finite jump in Θ^{exc}. Such a plot is given in fig. 2.5, which will be discussed in detail below. In the case of complete wetting F^{exc} is a continuously decreasing function of μ up to $\mu = \mu_0$ where the macroscopic phase is formed. The case of partial wetting requires some more explanation. For this system an infinite jump in Θ^{exc} occurs at $\mu = \mu_0$, which is equivalent to the formation of an adsorbed layer (1) in equilibrium with a droplet (2). In the symmetric system under study, the equilibrium conditions now read: $\mu^{(1)} = \mu^{(2)} = \mu_0$ and $\gamma^{(1)} = 2\gamma^{(2)} \cos\theta$, where $\gamma^{(1)} = \gamma_{13}$, $\gamma^{(2)} = \gamma_{12} = \gamma_{23}$, and $\theta = \theta_1 = \theta_3$ (for the symbols see fig. 2.1). So, from the excess free energies at $\mu = \mu_0$ the contact angle can be determined in the following way

$$\cos\theta = \frac{F^{\text{exc}}_{(1)}}{F^{\text{exc}}_{(2)}}, \tag{2.3.1}$$

where $F^{\text{exc}}_{(1)}$ denotes the excess free energy for the system with an adsorbed layer and $F^{\text{exc}}_{(2)}$ that of the system with a macroscopic layer.

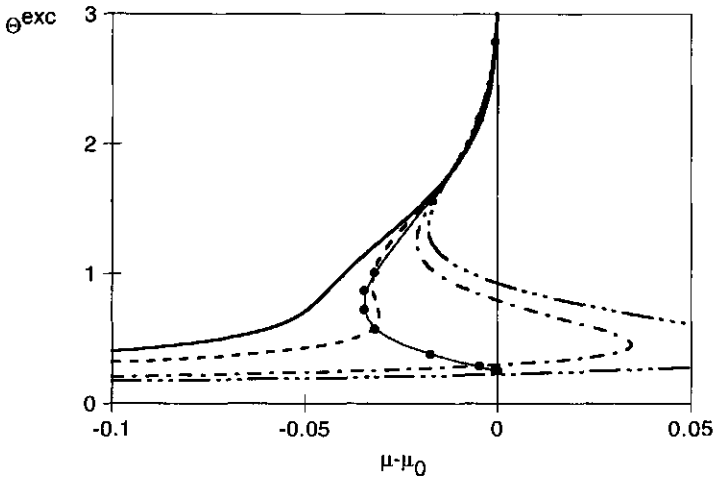

FIGURE 2.6. Adsorption isotherms for the flexible polymer B_{100} in the $A/B_{100}/C$ system with $\chi_{AC} = 2.2$. For the curves from left to right the interaction parameter χ is given by 1.01, 1.015, 1.025, and 1.03, respectively (see also fig. 2.7). The solid line with the filled circles indicates the prewetting region as determined from the adsorption isotherms (not all shown).

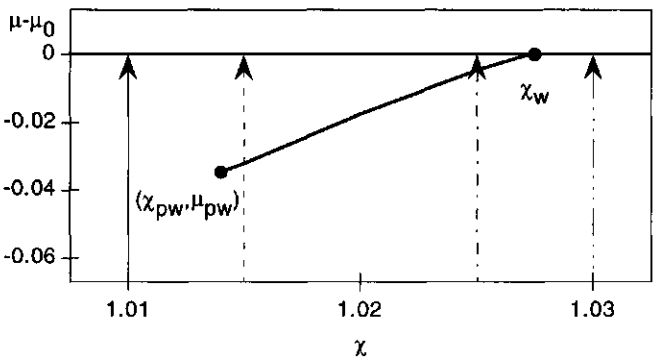

FIGURE 2.7. Wetting phase diagram for the system $A/B_{100}/C$ with a flexible polymer present and $\chi_{AC} = 2.2$. The arrows correspond to the adsorption isotherms shown in fig. 2.6. For further explanation see fig. 2.2 and the text.

With the above in mind it is easy to interpret the μ-dependence of the excess free energy as given in fig. 2.5 for different values of χ. With increasing χ we observe three principally different adsorption isotherms: from a complete wetting isotherm ($\chi = 1.01$) via a prewetting one ($\chi = 1.025$) to a partial wetting one ($\chi = 1.03$). In order to visualise this transition we plot a few typical adsorption isotherms in fig. 2.6. The positions of the finite jumps in Θ^{exc} are also indicated, through a pair of filled circles at the same μ for each jump. One observes that the magnitude of this jump increases

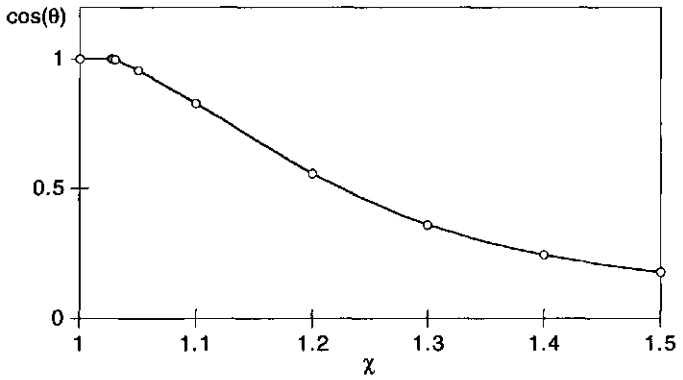

FIGURE 2.8. Contact angle for a B_{100}-rich phase in equilibrium with an A and a C-rich phase (partial wetting). The discontinuity in $\mathrm{d}\cos\theta/\mathrm{d}\chi$ around $\chi = \chi_w \approx 1.0275$ indicates a first-order phase transition.

when it occurs closer to $\mu = \mu_0$ and it diverges at $\mu = \mu_0$. This is similar to the observations made in section 2.1.2 for a solid surface. Clearly, the system undergoes a first-order wetting transition. In line with the introduction of this chapter (fig. 2.2), we plot a wetting phase diagram in fig. 2.7 based on the calculations from figs. 2.5 and 2.6. In this diagram the horizontal line represents the wetting line. Along this line there will be complete wetting for $\chi_c < \chi \leq \chi_w$, where $\chi_c \approx 0.605$ according to eq. (2.2.5) and $\chi_w \approx 1.0275$ as deduced from the SF SCF computations. Beyond χ_w, which we call the wetting interaction parameter, partial wetting will occur. The χ-interval for which a finite jump in the excess amount occurs in the adsorption isotherm is given by $\chi_{pw} < \chi < \chi_w$ where the prewetting interaction parameter $\chi_{pw} = 1.014$ (compare fig. 2.6).

One of the quantities that is experimentally accessible in a 3-phase system is the contact angle. This, of course, means that we should be studying a system in the partial-wetting regime. For the system discussed above, this implies that $\chi > \chi_w$. The contact angle θ, or better $\cos\theta$, is calculated with eq. (2.3.1) from the SF SCF excess free energies. Figure 2.8 shows the decrease of $\cos\theta$ with increasing χ. The discontinuity in the derivative of this function at $\chi \approx 1.0275$ implies that the phase transition is of *first* order. From the figure it can also be seen that a relatively small increase in the interaction between polymer and solvent suffices to cause the polymer-rich droplet to adopt an almost spherical shape. This observation should be no surprise, and can be explained in terms of interfacial tensions. The interfacial tension γ_{13} of an interface with a small amount of polymer deviates only slightly from that of the interface in the binary A/C system without polymer. However, the interfacial tension γ_{12} between the droplet and the A-rich phase depends strongly on the interaction parameter χ. This implies that $\cos\theta$ should indeed decrease rather strongly with increasing χ.

Effect of chain length on the wetting transition. Above we have shown that a simultaneous change of the solubility of a flexible polymer in two monomeric solvents can induce

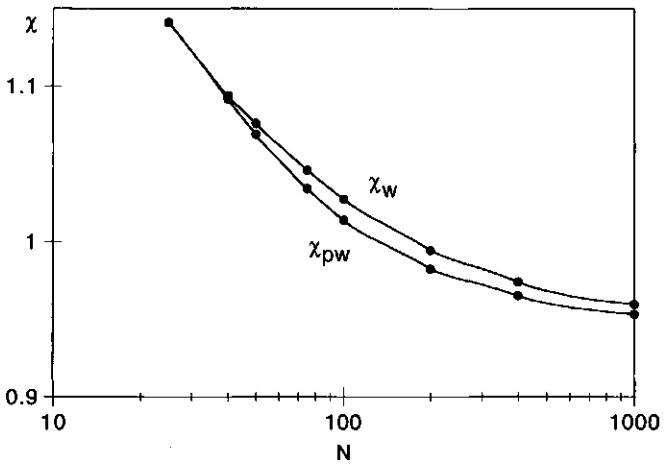

FIGURE 2.9. Wetting and prewetting interaction parameters (χ_w and χ_{pw}, respectively) as a function of the chain length N for the $A/B_N/C$ system with $\chi_{AC} = 2.2$.

a first-order wetting phase transition. Now we take a closer look at the transition itself. One way to do this is to change the polymer in such a way that the critical interaction parameter χ_c changes, by varying the polymer length N (see eq. (2.2.5)). We computed a number of adsorption isotherms for several values of N to find the characteristic points in the corresponding wetting phase diagrams: (χ_w, μ_0) and (χ_{pw}, μ_{pw}), see fig. 2.7.

The N-dependence of the prewetting interaction parameter χ_{pw} and of the wetting interaction parameter χ_w is depicted in fig. 2.9. The observed decrease of χ_w with increasing N is similar to that of the critical bulk interaction parameter χ_c, given by eq. (2.2.5), i.e. $\chi_c = \chi_w + \chi^*$, where χ^* is almost independent of N and is in this case given by $\chi^* \approx 0.423$. The fact that χ^* is almost independent of N can be traced to the weak N-dependence of the entropy loss per polymer segment upon transfer from bulk solution to the interfacial region. The arguments validating this statement are as follows. Within the interfacial region, parts of a polymer chain can freely adopt conformations of typical size ξ, the width of the interface. If we consider the chain to be subdivided in a number of blobs of size ξ, then the number of segments in such a blob is given by $N_\xi \propto \xi^2$. The entropy loss per 'bond' between two blobs can be approximated as $-\ln(2\lambda_1)$ (which is a positive quantity), so that the entropy loss per polymer segment is about

$$\Delta s \propto -\left(\frac{1}{\xi^2} - \frac{1}{N}\right) \ln(2\lambda_1) \qquad \text{for } N > \xi^2. \tag{2.3.2}$$

Clearly, this entropy loss depends only weakly on N for the values of N considered here in the system under study with $\chi_{AC} = 2.2$, which corresponds to $\xi \approx 2.35$.

A key observation is the fact that the prewetting line vanishes if the chain length approaches $N \approx 35$ from above. This is easily seen from fig. 2.10 where we plot the

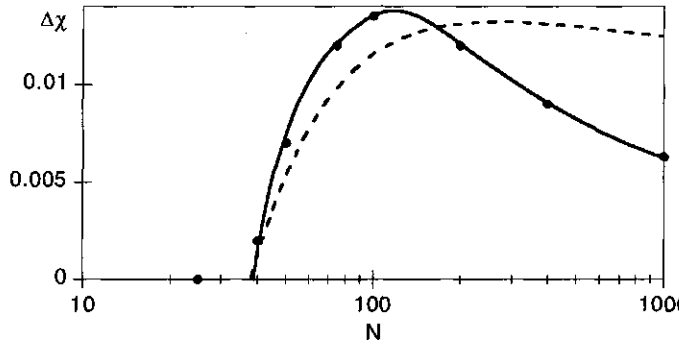

FIGURE 2.10. Location $\Delta\chi = \chi_w - \chi_{pw}$ of the prewetting critical point in the $A/B_N/C$ system with $\chi_{AC} = 2.2$ as a function of chain length. The dotted line indicates an estimate of $\Delta\chi$ based on a crude thermodynamic model as given by eq. (2.3.8). The used parameters are $\rho^* = 0.061$, $k_d = 0.841$, $d^* = 1.84$, $k_d = 13.25$, and $N_c = 38$.

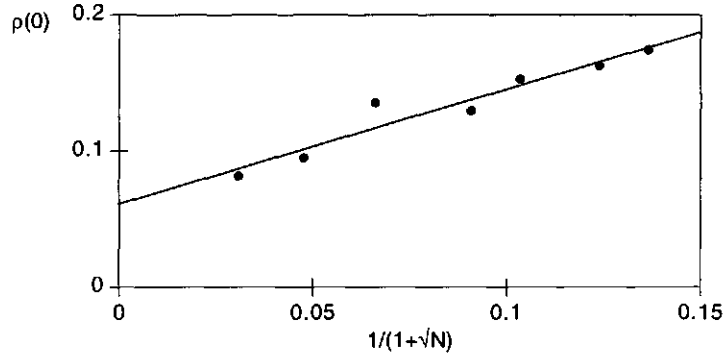

FIGURE 2.11. Reduced density of component B at $z = 0$ for the prewetting critical point as a function of $1/(1 + \sqrt{N})$.

difference $\Delta\chi \equiv \chi_w - \chi_{pw}$, i.e. the difference between the interaction parameter χ at the wetting transition and that at the prewetting critical point as a function of chain length. The vanishing prewetting line implies that the wetting transition becomes of second order for $N \lesssim 35$ under the given circumstances. The change of the order of this wetting transition as a function of N can be understood in terms of the ratio of the interfacial width of the 2-phase system and the coil-size of the polymer. A *first*-order wetting transition is characterised by the fact that a seed is needed to form an additional phase. If the radius of a polymer coil, which is proportional to $\sqrt{N}$, is smaller than the interfacial width, the third phase will form continuously without the need for a seed. This situation is referred to as *second*-order wetting.

At this stage it is worthwhile to pay attention to the extension of the prewetting line into the one-phase region, or more precisely to the prewetting critical point. To

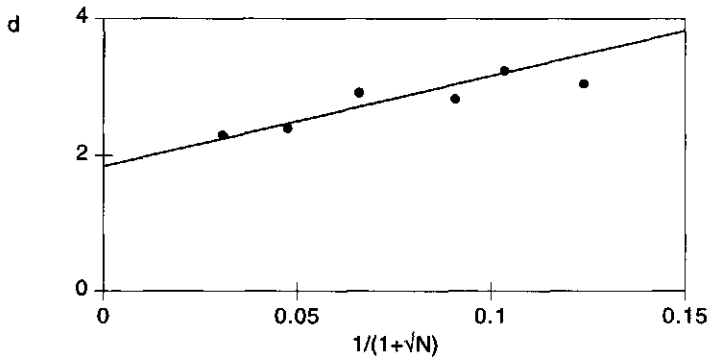

FIGURE 2.12. Width of the density profile at the interface for component B at the prewetting critical point as a function of $1/(1+\sqrt{N})$.

this end we again refer to fig. 2.10, where $\chi_w - \chi_{wp}$ is plotted as a function of N. The most remarkable feature of the prewetting critical point is the maximum in $\Delta\chi(N)$. The occurrence of such a maximum is far from trivial, and at present we are not able to provide a detailed explanation for this behaviour. Instead, we present some thermodynamic considerations which can at least explain why such a maximum could occur.

Consider a system for a certain value of N at its prewetting critical point. In terms of chemical potentials, this point is a distance $\Delta\mu = \mu_0 - \mu_{pw}$ away from the coexistence line. For $\mu_0 - \mu < \Delta\mu$ a finite jump in the adsorption isotherm occurs. At the prewetting critical point the extra negative contribution to the interfacial free energy relative to the system at coexistence, at which point a relatively thick layer is formed, is just balanced by the counteracting force to prevent the formation of such a layer before coexistence:

$$\Delta\chi\Delta\rho\,(1-\Delta\rho) \propto \frac{\Theta^{exc}\Delta\mu}{N}, \tag{2.3.3}$$

where $\Delta\mu$ and $\Delta\chi = \chi_w - \chi_{pw}$ are positive quantities by definition. The reduced density difference, $\Delta\rho = \rho(0) - \rho(\infty)$, can be approximated by $\rho(0)$, because the bulk reduced density is much smaller than that at the interface. In order to obtain some idea of the N-dependence of $\Delta\chi$ we first assume that $\Theta^{exc} \propto \rho(0)d$, with d the width of the density profile of component B. Furthermore, we expect that the reduced density at $z = 0$ will follow the critical density ρ_c for a binary system. We suggest the following empirical relationship:

$$\rho(0) = \rho^* + k_\rho\rho_c, \tag{2.3.4}$$

where k_ρ is a constant and ρ_c is given by

$$\rho_c = \frac{1}{1+\sqrt{N}}. \tag{2.3.5}$$

The threshold ρ^* is related to the reduced density at the interface for polymers with infinite chain length, which is necessarily non-zero for wetting. The N-dependence of d

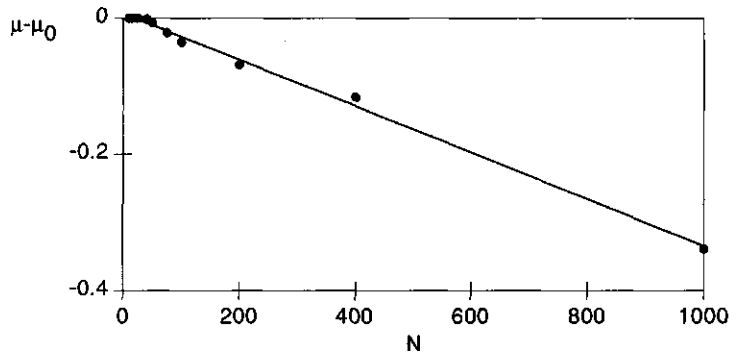

FIGURE 2.13. Chemical potential difference at the prewetting critical point as a function of N.

can not be principally different from that of $\rho(0)$, therefore we assume that

$$d = d^* + \frac{k_d}{1+\sqrt{N}}. \tag{2.3.6}$$

The numerical results show that eqs. (2.3.5) and (2.3.6) do indeed approximately hold, as can be seen from figs. 2.11 and 2.12, where we plot the reduced density at $z = 0$ and the distance d from the interface where $\rho(d) = \rho(0)/2$. The scatter in these figures is related to the indirect way in which the quantities are determined. The exact position of the prewetting critical point and the quantities derived from it, are extremely sensitive to the exact values of the selected Θ_B. Therefore, we can only use the density profiles *near*, and not *at*, the prewetting critical point. For this reason, it is unsurmountable that one introduces some scatter in the discussed quantities.

Returning to the balance in eq. (2.3.3) we finally have to consider the chemical potential difference $\Delta\mu$, already introduced above. The contribution of a segment of a polymer chain to the chemical potential difference can reasonably assumed to be an additive quantity. Note that this can only be the case for first-order wetting, i.e. $N > N_c$. So, we may assume

$$\Delta\mu \propto N - N_c, \tag{2.3.7}$$

where N_c is the critical chain length beyond which the wetting transition is of first order under the given circumstances (here $N_c \approx 35$). In fig. 2.13 we show the calculated $\Delta\mu$, which indicates that eq. (2.3.7) is a good approximation. With these rough arguments in mind, we may substitute the above results in eq. (2.3.3) and arrive at an approximation for the 'width' of the prewetting regime:

$$\Delta\chi \propto \frac{(N - N_c)\left(d^* + \frac{k_d}{1+\sqrt{N}}\right)}{N\left(1 - \rho^* - \frac{k_\rho}{1+\sqrt{N}}\right)}. \tag{2.3.8}$$

This expression always gives a maximum for $\Delta\chi$ as a function of N for physically feasible values of the introduced constants. An example of this feature is depicted in

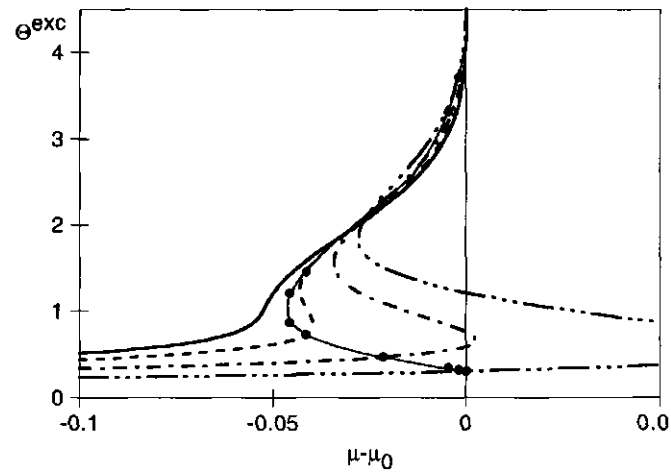

FIGURE 2.14. Adsorption isotherms for the semi-flexible polymer in the $A/B_{100}/C$ system with $\chi_{AC} = 2.2$ and $\chi = 0.94$. Depicted are the isotherms for $\Delta u_{tg} = -0.05$, 0, 0.1, and 0.25 (from left to right). The solid line with the filled circles indicates the prewetting region as determined from the adsorption isotherms (not all shown).

fig. 2.10, where we plot this function, where the values of the different parameters are taken from figs. 2.11 and 2.12, $N_c = 38$, and an arbitrary proportionality constant of 1/190 is assumed. Although the function does not entirely fit the data, it is able to describe the main features of $\Delta\chi$.

2.3.2. Semi-flexible polymer

In the preceding section we observed that a system with a liquid–liquid interface in the presence of a flexible polymer can undergo a first-order wetting transition if the solubility of the polymer in the two solvents is altered. In chapter 1 we studied the adsorption of a semi-flexible polymer at a liquid-liquid interface, and concluded that chain stiffness has a noticeable effect on the adsorption behaviour. The question arises whether the chain stiffness is also important for the wetting behaviour. In other words: is it possible to induce a wetting transition by only changing the chain stiffness? To answer this question we computed a number of adsorption isotherms for a semi-flexible polymer B_{100} with fixed interaction parameters. We choose $\chi = 0.94$ and varied the chain stiffness by taking different values for the energy difference Δu_{tg} between the *gauche* and the *trans* state.

Figure 2.14 shows the adsorption isotherms for a few values of Δu_{tg}, and fig. 2.15 gives the corresponding wetting phase diagram. One may wonder why in fig. 2.15 the wetting transition occurs at $\chi \approx 0.94$ for $\Delta u_{tg} = 0$, whereas in the case of the flexible polymer this transition was found at $\chi \approx 1.03$. The difference is caused by the fact that in the RIS scheme $\Delta u_{tg} = 0$ corresponds to $q = 3/2$, whereas first-order Markoff statistics

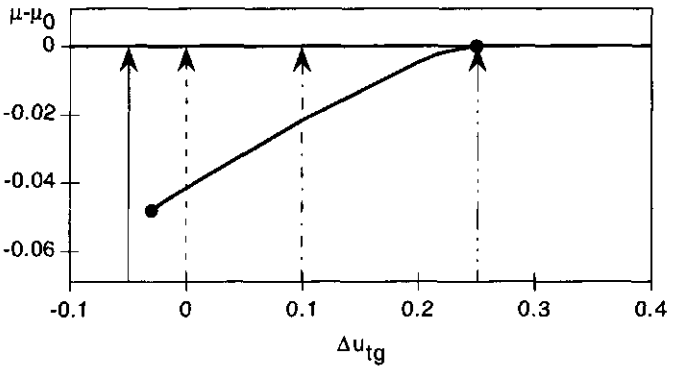

FIGURE 2.15. Wetting phase diagram for the $A/B_{100}/C$ system in the $(\Delta u_{tg}, \mu)$ space, with $\chi_{AC} = 2.2$ and $\chi = 0.94$. The arrows correspond to the isotherms in fig. 2.14.

on a cubic lattice imply $q = 5/4$. To achieve a persistence length of unity in the RIS scheme one should favour the *gauche* conformation by taking $\Delta u_{tg} = \ln(5/8) \approx -0.47$.

Clearly, the question put forward above regarding the chain flexibility can now be answered unambiguously: varying only the chain stiffness is indeed sufficient to induce a wetting transition. The prewetting range, a feature of a first-order transition, is in this case confined to the range $-0.03 < \Delta u_{tg} < 0.25$ or, equivalently, to $1.48 < q < 1.69$. In order to understand this effect of chain stiffness on the wetting behaviour of a polymer we return to the key conclusions of chapter 1. The adsorbed amount, at given μ, of a semi-flexible polymer at a liquid–liquid interface in the dilute regime decreases if q/ξ is increased up to the point where $q/\xi \approx 5$. Here, ξ represents the dimensionless interfacial width, which can be approximated as $\xi = \sqrt{2\lambda_1\chi_{AC}/(\chi_{AC} - 2)}$ (see eq. (1.2.6) in chapter 1). In the system studied here we have $\xi \approx 2.35$, which means that one expects the adsorbed amount to decrease for polymers with $q \lesssim 11$, i.e. $\Delta u_{tg} \lesssim 2.7$. The decrease in adsorbed amount with increasing χ is also found for a flexible polymer, in fact for any polymer. This phenomenon is a key effect needed for a wetting transition. We conclude that the predominantly entropic effect which modulates the adsorption behaviour of a semi-flexible polymer is also responsible for its wetting behaviour. However, the question remains what happens if we further increase the polymer stiffness.

To answer this question we calculated a number of adsorption isotherms for two values of χ (0.94 and 1.05) and values of Δu_{tg} ranging from 0 to 5. The isotherms for $\chi = 1.05$ (completely in the partial-wetting regime) are shown in fig. 2.16, now in a logarithmic plot in order to see the effect on the adsorbed amount more clearly. It can be seen that the adsorbed amount in the low-Θ^{exc} branch of the isotherm goes through a minimum as a function of Δu_{tg}. On the other hand, the high-Θ^{exc} branch does not show such a minimum. On first sight, one could expect that the observed effect on the adsorbed amount should have its impact on the contact angle θ. However, as can be

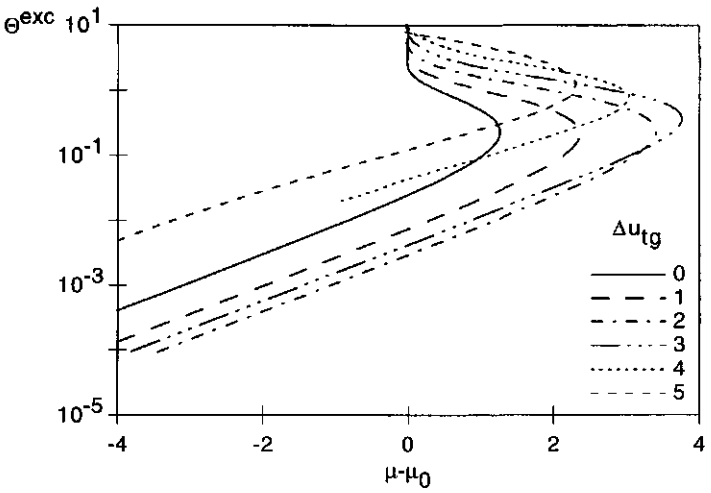

FIGURE 2.16. Adsorption isotherms in the partial-wetting regime for the semi-flexible polymer B_{100} in the $A/B_{100}/C$ system with $\chi_{AC} = 2.2$ and $\chi = 1.05$. The energy difference Δu_{tg} is indicated in the figure.

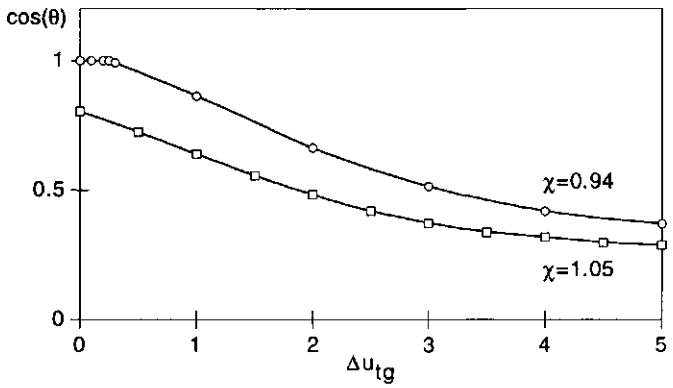

FIGURE 2.17. Contact angle for a B_{100}-rich phase in equilibrium with an A- and a C-rich phase with $\chi_{AC} = 2.2$ and two values of χ (as indicated). For $\chi = 0.94$ a first-order phase transition is visible.

seen in fig. 2.17, $\cos\theta$ is a continuously decreasing function of Δu_{tg} without anomalies. This apparent discrepancy can be understood when one realises that the effect of the adsorbed polymer on the interfacial tension γ_{13} is small in the low-Θ^{exc} branch as compared to the effect achieved by change in stiffness on the interfacial tension γ_{12} between de polymer-rich droplet and the A-rich phase.

2.4. CONCLUSIONS

The wetting behaviour of both flexible and semi-flexible polymers at a liquid–liquid interface has been shown to be extremely rich. With the aid of the SF SCF theory we were able to show that in a symmetric system, i.e. $\chi_{AB} = \chi_{BC} = \chi$, a change in the interaction parameter χ induces a wetting transition. For semi-flexible polymers it is possible to induce such a transition by solely changing the chain stiffness.

The order of the wetting transition is determined by the ratio of the interfacial width ξ of the binary A/C system and the coil size of the polymer. At fixed ξ there is a certain chain length N_c beyond which the wetting transition is of first order, whereas it is of second order for $N < N_c$. The features of the prewetting critical point are non-trivial. For the flexible polymer we found that the position $(\chi_w - \chi_{pw}, \mu_0 - \mu_{pw})$ of this point has a delicate N-dependence. We calculated and argued that $\Delta\chi$ has a maximum as a function of N. However, further theoretical considerations on this point are desirable.

The approach applied in this paper can be of relevance to wetting systems in polymer blends. The monomeric components used here can easily be replaced by polymeric ones. Also, the non-symmetric case can be analysed in detail with our methods. An example of a relevant non-symmetric system could be the wetting of a liquid–vapour interface by a polymer.

REFERENCES

[1] P. G. de Gennes. Wetting: statics and dynamics. *Rev Mod Phys*, 57:827–863, 1985.

[2] S. Dietrich. Wetting phenomena. In C. Domb and Lebowitz J. L., editors, *Phase transitions and critical phenomena*, volume 12, chapter 1. Academic Press, London, 1988.

[3] M. Schick. Introduction to wetting phenomena. In J. Charvolin, Joanny J.-F., and J. Zinn-Justin, editors, *Les Houches, Session XLVIII, 1988 — Liquides aux interfaces/Liquids at interfaces*, pages 415–497. Elsevier Science Publishers, 1990.

[4] J. M. H. M. Scheutjens and G. J. Fleer. Statistical theory of the adsorption of interacting chain molecules. I. Partition function, segment density distribution and adsorption isotherms. *J Phys Chem*, 83:1619–1635, 1979.

[5] J. M. H. M. Scheutjens and G. J. Fleer. Statistical theory of the adsorption of interacting chain molecules. II. Train, loop, and tail size distribution. *J Phys Chem*, 84:178–190, 1980.

[6] F. A. M. Leermakers and J. M. H. M. Scheutjens. Statistical thermodynamics of associated colloids. I. Lipid bilayer membranes. *J Chem Phys*, 89:3264–3274, 1988.

[7] P. Linse. *Polymer, release 2.6.9.* Lund University, 1995. Computer programme.

CHAPTER 3

Adsorption kinetics of the polysaccharide xanthan on ZrO_2

ABSTRACT

The adsorption kinetics of the polysaccharide xanthan from aqueous solution on zirconium oxide were studied as a function of pH and ionic strength. The adsorption was monitored by reflectometry in a stagnation-point flow setup. At intermediate pH and ionic strength, xanthan is present in a helical form and it can be viewed as a semi-flexible polymer under these conditions. By lowering the salt concentration or increasing the pH a helix–coil transition takes place. This transition is caused by the mutual electrostatic repulsion of the short side chains of xanthan. The so-formed coil can be considered as a Gaussian chain, with a large radius of gyration. The conformation of the polysaccharide is roughly reflected in its adsorption behaviour. It is, however, deduced that the electrostatic interaction between polymer and surface influences the stability of the helix. The adsorption process can be divided in two regimes. At low surface coverage the rate of adsorption is transport-limited, which in a stagnation-point flow leads to a linear time dependence of the adsorbed amount. The adsorption rate in this regime hardly changes with ionic strength or pH. The time range over which it holds, however, does, which can be understood in terms of electrostatic effects. At higher surface coverage two types of behaviour are observed. At low ionic strength and on a highly charged surface the adsorbed amount saturates abruptly. This kind of kinetics resemble those of flexible polymers. In this case the xanthan presumably adsorbs in a coil-like conformation, because the helix becomes unstable in the vicinity of the surface. At higher ionic strength and on a weakly charged surface, the adsorbed amount increases gradually over very long times. Under these conditions, the helix conformation is more stable so that we ascribe this slow process to tentatively rearrangement and alignment processes of the stiff chains on the surface.

3.1. INTRODUCTION

The adsorption of polymers onto solid surfaces has been investigated by many researchers. Usually, the focus is on the "equilibrium" adsorbed amount of polymer as a function of, e.g. concentration, charge or pH. Much less attention is paid to the kinetic aspects of this process. The kinetics are, however, important if the buildup of an adsorption layer does not follow a path of equilibrium conformations, which may well be the case. So far, kinetic studies mainly focussed on the adsorption of flexible polymers such as poly(ethylene oxide), poly(vinyl-4-pyridine) and polystyrene [1–3]. Semi-flexible and rigid chain molecules have received hardly any attention at all. On the other hand,

such polymers have been subject to many investigations as far as solution properties are concerned. It is our goal to pay attention to the adsorption kinetics of semi-flexible polymers.

It is important to choose a well-defined model polymer. One candidate is the polysaccharide xanthan, produced by the plant-pathogenic bacterium *Xanthomonas campestris*. This polyelectrolyte is known to exhibit a helical structure at intermediate pH and ionic strength. Xanthan is used extensively in physico–chemical studies [4–7], and it should be possible to compare its adsorption behaviour with its solution properties. It is therefore useful to summarise the latter properties first, before discussing any adsorption experiments. An important property for adsorption experiments is the secondary structure as a function of ionic strength, pH, and possibly temperature. It should be realised that a change in structure of the polymer may also be due to the presence of an interface: the helix–coil transition may shift upon adsorption. Hence, a comparison of adsorption properties with solution properties can only be made on a qualitative level.

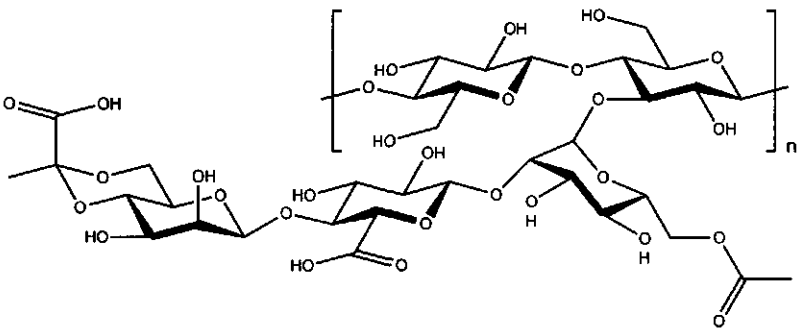

FIGURE 3.1. Monomer unit of xanthan.

The primary structure of the bacterial polysaccharide xanthan was established by Jansson et al. [8] and is shown in fig. 3.1. The monomeric unit consists of five saccharide rings, some of which contain side groups. The amount of acetate and acidic pyruvate groups depends on the origin of the xanthan. In our xanthan the pyruvate group content is approximately 50% and the acetate group content is almost 100%. From the primary structure the kind of interactions with an oxide surface can, at least qualitatively, be deduced. Two kinds of interactions are likely to occur. First, xanthan is a polyacid. Hence, electrostatic interactions can lead to adsorption as long as the oxide surface carries positive charges, i.e. $pH < pH_0$, where pH_0 is the point of zero charge of the surface. Secondly, specific short-range interactions between monomer units and the surface may drive adsorption. It is believed that polysaccharides adsorb tenaciously on various metal oxides because of the formation of a strong coordination complex of the sugar ring with metal ions [9].

Another, relevant feature of xanthan is its ability to form a helix in aqueous solution. Such a helix may be viewed upon as a semi-flexible object, which is likely to affect the adsorption behaviour. Although there is still some uncertainty as to whether the

secondary structure is a single or a double helix (a discussion about this subject is given by Bezemer et al. [7]), we will simply consider xanthan in its helical form as a semi-flexible chain, without specifying the exact structure of the helix. At an ionic strength of 5–10 mol m^{-3} ($pH = 7$, $T = 298$ K) the contour length of this semi-flexible chain, for the native product as used in this study, is of the order of 500 nm with a persistence length $q \approx 70$ nm [6].

For describing the secondary structure as a function of ionic strength, roughly three regimes can be distinguished. Milas and Rinaudo [4] investigated the low and intermediate ionic strength regime at different temperatures. At very low ionic strength ($I < 5$ mol m^{-3}), where electrostatic screening is negligible, the strong mutual repulsion of the side groups of the xanthan molecule will break up the helix so that a coil conformation results. A reversible coil–helix transition is found to occur upon increasing the ionic strength. At room temperature, without any buffer, this transition occurs at an ionic strength $I \approx 5$ mol m^{-3}. Increasing the ionic strength further will cause the charged side groups of xanthan to fold around the backbone. At still higher ionic strength ($I > 1000$ mol m^{-3}), i.e. full electrostatic screening, one finds aggregation of the helices.

3.2. EXPERIMENTAL

Commercial food grade Rhodigel-23 xanthan gum was used. This product was dissolved in water with addition of sodium chloride (up to 100 mol m^{-3}). In order to prevent biological degradation of the xanthan, 1 mol m^{-3} sodium azide (NaN_3) was added. The solution was stirred for 48 h, after which it was centrifuged for 2–12 h to remove undissolved matter (mainly cell material). After this purification step, the reagent Coomassie brilliant blue R250 was used to check on residual protein contaminations [10], which were found to be less that 1%. All manipulations were carried out at $T \approx 294$ K. The xanthan concentrations are determined by a colorimetric method using phenol and sulfuric acid, as described by Dubois et al. [11] for saccharides. The ionic strength of a solution was controlled by adding sodium chloride. The pH of a solution was held constant by using a approximately 5 mol m^{-3} barbital sodium-acetate buffer.

ZrO_2 films were prepared on silicon wafers by conventional sputtering techniques. The resulting layer thickness was found to be 68 nm. ZrO_2 has a point of zero charge $pH_0 \approx 6$.

The adsorbed amount of polymer was measured by reflectometry, as extensively described by Dijt et al. [1, 12]. A stagnation-point flow cell is used in these experiments to control the polymer flux J towards the surface. In such a setup the polymer concentration as well as the flow rate can be varied. The flux of polymer to the surface, in a steady-state situation, is described by the following equation [13]:

$$J = 0.776\nu^{1/3}R^{-1}D^{2/3}(\bar{\alpha}Re)^{1/3}(c_p - c_s). \tag{3.2.1}$$

Here, ν is the kinematic viscosity, R the radius of the inlet tube, D the polymer diffusion coefficient, $\bar{\alpha}$ a dimensionless stream intensity parameter, Re the Reynolds number, c_p the polymer bulk concentration and c_s the subsurface concentration, which is negligibly small as long as the adsorbed amount is low. We will write J_0 instead of J in the case that $c_s \ll c_p$.

3.3. RESULTS AND DISCUSSION

The adsorption of xanthan from aqueous solution is influenced by several physico–chemical properties of the system. The negative charge of the polymer causes an attraction between polymer and the ZrO_2-substrate at a $pH < pH_0$. A specific interaction with the surface in the form of a coordination complex is probably a second driving force for adsorption. The electrostatic interactions can be influenced by changing the pH or ionic strength. However, this also changes the internal electrostatic interactions of xanthan and thus its conformation. It is therefore not possible to study the effects of the two driving forces for adsorption separately without changing the xanthan conformation. Hence, only qualitative remarks will be made on this point. The possibility that the stiffness of xanthan in its helical form leads to the formation of a ordered phase near the solid–liquid interface may play an important role in adsorption studies. It is expected that if a, possibly surface-induced, coil–helix transition occurs, this must be reflected in the adsorption behaviour. The xanthan conformation can be influenced by changing ionic strength, pH or temperature. For convenience, temperature is held constant, whereas pH and ionic strength (I) are varied.

As was noted before, at given pH, xanthan exhibits conformational transitions as a function of ionic strength. Starting at low ionic strength, xanthan undergoes a coil-to-helix transition at intermediate I, and finally aggregates of helices are formed at high ionic strength. We used the ionic strength mainly as a control parameter for the xanthan conformation, whereas the pH was assumed to change mainly the charge of the ZrO_2 surface. As was discussed above, this approach can be only a first-order approximation since I affects also the surface charge and the pH has also an effect on the polymer conformational properties. Figures 3.3 shows examples of the adsorption kinetics of xanthan onto ZrO_2 at different pH-values and for various ionic strengths. Below, we will discuss some aspects of these adsorption kinetics measurements. It should be noted that in these figures the horizontal axis has been scaled by multiplying time t by the polymer concentration c_p. In this way the initial slopes are identical as long as the adsorption is transport limited. This means that, initially, the adsorbed amount can be described by $\Gamma = J_0 t$; the initial slope $(\mathrm{d}\Gamma/\mathrm{d}(c_p t))_0$ should then be constant according to eq. (3.2.1).

Within experimental error, the scaled initial adsorption rates $(\mathrm{d}\Gamma/\mathrm{d}(c_p t))_0$ are the same over a wide range of ionic strengths ($5 \leq I \leq 500$ mol m^{-3}) and independent of pH. According to eq. (3.2.1), a difference in initial adsorption rate upon varying the ionic strength or pH can only be accounted for by a change in diffusion coefficient

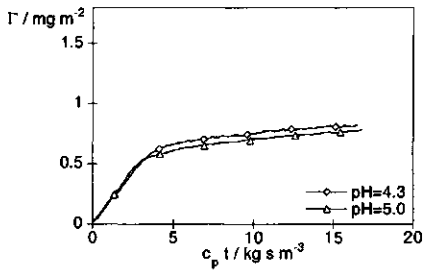

(a) $I = 5.4$ mol m^{-3}

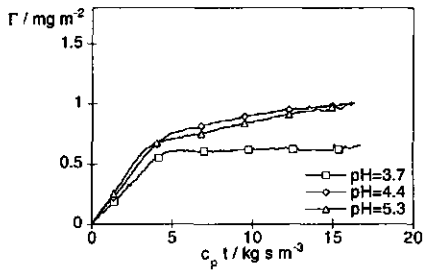

(b) $I = 10$ mol m^{-3}

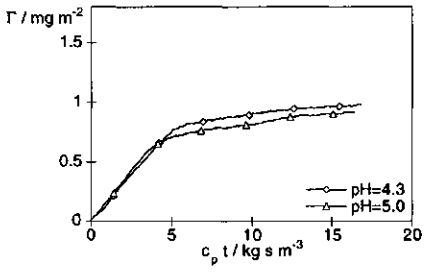

(c) $I = 20$ mol m^{-3}

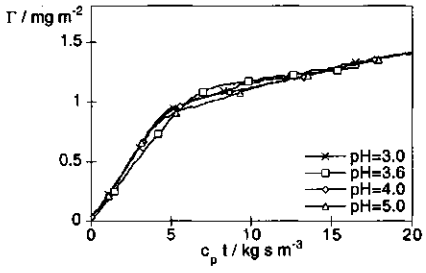

(d) $I = 100$ mol m^{-3}

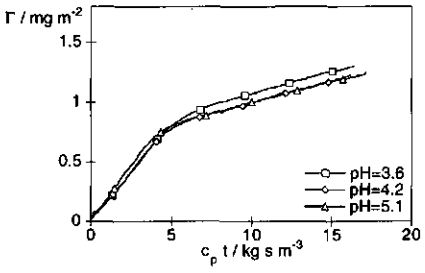

(e) $I = 500$ mol m^{-3}

FIGURE 3.2. Adsorption of xanthan onto ZrO_2 at $I = 5.4$–500 mol m^{-3} with $c_p = 40$ g m^{-3} ($c_p = 50$ g m^{-3} for $I = 100$ mol m^{-3} and $pH = 3.6$) for various pH values. The symbols are only drawn for clarity

of xanthan. Apparently the changes in conformation of xanthan with ionic strength, whatever they may be, are not reflected in its diffusion coefficient.

Although the initial (transport-limited), part of the kinetic curves is approximately the same over a large range of ionic strengths, significant differences occur at larger Γ. Qualitatively, we can make two observations. The first is that the point where the transport-limited regime ends, i.e. the bending point in the adsorption curve, shifts

with ionic strength and pH. Secondly, it should be noted that the adsorption rate beyond the bending point does, in most cases, not go to zero, but it remains finite over the adsorption times considered in these experiments. The latter observation is in sharp contrast with adsorption experiments on flexible polymers like poly(ethylene oxide) [1], poly(vinyl-4-pyridine) [2] and polystyrene [3], where a rather abrupt saturation is usually found.

3.3.1. Transport-limited regime

With respect to the duration of the transport-limited regime the following observations and considerations can be made. Comparing results for increasing pH-values at a fixed ionic strength in fig. 3.3, we see that the adsorbed amount at the bending point shows a monotonic decrease. This decrease is illustrated in fig. 3.3(a). If, however, we consider the same effect at increasing ionic strengths and fixed pH (4.3), we find that the adsorbed amount at the bending point of the adsorption curve shows a maximum at $I \approx 100$ mol m^{-3}. The latter effect is shown in fig. 3.3(b).

The shift of the bending point with increasing pH (fig. 3.3(a)) is easily explained. An increase in pH leads to an increase of the number of negatively charged groups of the polyacid xanthan, whereas the positive surface charge of ZrO_2 decreases. Due to the strong electrostatic interaction between surface and polymer, this interaction will initially be the most important one. The large number of negatively charged groups on the polymer at high pH, in comparison with the small number of positively charged sites on the surface, will lead to a large occupied surface area per polymer chain. Hence, the higher the pH, the lower the coverage where newly arriving polymers start to be repelled so that $\mathrm{d}\Gamma/\mathrm{d}t$ drops. In other words, the transport-limited regime is shorter at high pH because the extent of spreading of the polymer is larger.

The second effect requires some more considerations before any conclusions can be drawn about the nature of the maximum in the adsorbed amount at the bending point. The increase of the adsorbed amount at the bending point of the adsorption curve at increasing ionic strength up to $I = 100$ mol m^{-3} is mainly caused by the difference in screening of the electrostatic interactions. The Debye screening length κ^{-1} decreases from 4.2 nm at $I = 5.4$ mol m^{-3} to 0.96 nm at $I = 100$ mol m^{-3}. The effects screening has on the initial adsorption behaviour is mainly a steric one. The mutual repulsion between xanthan molecules becomes less pronounced as the ionic strength increases, allowing the polymers to be closer packed at the surface, allowing more space for newly arriving polymers. This tends to stretch the transport-limited regime to higher Γ. If xanthan were a simple polyelectrolyte this increase would continue (or possibly drop to zero) at still higher I. As it is, we have to find an explanation for the decrease in the adsorbed amount above $I = 100$ mol m^{-3}. So far, we have only discussed the electrostatic interactions between the polymer and the surface and ignored the specific interaction due to a coordination complex formalism. When the screening of the electrostatic polymer–surface interaction becomes large, this specific interaction is likely to become more important. When this interaction is dominating over the electrostatic, one could again visualise that the xanthan molecules spread as much as possible to profit

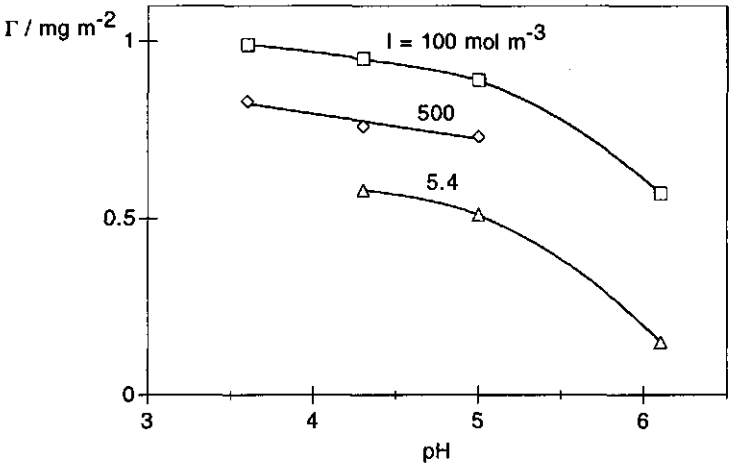

(a) Γ as a function of pH for different ionic strengths.

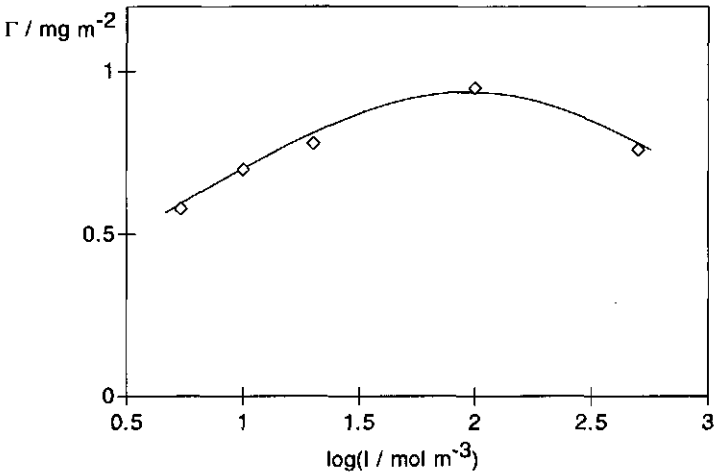

(b) Γ as a function of I at $pH = 4.3$.

FIGURE 3.3. Adsorbed amount of xanthan on ZrO_2 at the bending point of the kinetic adsorption curve. Flow conditions are identical for all measurements: Flow rate $Q = 11 \times 10^{-9}$ m^{3}s^{-1} and $c_p = 40$ g m^{-3}. The drawn lines only serve as a guide to the eye.

from as many coordination complexes as possible, so that Γ at the bending point would again become smaller. At present, we do not have enough data to fully corroborate this picture, and therefore we consider this only as a rather speculative explanation.

3.3.2. Long-term adsorption kinetics

As discussed above the adsorption kinetics of xanthan initially are transport-limited, as is the case for most adsorption or deposition processes from solution in a stagnation-point flow (see, e.g. refs. [1, 14]). Above, this initial adsorption process was described without considering explicitly the helix-forming ability of xanthan. However, the secondary structure of xanthan is likely to be of great importance for the adsorption kinetics on a highly covered surface (i.e. after the bending point). We will show that in this region there are significant differences with the adsorption kinetics of regular flexible polymers.

The semi-flexible nature of xanthan reveals itself when the structure of the adsorbed polymer layer starts influencing the adsorption rate. In the case of flexible polymers the conformational changes near the surface are, at least at workable Reynolds numbers ($4 \leq Re \leq 40$), much faster than the transport of new polymers, whereas conformational changes in xanthan are relatively slow due to the intrinsic stiffness of the helical structure. We can give a rough estimate of the time scales involved in the adsorption process. For this we define τ_f as a characteristic time needed to fill up the surface. In its most simple form this is the ratio between the adsorbed amount at the bending point and the initial flux:

$$\tau_f = \frac{\Gamma_{tlr}}{J_0}. \tag{3.3.1}$$

A typical value for Γ_{tlr} is 1 mg m^{-2} and the initial flux J_0 can roughly vary between 10^{-4} and 1 mg m^{-2}s^{-1}. Therefore, conformational changes of a polymer that occur within the range of 1–10^4 s will probably have an influence on the adsorption kinetics. Faster processes will have no measurable influence, whereas slower ones will only be noticeable in the long time behaviour. Investigations of Adachi et al. [15] point in the direction that for flexible polymers an unfolding time of less than 1 s is likely. This is the reason that for flexible polymers, the final adsorbed amount is reached rather quickly after the transport-limited regime has ended. Then the kinetic curves reach a plateau value characterised by $d\Gamma/dt \to 0$.

As already seen in fig. 3.3, for xanthan the adsorbed amount does not level off after the transport-limited regime, but it continues to increase, albeit more slowly than initially. In these figures there is only one exception to this rule, namely for low pH ($pH = 3.7$) and relatively low ionic strength ($I = 10$ mol m^{-3}) in fig. 3.2(b). A similar curve was found (but not displayed here) for $pH = 3.6$, without added salt (corresponding to $I \approx 6$ mol m^{-3} due to buffer). In the following part we try to discuss these observations systematically, thereby making the comparison to known solution properties of xanthan.

First, we discuss the adsorption behaviour of xanthan at low pH and low ionic strength. In fig. 3.2(b) one example of such an experiment is shown ($pH = 3.7$ and

$I = 10$ mol m^{-3}). In this case the adsorption kinetics resemble those of flexible polymers, i.e. $\mathrm{d}\Gamma/\mathrm{d}t \to 0$ beyond the bending point. In this case the final adsorbed amount is relatively low. This is a reason to believe that xanthan is now in a coil conformation. At $pH = 3.7$ the polymer itself is negatively charged and the surface has a high positive charge. The low ionic strength ($I = 10$ mol m^{-3}) cannot sufficiently screen the electrostatic interactions, which are the driving force for the helix–coil transition. In solution at $pH \approx 7$ the coil–helix transition occurs at $I \approx 5$ mol m^{-3} [6]. A lower pH will favour the helix conformation and even further decrease the ionic strength at which this transition occurs. Hence, under the conditions where in fig. 3.2(b) a plateau is reached ($pH = 3.7$ and $I = 10$ mol m^{-3}), xanthan in solution is in the helical conformation. Yet, the adsorption behaviour points to a coil behaviour. We therefore assume that the surface has an influence on the transition. This is possible because the electrostatic interactions due to the charged surface may destabilise the helix and induce a helix–coil transition, so that a flexible molecule with a large radius of gyration is formed. Due to this probable conformational transition, this polymer chain will adsorb in the same manner as charged flexible polymers do. The low final adsorbed amount is typical for flexible polymers, particularly when they are charged [2]. At higher values of the pH the charge of the surface is probably too low to induce the helix–coil transition at $I = 5$ mol m^{-3}, and xanthan is in the helix conformation also on the surface. Experiments at very low ionic strength might give evidence for uncoiling at higher pH, but with the present system this is experimentally impossible. In order to have sufficient adsorption at low I the ZrO_2 must be positively charged, i.e. the pH must ne lower than 6. At low pH the ionic strength automatically is too high due to the added acid, and at high pH a buffered solution is needed, which again makes the lowest possible value for the ionic strength around 5 mol m^{-3}.

We tentatively conclude that the continued increase of $\Gamma(t)$ after the bending point for most of the curves in fig. 3.3 (i.e. for all cases when I and pH are not very low) must be related to xanthan adsorbing in a helical conformation. In some way or another, this adsorption of helices is a continuing process, even after prolonged exposure of the surface to xanthan solutions.

The data reported in fig. 3.3 were limited to the adsorption kinetics for relatively short times, not far beyond the transport limited part. It is also interesting to consider the long-time behaviour. Figure 3.4 shows an example of the adsorption of xanthan from a solution at intermediate ionic strength at $pH = 4.3$ over a time range of the order of $10\tau_{\mathrm{tlr}}$, where τ_{tlr} is the length of the transport-limited regime. In order to bring out sufficient detail, $\Gamma(t)$ was plotted on logarithmic axes. It is clear that even after very long times the adsorbed amount does not reach an "equilibrium". In order to understand this behaviour we consider xanthan as a charged semi-flexible object, without taking into account too much details. At the rather low concentration used in the experiments ($c_{\mathrm{p}} = 40$ g m^{-3}) and the low value of Re, the solution with semi-flexible helices will be isotropic and the molecules will have no preferential orientation when arriving at the surface. However, in the vicinity of the surface the local concentration

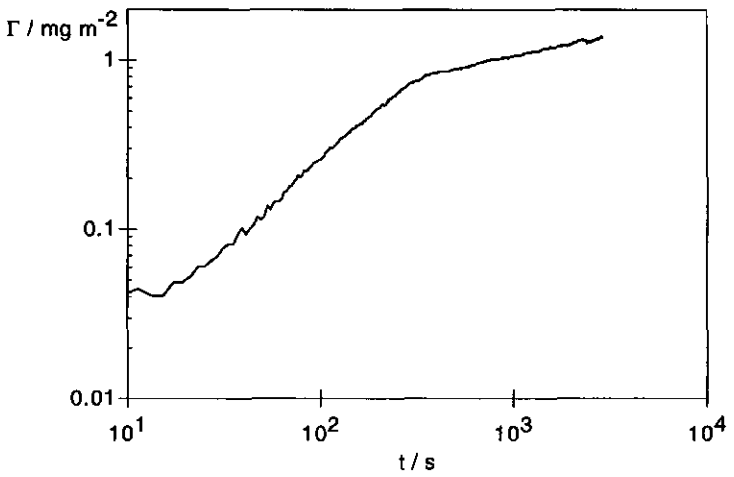

FIGURE 3.4. Long-time adsorption behaviour of xanthan onto ZrO_2 as measured by reflectometry in stagnation-point flow at $pH = 4.3$, $I = 10$ mol m^{-3}, $c_p = 27$ g m^{-3}, and flow rate $Q = 5 \times 10^{-9}$ m^{3}s^{-1}.

is much higher so that alignment of (parts of the) molecules could occur. Also, the presence of the solid surface itself might favour alignment. This process is likely to be slow, occurring on time scales larger than that of the initial adsorption process. The slow nature of this rearrangement process probably related to the exchange mechanism that has to occur to allow the xanthan molecule to move along the surface. In other words, parts of a polymer have to detach from one site and attach at another. The attractive interaction between a metal oxide and a polysaccharide is large [9], and detachments of a part of the molecule will occur with a low frequency. When alignment takes place within the adsorbed layer, the available free area for new incoming polymer increases, and therefore the adsorbed amount will increase as well. Hence, the adsorption rate will be non-zero even at long time scales. It will mainly depend on the rate of reorientation, as long as the polymer flux is not the limiting factor. We therefore propose that the adsorbed layer locally forms an oriented phase due to alignment of parts of the xanthan helix, and that this process is responsible for the slow increase of the adsorbed amount as a function of time.

It should also be noted that at $I = 500$ mol m^{-3} (fig. 3.2(e)) the adsorption rate increases slightly compared to that at lower ionic strengths. This effect is probably caused by the onset of aggregation of xanthan helices. Due to this effect it was not possible to perform adsorption experiments beyond $I = 500$ mol m^{-3}, because at these high salt concentrations the process is most likely dominated by aggregation, so that the adsorption kinetics as such can no longer be studied.

3.4. CONCLUSIONS

The adsorption process of a semi-flexible polymer differs substantially from that of a flexible one. We have shown that an increased rigidity of a chain, in this case the xanthan helix, causes the adsorption kinetics to change drastically. Using the ionic strength of the xanthan solution as a tuning parameter for the coil–helix transition, we were able to see a remarkable change in kinetics. At a pH below 4 and at very low ionic strength, xanthan is supposed to undergo a helix–coil transition in the vicinity of the positively charged ZrO_2-surface. The adsorption process is in that case comparable to that of a flexible polymer. In this regime the adsorption is initially transport-limited, followed by a fast saturation of the adsorbed amount. We like to emphasise that not the solution properties alone determine the adsorption behaviour; especially the ratio between polymer charge and the surface charge is important as well. Beyond a certain, pH-dependent, threshold of the ionic strength ($I \gtrsim 10$ mol m^{-3} at $pH \approx 4$), the adsorption kinetics do no longer show the fast levelling off. Instead, a gradual increase in the adsorbed amount is found, which is most likely due to the slow rearrangement of the stiff helices near the interface. We suppose that this rearrangement is slow, because it involves an exchange mechanism in which a section of one chain at has to detach from the surface before it can be replaced by one of another chain. This process will increase the packing efficiency near the surface, and hence, also the adsorbed amount. In comparison to experimental time scales the exchange is slow, because the binding of polysaccharides to a metal oxide surfaces is rather strong [9], and thus the energy barrier is high.

REFERENCES

[1] J. C. Dijt, M. A. Cohen Stuart, J. E. Hofman, and G. J. Fleer. Kinetics of polymer adsorption in stagnation-point flow. *Colloids Surfaces*, 51:141–158, 1990.

[2] E. Pefferkorn and A. Elaissari. Adsorption–desorption processes in charged polymer/colloid systems; structural relaxation of adsorbed macromolecules. *J Colloid Interface Sci*, 138:187–194, 1990.

[3] J. C. Dijt, M. A. Cohen Stuart, and G. J. Fleer. Kinetics of adsorption and desorption of polystyrene on silica from decalin. *Macromolecules*, 27:3207–3218, 1994.

[4] M. Milas and M. Rinaudo. Conformational investigation on the bacterial polysaccharide xanthan. *Carbohydr Res*, 76:189–196, 1979.

[5] A. Gamini, J. de Bleijser, and J. C. Leyte. Physico-chemical properties of aqueous solutions of xanthan: An n.m.r. study. *Carbohydr Res*, 220:33–47, 1991.

[6] A. Gamini and M. Mandel. Physicochemical properties of aqueous xanthan solutions: static light scattering. *Biopolymers*, 34:783–797, 1994.

[7] L. Bezemer, J. B. Ubbink, J. A. Dekooker, M. E. Kuil, and J. C. Leyte. On the conformational transitions of native xanthan. *Macromolecules*, 26:6436–6446, 1993.

[8] P.-E. Jansson, L. Kenne, and B. Lindberg. Structure of the extracellular polysaccharide from Xanthomonas campestris. *Carbohydr Res*, 45:275–282, 1975.

[9] Q. Liu and J. S. Laskowski. The role of metal hydroxides at mineral surfaces in dextrin adsorption, i. studies on modified quartz samples. *Int J Miner Process*, 26:297–316, 1989.

[10] S. Fazekas de St. Groth, R. G. Webster, and A. Datyner. Two new staining procedures for quantitative estimation of proteins on electrophoretic strips. *Biochim Biophys Acta*, 71:377–391, 1963.

[11] M. Dubois, K. A. Gilles, J. K. Hamilton, P. A. Rebers, and F. Smith. Colorimetric method for determination of sugars and related substances. *Anal Chem*, 28:350–356, 1956.

[12] J. C. Dijt, M. A. Cohen Stuart, and G. J. Fleer. Reflectometry as a tool for adsorption studies. *Adv Colloid Interface Sci*, 50:79–101, 1994.

[13] T. Dąbroś and T. G. M. van de Ven. A direct method for studying particle deposition onto solid surfaces. *Colloid Polym Sci*, 261:694–707, 1983.

[14] T. Dąbroś and T. G. M. van de Ven. Deposition of latex particles on glass surfaces in an impinging jet. *PhysicoChemical Hydrodynamics*, 8:161–172, 1987.

[15] Y. Adachi, M. A. Cohen Stuart, and R. Fokkink. Dynamic aspects of bridging flocculation studied using standardized mixing. *J Colloid Interface Sci*, 167:346–351, 1994.

CHAPTER 4

Competition between transport and spreading in protein adsorption kinetics

ABSTRACT

The saturation adsorbed amount of polymers on solid surfaces is mostly found to be independent of the polymer transport rate, or flux J, to the surface. In most cases this is because the experimental rate of transport strongly deviates from the relaxation rate in the polymer layer. We studied the adsorption of both immunoglobulin G and savinase on SiO_2 from aqueous solution and found that the transport rate is an important parameter in the adsorption kinetics. The adsorption process can be viewed as an attachment to, followed by the spreading over the surface of a polymer molecule. In this way the adsorbed amount strongly depends on J if the time for transport to the surface is in the same range as the spreading time. Using an analytical "growing disk" model for the polymer adsorption, we are able to, at least qualitatively, describe the adsorption kinetics.

4.1. INTRODUCTION

The process by which a polymer layer near a solid surface builds up is, in general, one which runs through a series of nonequilibrium states. The extent to which an adsorbed polymer layer can relax towards its equilibrium structure, described by the widely accepted statistical theories (see, e.g. ref. 1), is currently under investigation. It should be no surprise that evidence for very slow, or even completely suppressed, equilibration is now accumulating. As may be anticipated, relaxation becomes more difficult as the polymer–surface interaction gets stronger. An example for this effect is the adsorption of polymer from organic solvents on mineral surfaces. Here, strong hydrogen bonds are the driving force for adsorption and quenched states are therefore likely to be formed.

A recent study by Schneider et al. [2] provides an example of such quenching. It was found by means of infrared spectrometry that poly(methyl methacrylate) molecules adsorbed on silica from CCl_4 have, in the terms of the authors, a "bimodal energy landscape": molecules arriving at an early stage of the adsorption will flatten to a large extent and develop a high fraction of polymer–surface contacts (bound fraction), whereas a significant population of molecules that arrive later will adsorb with a low bound fraction. This distribution proved to be quite stable, even though it is nowhere near thermodynamic equilibrium.

An immediate implication of this observation is that the rate at which polymer molecules arrive at an interface should have an effect on the adsorbed amount. As Schneider

et al. point out at the very end of their paper, the outcome of an adsorption experiment must depend on the relative rates of surface impingement on the one hand and surface spreading on the other hand. If spreading occurs relatively fast, more molecules will lay flat so that the adsorbed mass is low. If, however, the rate of polymer supply to the surface can be made higher than the rate of spreading, the dominant adsorbed species will be in a more coiled conformation and the adsorbed mass will be higher. A family of macromolecules which will presumably exhibit a slow spreading process are proteins. Their relatively rigid structure in solution will give rise to slow rearrangement in the vicinity of an attractive wall. Measurements on the adsorption of monoclonal immunoglobulin G already give an indication in this direction [3]. In the present paper we report two more pronounced examples of the competition between transport to and slow spreading at an interface. More importantly, we derive expressions for the rate of adsorption of spreading molecules and use these to analyse the data.

4.2. EXPERIMENTAL

We will briefly describe experiments on the adsorption of the enzyme savinase on SiO_2 as they were presented by Maste [4]. However, we will give a somewhat different interpretation of the results as they were given in the PhD thesis by Maste. Furthermore, we will desribe similar experiments, which were carried out on the immunoglobulin G–SiO_2 system [5].

4.2.1. Materials

A wild-type alkalophilic serine proteinase produced by *Bacillus lentus* was used. This enzyme is commercially available as savinase. The savinase was irreversible inhibited by phenylmethylsulfonyl fluoride (PMSF), which reacts with the active site of the protein. Aqueous solutions of the protein were used, where a sodium tetraborate buffer (borax) was used to set $pH = 8$. The ionic strength of the solution was controlled by addition of sodium chloride and set to $I = 10$ mol m^{-3}.

Monoclonal immunoglobulin G (IgG) with an isoelectric point $pH_0 \approx 6$ was used. IgG consists of four polypeptide chains linked by disulphide bonds. The folded chains form an Y-shaped molecule, giving the protein a anisotropic character. Buffered aqueous solutions of this protein were prepared using a phosphate buffer at $pH = 6.0$ and ionic strength $I = 5$ mol m^{-3}. Before performing the adsorption experiments the solutions were filtered over a 0.2 μm Acrodisc to remove possible aggregates.

SiO_2 films were prepared on silicon wafers by oxidation in ambient air at $T = 1270$ K for approximately 1 h, resulting in a film thickness of about 100 nm.

4.2.2. Reflectometry

The adsorption was measured as a function of time by means of reflectometry, as described extensively by Dijt et al. [6, 7]. All measurements were carried out at $T \approx 294$ K. In these experiments, the flux of polymer toward the surface is controlled by the use of a stagnation point flow cell. In such a setup the flow rate as well as the polymer

concentration can be varied. In a steady state situation the polymer flux is described by the following equation [8]:

$$J = 0.776\nu^{1/3}R^{-1}D_{\mathrm{p}}^{2/3}(\bar{\alpha}Re)^{1/3}(c_{\mathrm{p}} - c_{\mathrm{s}}). \tag{4.2.1}$$

Here, ν is the kinematic viscosity, R the radius of the inlet tube, D_{p} the diffusion coefficient of the polymer, and $\bar{\alpha}$ a stream intensity parameter depending on both the dimensions of the cell and the Reynolds number Re. The polymer concentration near the interface and in the bulk are denoted by c_{s} and c_{p}, respectively. In the case of high affinity adsorption and as long as the surface coverage θ (or adsorbed amount Γ) is low, c_{s} can be neglected. As long as the adsorption is transport limited, which is usually the case with a bare surface, the adsorption can be described by $\mathrm{d}\Gamma/\mathrm{d}t = J_0$. To compare different experiments, it is convenient to rescale time to J_0t leading to an initial slope of unity for all cases. The point where this slope deviates from unity is denoted as the end of the transport limited regime. All plots of Γ against time are rescaled this way.

4.3. RESULTS AND DISCUSSION

As most proteins, both savinase and IgG contain hydrophilic as well as hydrophobic domains. Both electrostatic and hydrophobic interactions can therefore be important in the adsorption from aqueous solutions. Both proteins are found to have a high affinity for hydrophobic surfaces (see, e.g. refs. 4, 9), which indicates the importance of nonelectrostatic interactions. The strong adsorption is very likely to cause surface relaxation processes to be slow.

To compare the present results on a system with strong polymer–surface interaction with a system with much weaker interactions, it is useful to take the adsorption of polystyrene (PS, $M_{\mathrm{w}} = 3040$ kg mol^{-1}) from decalin on SiO_2 as an example [7]. These experiments are also carried out in a stagnation-point flow setup. Figure 4.1 shows the adsorbed amount Γ for PS as a function of the scaled time J_0t for various polymer concentrations (a measure of J_0). Clearly, in this case there are no significant differences, within the experimental window, in the adsorbed amount as a function of polymer flux J_0. This indicates a spreading process that is much faster than the transport of polymer to the surface. Similar adsorption behaviour is found for, e.g. poly(ethylene oxide) on SiO_2 from aqueous solution studied by means of reflectometry [6].

In fig. 4.2 we plot the adsorbed amount Γ for savinase as a function of scaled time J_0t for adsorption at constant flow rate but varying polymer concentration. Figure 4.3 shows the adsorption kinetics for IgG. For both polymers it can be seen that the adsorbed amount first increases linearly with time (as is to be expected for a constant flux), and then levels off. However, the adsorbed amount reached under conditions of low polymer concentration is significantly lower than that found for higher concentrations.

We conclude that in this particular case the spreading rate on the bare surface was indeed small, so that fast filling of the surface could prevent it to a large extent. Spreading on the fully covered surface, however, did not occur, just as in the experiments reported

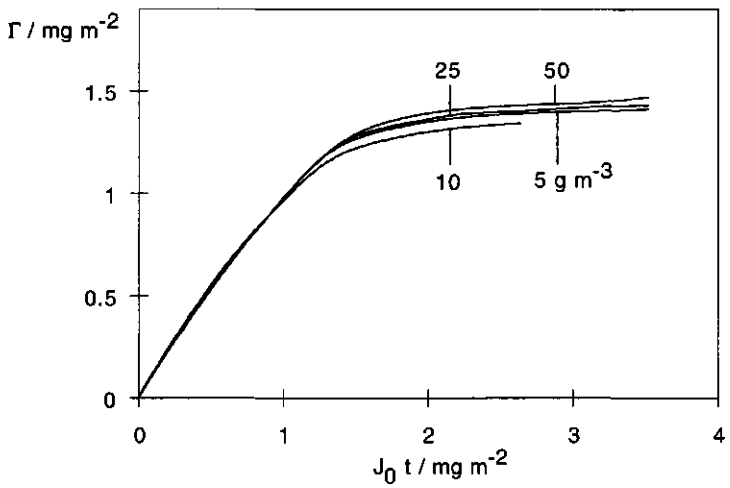

FIGURE 4.1. Effect of polymer concentration c_p on the adsorption of polystyrene on SiO_2 from decalin with $M_w = 3040$ kg mol^{-1}, $Q = 21.8$ μl s^{-1}, and c as indicated. $J_0 = 0.0022$, 0.0044, 0.0110, and 0.0220 mg m^{-2}s^{-1} for the different polymer concentrations.

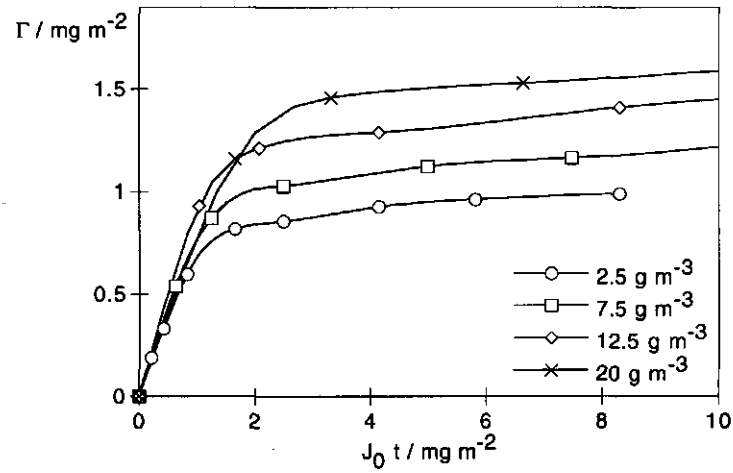

FIGURE 4.2. Effect of polymer concentration c_p on the adsorption kinetics of savinase on SiO_2 for c_p as indicated. $I = 10$ mol m^{-3}, $pH = 8$, and $J_0 = 0.014$, 0.042, 0.069, and 0.111 mg m^{-2}s^{-1} for the different savinase concentrations. The symbols are only plotted for clarity.

by Schneider et al. [2]. Apparently, the combination of a strong segmental binding with a crowded surface has that effect.

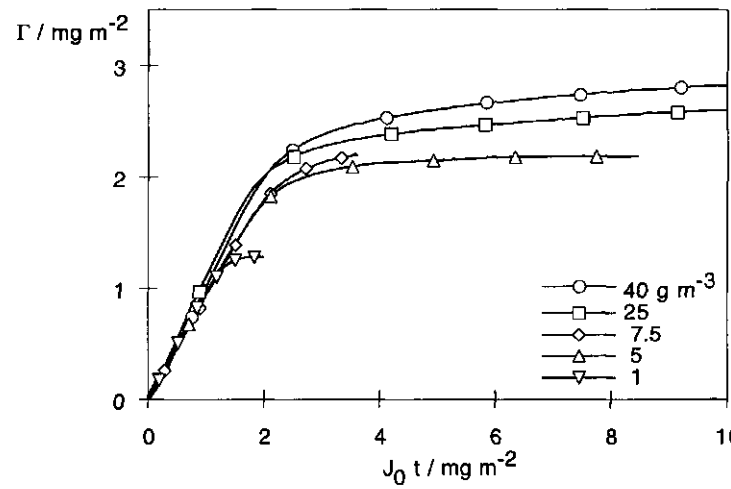

FIGURE 4.3. Effect of polymer concentration c_p on the adsorption kinetics of IgG on SiO_2 for c_p as indicated. $I = 5$ mol m^{-3}, $pH = 6$, and $J_0 = 0.0014$, 0.0069, 0.0103, 0.0342, and 0.0548 mg m^{-2}s^{-1} for the different IgG concentrations. The symbols are only plotted for clarity. Data taken from ref. [5].

What are the timescales involved? The time τ_f needed for filling up the surface can be defined as the ratio between saturation coverage and initial flux:

$$\tau_f = \frac{\Gamma_{max}}{J_0}. \tag{4.3.1}$$

As a typical value of Γ_{max} we can take 1 mg m^{-2}. Values of J_0 that can be experimentally realised depend on the diffusion coefficient of the polymer, the flow rate, and the concentration, and range in most of our experiments between 10^{-4} and 1 mg m^{-2} s^{-1}. This means that only polymers having a spreading time τ_s in the range 1–10^4 s can respond to changes in the supply rate with a change in adsorbed mass. There is some evidence [10] that flexible polymers unfold at time scales of about 1 s or less, which is, indeed, not inside this range. For savinase and IgG, apparently, τ_s is around 100, and 1000 s, respectively, which is remarkably slow but consistent with the strong interaction this protein has with the surface. One should bear in mind that a structural change of the adsorbed layer involves a detachment/reattachment process of polymer segments with an obviously high energy barrier. We also argue that the fact that these proteins have a strong internal structure plays a role, too. Especially the fact that both proteins have a hydrophobic core, which has a high affinity for the surface [4, 9], causes a partial denaturation of the protein near the surface. This leads to a higher surface coverage, but a smaller adsorbed amount, if J_0 is low. A further property of IgG that influences its spreading behaviour, is the anisotropy of the molecule. It enables reorientation near an interface, which is in fact nothing else than spreading.

One could argue that the presence of savinase fragments, due to possible autocatalytic cleavage of the enzyme, plays a role in the adsorption behaviour. In the case of IgG fragments could also be present, this is, however, unlikely. We will show that the presence of fragments can not explain the observed behaviour. When a short adsorbed chain is replaced by a longer one, this leads to a small increase in the translational entropy, therefore leading to preferential adsorption for long polymers. It should however be noted that this only describes the thermodynamic equilibrium situation. In the following comparison of our system with the adsorption of bidisperse polymer samples, we will show that it is very unlikely that fragmentation plays a significant role in the observed effects, i.e. the dependence of the maximum adsorbed amount on the polymer transport rate. Dijt et al. [11] studied the exchange kinetics of both polystyrene and poly(ethylene oxide) differing in length only. For these polymers they indeed found that short polymers are replaced by long ones. Using a stagnation point flow setup and a solution with equal concentrations of short and long polymers, the transport rate to the surface of the short polymers will be larger than that of the long ones ($J_0 \propto D^{2/3}$), so that initially only short chains adsorb. If the observed differences in final adsorbed amount for the our protein case would be caused by the presence of fragments, then by decreasing the transport rate one would eventually expect the adsorbed amount to increase, i.e. only long chains are adsorbed. However, the opposite is the case, which is, in our opinion, a strong indication that fragmentation is of minor importance.

4.4. ANALYTICAL MODEL

As a simple descriptive model, it should be relevant to use the "growing disk" idea, originally proposed by Pefferkorn et al. [12]. In this model, each molecule is described as a disk of initial area a_0 that is deposited on the surface. Immediately after surface attachment, the disk starts to grow exponentially with a growth rate characterised by the time τ_s and a limiting size $a_0 + \alpha$. For a single disk adsorbed at time t' the following equation for the occupied area is supposed:

$$a(t;t') = a_0 + \alpha\left(1 - e^{-(t-t')/\tau_s}\right). \tag{4.4.1}$$

As a first approximation we assume that the adsorption rate is proportional to the free surface area fraction β,

$$\frac{\mathrm{d}\Gamma}{\mathrm{d}t} = J_0\beta, \tag{4.4.2}$$

where Γ is simply the number of disks per unit area. We start an adsorption experiment at $t = 0$ and follow the adsorbed amount in time. During a time interval $\mathrm{d}t'$ the adsorbed amount will increase by an amount $\mathrm{d}n = J_0\beta(t')\,\mathrm{d}t'$. At time t, these disks will contribute to the fraction of occupied area $1 - \beta$ by an amount $J_0\beta(t')a(t;t')\mathrm{d}t'$. The time dependence of β is now found by integrating over all populations, i.e. all values of t':

$$\beta(t) = 1 - J_0\int_0^t \mathrm{d}t'\,\beta(t')\left[a_0 + \alpha\left(1 - e^{-(t-t')/\tau_s}\right)\right]. \tag{4.4.3}$$

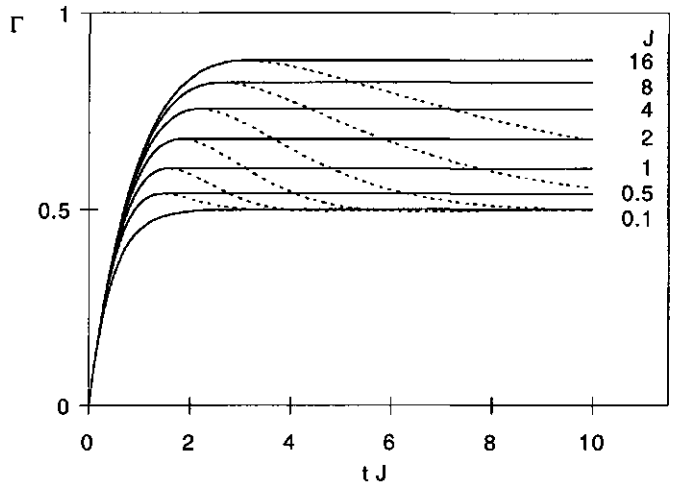

FIGURE 4.4. *Calculated adsorption kinetics using the "growing disk" model. Variables scaled as in eq. (4.4.4), $\alpha = 1$. No desorption is taken into account. The solution of the differential equation after the time that $\Gamma_{\max}$ is reached is dotted.*

In order to solve this equation and find a general expression for the adsorption behaviour it is useful to switch to dimensionless variables. Using the following rescaling

$$t/\tau_s \to t, \qquad J_0 a_0 \tau_s \to J, \qquad \alpha/a_0 \to \alpha, \tag{4.4.4}$$

we can write eq. (4.4.3) as

$$\beta(t) = 1 - J \int_0^t \mathrm{d}t' \, \beta(t') \left[1 + \alpha \left(1 - e^{-(t-t')}\right)\right]. \tag{4.4.5}$$

After differentiating this equation twice with respect to t and some rewriting, we arrive at the following linear, homogeneous second-order differential equation:

$$\frac{\mathrm{d}^2\beta}{\mathrm{d}t^2} + (1 + J)\frac{\mathrm{d}\beta}{\mathrm{d}t} + J(1 + \alpha)\beta(t) = 0. \tag{4.4.6}$$

This equation is the analog of the differential equation describing the movement of a damped pendulum. The solution can be found in any mathematical or physical handbook (see, e.g. ref. 13).

In solving eq. (4.4.6) we use the following boundary conditions

$$\beta(0) = 1, \qquad \left(\frac{\mathrm{d}\beta}{\mathrm{d}t}\right)_{t=0} = -J, \tag{4.4.7}$$

and we define the discriminant D as follows

$$D = (1 + J)^2 - 4J(1 + \alpha). \tag{4.4.8}$$

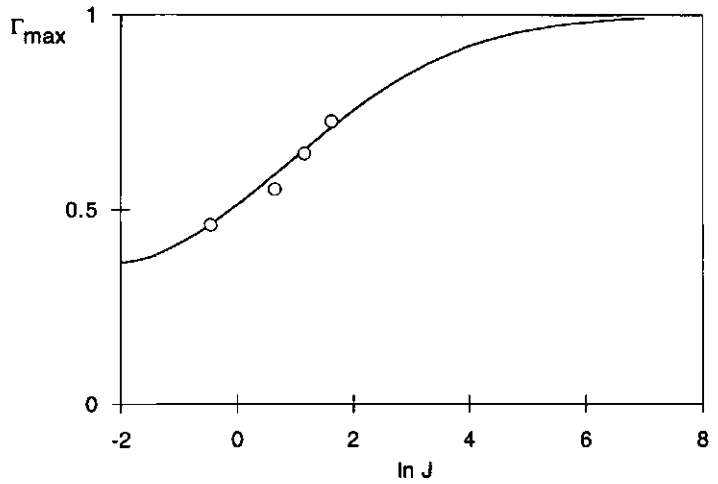

(a) Savinase/SiO_2 system, data taken from fig. 4.2 (∘) with $a_0 = 0.46\ \mathrm{m^2mg^{-1}}$, $\alpha/a_0 = 1.75$, and $\tau_s = 100$ s.

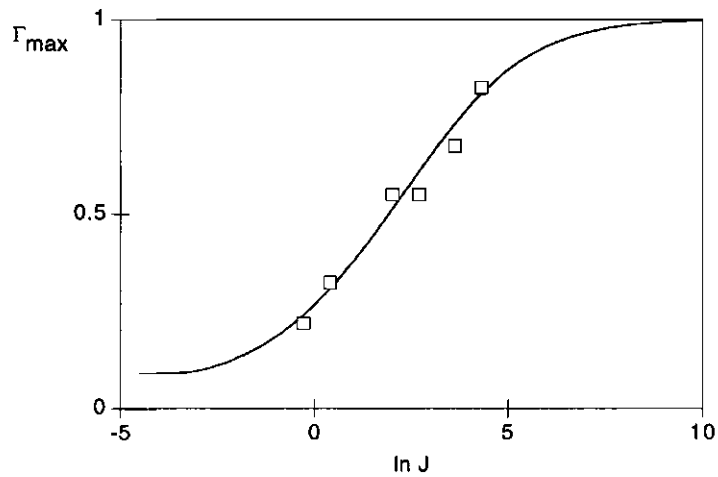

(b) IgG/SiO_2 system (□) with $a_0 = 0.25\ \mathrm{m^2mg^{-1}}$, $\alpha/a_0 = 10$, and $\tau_s = 4\times10^3$ s.

FIGURE 4.5. Maximum adsorbed amount as function of the flux as calculated by the "growing disk" model (solid lines) compared with the experimental results for savinase and IgG. Variables scaled as in eq. (4.4.4).

This leads to three different solutions:

$$\beta = \begin{cases} \left(1 + \frac{1-J}{2}t\right) e^{-t(J+1)/2} & \text{if } D = 0, \\ \frac{J-1+\sqrt{D}}{2\sqrt{D}} e^{-t(J+1+\sqrt{D})/2} - \frac{J-1-\sqrt{D}}{2\sqrt{D}} e^{-t(J+1-\sqrt{D})/2} & \text{if } D > 0, \\ \left(\cos\frac{t\sqrt{-D}}{2} + \frac{1-J}{\sqrt{-D}} \sin\frac{t\sqrt{-D}}{2}\right) e^{-t(J+1)/2} & \text{if } D < 0, \end{cases} \tag{4.4.9}$$

where only the solutions for positive, real values of J and α are physically realistic. The adsorbed amount is found by using eq. (4.4.2), thus integrating eq. (4.4.9):

$$\Gamma = J \int_0^t \mathrm{d}t' \, \beta(t'). \tag{4.4.10}$$

All three cases can be solved analytically. It should, however, be noted that eq. (4.4.10) should only be used as long as Γ increases, because eq. (4.4.2) is not intended to describe desorption. Therefore, we retain only the solutions of this integral until the time where $\beta(t) = 0$ for the first time (here $\Gamma = \Gamma_{\max}$). In the case of strong adsorption, as is the case for savinase or IgG on SiO_2, desorption is very slow, and hence, we consider the adsorbed amount as constant after the aforementioned time. As an example of the abilities of the model, fig. 4.4 shows the adsorption kinetics for the adsorbing disks with $\alpha = 1$ for a few values of J. Figure 4.5(a) shows $\Gamma_{\max}$ as function of J for $\alpha = 1.75$, and for comparison the data of savinase is also plotted. In fig. 4.5(b) this procedure is repeated for IgG with $\alpha = 10$. The used values for the model parameters (non-rescaled) are depicted in table 4.1.

TABLE 4.1. Model parameters for savinase and IgG adsorption on SiO_2.

Protein	$a_0/\mathrm{m^2mg^{-1}}$	α/a_0	τ_s/s
Savinase	0.46	1.75	100
IgG	0.25	10	4×10^3

Although there is no exact agreement of the adsorption kinetics of the two proteins with the "growing disk" model, the main effects are predicted well. The model could be improved by also introducing a desorption mechanism and by examining the validity of eqs. (4.4.1) and (4.4.2).

ACKNOWLEDGEMENTS

We thank Marcel Minor and Frans Leermakers for very helpful discussions, and Monique Bremer for carrying out the experiments on IgG.

REFERENCES

[1] G. J. Fleer, M. A. Cohen Stuart, J. M. H. M. Scheutjens, T. Cosgrove, and B. Vincent. *Polymers at Interfaces.* Chapman & Hall, London, 1993.

[2] H. M. Schneider, P. Frantz, and S. Granick. The bimodal energy landscape when polymers adsorb. *Langmuir*, 12:994–996, 1996.

[3] J. Buijs, P. A. W. van den Berg, J. W. Th. Lichtenbelt, W. Norde, and J. Lyklema. Adsorption dynamics of IgG and its $F(ab')_2$ and Fc fragments studied by reflectometry. *J Colloid Interface Sci*, 178:594–605, 1996.

[4] M. C. L. Maste. *Proteolytic stability in colloidal systems; interactions of proteins with the solid-water interface.* PhD thesis, Wageningen, 1996. Chapter 3.

[5] M. G. E. G. Bremer and W. Norde. The adsorption of IgG on solid surfaces: electrostatic interactions. To be submitted.

[6] J. C. Dijt, M. A. Cohen Stuart, J. E. Hofman, and G. J. Fleer. Kinetics of polymer adsorption in stagnation point flow. *Colloids Surfaces*, 51:141–158, 1990.

[7] J. C. Dijt, M. A. Cohen Stuart, and G. J. Fleer. Reflectometry as a tool for adsorption studies. *Adv Colloid Interface Sci*, 50:79–101, 1994.

[8] T. Dąbroś and T. G. M. van de Ven. A direct method for studying particle deposition onto solid surfaces. *Colloid Polym Sci*, 261:694–707, 1983.

[9] A. V. Elgersma, R. L. J. Zsom, W. Norde, and J. Lyklema. The adsorption of different types of monoclonal immunoglobulin on positively and negatively charged polystyrene latices. *Colloids Surfaces*, 54:89–101, 1991.

[10] Y. Adachi, M. A. Cohen Stuart, and R. Fokkink. Dynamic aspects of bridging flocculation studied using standardized mixing. *J Colloid Interface Sci*, 167:346–351, 1994.

[11] J. C. Dijt, M. A. Cohen Stuart, and G. J. Fleer. Competitive adsorption kinetics of polymers differing in length only. *Macromolecules*, 27:3219–3228, 1994.

[12] E. Pefferkorn and A. Elaissari. Adsorption-desorption processes in charged polymer/colloid systems; structural relaxation of adsorbed macromolecules. *J Colloid Interface Sci*, 138:187–194, 1990.

[13] R. C. Weast and M. J. Astle, editors. *CRC Handbook of Chemistry and Physics*, page A87. CRC Press, Boca Ranton, 62nd edition, 1981.

CHAPTER 5

Adsorption and spreading of polymers at plane interfaces; theory and molecular dynamics simulations

ABSTRACT

Nonequilibrium processes play a key role in the adsorption kinetics of macromolecules. It is expected that the competition between transport of polymer towards an interface and its subsequent spreading has a significant influence on the adsorbed amount. An increase of the transport rate can lead to an increase of the adsorbed amount, especially when the polymer has too little time to spread at the interface. In this study we present both molecular dynamics simulations and analytical calculations to describe some aspects of the adsorption kinetics. From MD simulations on a poly(ethylene oxide) chain in vacuum near a graphite surface, we conclude that the spreading process can, in first approximation, be described by either a simple exponential function or by first-order reaction kinetics. Combining these spreading models with the transport equations for two different geometries (stagnation-point flow and overflowing cylinder) we are able to derive analytical equations for the adsorption kinetics of polymers at solid–liquid and at liquid–fluid interfaces.

5.1. INTRODUCTION

The adsorption process of polymers frequently involves long-lived nonequilibrium states. The equilibrium structure of a polymer layer, as described by numerous statistical theories (see, e.g. ref. 1), is insufficient to describe various effects observed in adsorption kinetics and statics. Several experimental studies report significant nonequilibrium processes in polymer adsorption [2–5]. One of the important parameters in the surface relaxation is the strength of the polymer–surface interaction. If the interaction energy of a single polymer segment with the interface exceeds $1kT$, then thermal fluctuations are not able to *release* parts of the polymer easily, which is necessary for its spreading. Polymers adsorbed from organic solvents on mineral surfaces interact by strong hydrogen bonds, and are therefore likely to form long-living nonequilibrium states.

Such a system was studied by Schneider et al. [4]. From their adsorption experiments with poly(methyl methacrylate) on silica from CCl_4 they concluded that as long as the surface coverage is low, arriving polymers will flatten and a relatively large number of polymer–surface contacts will be achieved, whereas molecules arriving at a later stage in the adsorption process will adsorb with a low bound fraction. This nonequilibrium

situation turned out to be quite stable. This observation implies that polymer flux towards an interface together with the time dependent adsorbed amount $\Gamma(t)$ should have an effect on the state in which a polymer adsorbs. A slow spreading process will initially lead to a relatively small area per molecule, and thus to a relatively high adsorbed amount. Subsequent relaxation by spreading leads to an increased area per molecule, which is only possible when it is accompanied by a desorption process. This delayed spreading will lead to a decrease of $\Gamma(t)$. In this scenario a maximum (*overshoot*) in the adsorption curve will be found.

Overshoots have indeed been observed in a number of cases, both for proteins [5, 6] and for synthetic polymers [2–4]. In addition, spreading plays a role in polymer–polymer exchange processes [7]. As yet, very little is known about the factors controlling the rate of the spreading process. Moreover, apart from a scaling calculation in a recent paper by Semenov and Joanny [8], the consequences of spreading for the overall adsorption kinetics have hardly been investigated.

In this paper two cases are considered: adsorption from flowing solution onto a solid surface, and adsorption onto an expanding liquid-gas or liquid–liquid interface. In the latter case, the rate of expansion of the interface enters the problem as a additional timescale. Pefferkorn and Elaissari [2] have introduced the "growing disk" model. In this model, each molecule is described as a disk with initial radius $S(0)$ that arrives at the interface. Immediately after attachment, the disk starts to grow exponentially with a growth rate characterised by a spreading time τ and a limiting size $S(\mathrm{eq})$. As described in chapter 4, we already successfully applied an analytical version of this model to the adsorption of savinase (see also ref. 5) and immunoglobulin G on SiO_2. It should be important to see how realistic the "growing disk" model is. To this end we carried out molecular dynamics simulations on individual chains near a solid surface. We divided this study into two parts. In the first one, we introduce the relevant transport and spreading processes and also explore the latter at its molecular level. Secondly, we present analytical calculations based on the "growing disk" approach together with the two geometries in order to describe adsorption processes where spreading occurs on experimental timescales. Special attention is paid to two different spreading models.

5.2. TRANSPORT AND SPREADING

The adsorption kinetics of polymers can conveniently be subdivided into three stages. Firstly, a polymer has to reach the interface by, e.g. convection or diffusion. For this, the fluid dynamics of the studied system are of major importance. Secondly, an attachment of the polymer to the interface has to occur. Here several kinds of interactions may play a role, such as electrostatic or hydrophobic ones. Finally, a spreading of the molecule at the interface will occur. This spreading process will be governed by the gain or loss in the number of interaction sites between polymer and interface. Especially the characteristic times of the first and the last step in the adsorption process are of great importance for the final kinetics. Pefferkorn and Elaissari [2] applied a "growing disk" model to the adsorption kinetics of polyelectrolytes at a solid surface. They used

numerical calculations to arrive at their final results. Here, we will discuss an analytical version of a comparable model, but we will also introduce a more general n-state model to address adsorption kinetics.

In the following, we will present the transport process for the case of two widely used experimental setups. Subsequently we will concentrate on two spreading models that will be used in the description of adsorption kinetics of macromolecules. We have applied molecular dynamics simulations to elucidate the spreading behaviour. These simulations justify our spreading models.

5.2.1. Transport to the interface

The first step in trying to describe the adsorption kinetics of polymers, is deriving expressions for the transport of the molecules to the interface. In order to keep the equations relatively simple, it is necessary to work with well-defined geometries for which fluid-dynamical relations can be derived easily. In the following, we will first discuss adsorption from solution to a solid surface in a stagnation-point flow (for a rigourous fluid-dynamical approach see ref. 9). This setup gained much interest in reflectometric studies on polymer adsorption. A description of this technique in combination with a stagnation-point flow is given by Dijt et al. [10, 11]. Another widely used setup which will be treated is the overflowing cylinder. This geometry is used for studying the adsorption of, e.g. proteins at an air-water interface. The fluid dynamics of this geometry are described by Bergink-Martens et al. [12].

Stagnation-point flow. Figure 5.1 shows a schematic representation of a stagnation-point flow. The axial symmetry in the problem makes the use of cylindrical coordinates obvious. The radius of the tube is denoted by R and the distance between the outlet of the tube and the plane is given by h. We choose the stagnation-point (i.e. where the fluid velocity $\mathbf{v} = \mathbf{0}$) as the origin of our coordinate system, where r denotes the radial direction, z the direction along the symmetry axis into the fluid, and ϕ the rotation around this axis. Dąbroś and Van de Ven [9] derived the following expressions for the three components of the velocity near the stagnation point for an incompressible Newtonian fluid (in dimensionless form):

$$v_r = \hat{\alpha} z r \tag{5.2.1a}$$

$$v_z = -\hat{\alpha} z^2 \tag{5.2.1b}$$

$$v_\phi = 0, \tag{5.2.1c}$$

where $\hat{\alpha}$ is a dimensionless flow intensity parameter depending on the Reynolds number Re and the ratio h/R. The distances r and z are made dimensionless with respect to R, and the velocity $\mathbf{v}$ with respect to the average fluid velocity U at $z = h/R$. We will use this flow field near the stagnation point for the solution of the convective diffusion equations for the transport of polymer to the interface. As flow intensity parameter we will use α which is defined as $\alpha = \hat{\alpha} U/R^2$, retaining the appropriate dimensions for the variables.

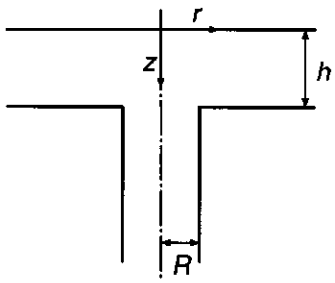

FIGURE 5.1. Geometry of a stagnation-point flow setup. Fluid moves along the axes of symmetry in a tube of radius R and enters between two planes distance h apart. The stagnation point is the origin of a cylindrical coordinate system r, z, and ϕ (not shown).

Using conservation of mass, we write for the transport of solute i

$$\frac{\partial c_i}{\partial t} = -\nabla \cdot \mathbf{J}_i, \tag{5.2.2}$$

where $\mathbf{J}_i$ is the net flux and c_i the concentration of the solute (polymer). In the mentioned stagnation-point flow, diffusion and convection determine the flux. Due to the axial symmetry of the system only the r and z-components of the flux are non-zero and are given by

$$J_{ri} = c_i v_r - D_i \frac{\partial c_i}{\partial r}, \tag{5.2.3a}$$

$$J_{zi} = c_i v_z - D_i \frac{\partial c_i}{\partial z}, \tag{5.2.3b}$$

where D_i is the diffusion coefficient for component i. It must be noted that these equations are valid only under the assumption that hydrodynamic interactions are cancelled by the specific interactions between the interface and the solute [13] (Smoluchowski-Levich approximation). If we neglect radial diffusion (i.e. $D_i \partial c_i/\partial r \ll c_i v_r$) then substitution of these equations in eq. (5.2.2), where we take $\nabla \cdot \mathbf{v} = 0$ because of the incompressibility constraint, gives for the stationary state

$$\frac{\partial}{r\partial r}(r c_i v_r) + \frac{\partial c_i v_z}{\partial z} = D_i \frac{\partial^2 c_i}{\partial z^2}. \tag{5.2.4}$$

Substituting eq. (5.2.1) into this equation gives us

$$\alpha r z \frac{\partial c_i}{\partial r} - \alpha z^2 \frac{\partial c_i}{\partial z} = D_i \frac{\partial^2 c_i}{\partial z^2}. \tag{5.2.5}$$

Symmetry implies that $\partial c_i/\partial r = 0$ at the stagnation point, thus for $r = 0$ we rewrite eq. (5.2.5) as the linear differential equation

$$-\alpha z^2 \frac{\partial c_i}{\partial z} = D_i \frac{\partial^2 c_i}{\partial z^2}. \tag{5.2.6}$$

We are now able to derive an analytic expression for the flux J_{zi} at the stagnation point. The solution of eq. (5.2.6) is

$$\frac{\partial c_i}{\partial z} = K_i \exp\left(-\frac{\alpha z^3}{3D_i}\right). \tag{5.2.7}$$

The constant K_i can be found by noticing that c_i must be equal to the bulk concentration far away from the interface and c_i^0 to that in the vicinity of the interface. This subsurface concentration can in principle be found by assuming local equilibrium, implying a direct relationship between the adsorbed amount and c_i^0. We write

$$\int_0^\infty \mathrm{d}z \frac{\partial c_i}{\partial z} = c_i^\mathrm{b} - c_i^0, \tag{5.2.8}$$

from which we can calculate

$$K_i = \frac{(c_i^\mathrm{b} - c_i^0)}{\Gamma\left(\frac{1}{3}\right)} \left(\frac{9\alpha}{D_i}\right)^{\frac{1}{3}}, \tag{5.2.9}$$

where $\Gamma(x) = \int_0^\infty \mathrm{d}t\, e^{-t} t^{x-1}$ denotes the Gamma function. The flux of polymer i towards the stagnation point is now given by

$$\begin{aligned} J_{zi}(0) &= D_i \frac{\partial c_i}{\partial z}\bigg|_{z=0} \\ &= \frac{(c_i^\mathrm{b} - c_i^0) D_i^{\frac{2}{3}} (9\alpha)^{\frac{1}{3}}}{\Gamma\left(\frac{1}{3}\right)}. \end{aligned} \tag{5.2.10}$$

We will also use the limiting flux J_{0i}, which is defined as the flux $J_{zi}(0)$ for the situation where $c_i^0 = 0$.

Overflowing cylinder. A schematic representation of the overflowing cylinder is given in fig. 5.2. In this setup, again, a stagnation point exists. We choose this as the origin of our cylindrical coordinate system. In contrast to the stagnation-point flow discussed above, we are now dealing with an *expanding* interface, which introduces a new timescale. Bergink-Martens et al. [12] showed that if $r \ll R$, the relative expansion rate of the surface $\vartheta = \mathrm{d}A/(A\,\mathrm{d}t)$ is constant. The fluid velocities near the stagnation point are given by

$$v_r = \frac{\vartheta r}{2}, \tag{5.2.11a}$$

$$v_z = -\vartheta z, \tag{5.2.11b}$$

$$v_\phi = 0. \tag{5.2.11c}$$

The equations that describe the flux have already been discussed; again eqs. (5.2.2)–(5.2.4) can be used to obtain an expression for the flux towards the interface in the vicinity of the stagnation point. We substitute eq. (5.2.11) into eq. (5.2.4) to arrive at

$$\frac{\vartheta r}{2}\frac{\partial c_i}{\partial r} - \vartheta z \frac{\partial c_i}{\partial z} = D_i \frac{\partial^2 c_i}{\partial z^2}. \tag{5.2.12}$$

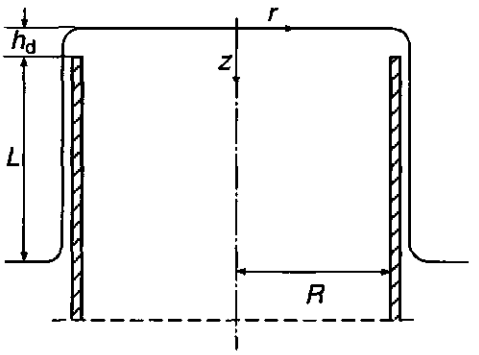

FIGURE 5.2. Geometry of an overflowing cylinder. Fluid moves upwards in a cylinder of radius R, which will overflow, giving rise to a free expanding surface. The height L of the falling film together with the flow rate Q determine the relative expansion rate $\vartheta = \mathrm{d}A/(A\,\mathrm{d}t)$. Again, the stagnation point is the origin of a cylindrical coordinate system r, z, and ϕ (not shown).

Symmetry implies that $\partial c_i/\partial r$ is zero at the stagnation point and negligible in its neighbourhood. Equation (5.2.12) then simplifies to

$$-\vartheta z \frac{\partial c_i}{\partial z} = D_i \frac{\partial^2 c_i}{\partial z^2}, \tag{5.2.13}$$

which is easily solved to obtain

$$\frac{\partial c_i}{\partial z} = K_i \exp\left(-\frac{\vartheta z^2}{2D_i}\right). \tag{5.2.14}$$

We use the boundary condition given by eq. (5.2.8) and obtain an expression for the integration constant

$$K_i = (c_i^{\mathrm{b}} - c_i^0)\left(\frac{2\vartheta}{D_i \pi}\right)^{\frac{1}{2}}. \tag{5.2.15}$$

With this equation we calculate the flux of solute i towards the interface at the stagnation point

$$\begin{aligned} J_{zi}(0) &= D_i \left.\frac{\partial c_i}{\partial z}\right|_{z=0} \\ &= (c_i^{\mathrm{b}} - c_i^0)\left(\frac{2\vartheta D_i}{\pi}\right)^{\frac{1}{2}}. \end{aligned} \tag{5.2.16}$$

Again, J_{0i} will be used to express the limiting flux for $c_i^0 = 0$. The main difference of the flux between a stagnation-point flow and an overflowing cylinder setup is the different dependence on the diffusion coefficient ($D_i^{2/3}$ vs. $D_i^{1/2}$).

5.2.2. Spreading models

We are now able to describe the transport of a polymer towards an interface, but are still left with the problem of rearrangements after attachment. We will model this process as a spreading of polymer molecules at the interface. First, we will describe the rather crude, but useful, "growing disk" model, which was also used by Pefferkorn and Elaissari to model polymer adsorption kinetics [2]. Subsequently, we will discuss a simple n-step model based on first-order reaction kinetics.

In the "growing disk" model we assume that a polymer attaches to the interface in a coil conformation ($\mathcal{C}$) comparable to that in solution. After attachment the polymer will spread to its final conformation, denoted by $\mathcal{S}$. The process is then given by

$$\mathcal{C} \xrightarrow{\text{growing disk}} \mathcal{S}. \tag{5.2.17}$$

We take a simple exponential function for this spreading process, such that the area occupied by a polymer attached at time t' is given by

$$s(t-t') = s_c + (s_s - s_c)\left(1 - e^{-\frac{t-t'}{\tau_s}}\right), \tag{5.2.18}$$

where s_c and s_s are the initial and final occupied area of the molecule per unit mass, respectively.

A discrete form of the "growing disk" model is obtained if we assume that the polymer can be present at the interface in $n+1$ different conformations. Schematically the spreading process can then be depicted as

$$\mathcal{P}_0 \underset{k_{-1}}{\overset{k_{+1}}{\rightleftarrows}} \mathcal{P}_1 \cdots \mathcal{P}_{n-1} \underset{k_{-n}}{\overset{k_{+n}}{\rightleftarrows}} \mathcal{P}_n, \tag{5.2.19}$$

where k_{+i} and k_{-i} are reaction rate constants for the surface processes. The areas per unit mass for the $n+1$ states are denoted by s_i. We can simply apply first-order reaction kinetics to calculate the adsorbed amounts of the different conformations. There also exists a direct relation between the adsorbed amounts and the surface coverage θ:

$$\theta = \sum_{i=0}^{n} \Gamma_i s_i, \tag{5.2.20}$$

In practice it is useful to use the one-step version of this model, defining $k_f \equiv k_{+1}$ and $k_b \equiv k_{-1}$ as reaction rate constants, and take s_c and s_s as the area of the polymer in the initial and final state, respectively.

5.2.3. Molecular dynamics

Before proceeding to an analytical description of the adsorption kinetics of spreading polymers, we would like to give a possible justification on a molecular level for the introduced spreading models. To this end, we carried out some molecular dynamics simulation on a fairly simple model system, from which we are able to extract the spreading behaviour near a solid surface.

Model system and procedure. One of the aspects to keep in mind when trying to simulate the spreading of a polymer near an interface, is the accessible timescale. It should be clear that we should pick a model system where spreading will be fast, and as a consequence we have to limit ourselves to relatively small flexible molecules at a very low density.

The systems we studied all consist of a single chain of poly(ethylene oxide) (PEO) with protons as end groups near a graphite surface. We will denote these polymers as EO_n, where n is the number of ethylene oxide groups. The graphite surface is a single layer consisting of 1881 C-atoms. All simulations on the PEO system were carried out using the commercially available software Insight II 4.0.0 from MSI together with the Discover 96.0/4.0.0 module. To get reliable results on the spreading behaviour of PEO, each simulation was build up in four stages. Before going in these details, we first mention some characteristics of the MD simulation.

The microscopic state of a system of N atoms can be described in terms of the positions ($\mathbf{r}_i$) and momenta ($\mathbf{p}_i$) of the contained atoms. To characterise the system we will use a convenient condensed notation

$$\mathbf{r} = (\mathbf{r}_1, \mathbf{r}_2, \ldots, \mathbf{r}_N) \tag{5.2.21a}$$

$$\mathbf{p} = (\mathbf{p}_1, \mathbf{p}_2, \ldots, \mathbf{p}_N). \tag{5.2.21b}$$

As is common, we write the Hamiltonian of the system as a sum of potential and kinetic energy terms:

$$\mathcal{H}(\mathbf{r}, \mathbf{p}) = \mathcal{V}(\mathbf{r}) + \mathcal{K}(\mathbf{p}). \tag{5.2.22}$$

We use the consistent valence force field from the Discover module without cross terms arriving at the following expression for the potential energy contribution to the Hamiltonian:

$$\begin{aligned} \mathcal{V}(\mathbf{r}) = & \sum_i k_{bi} \left(b_i - b_i^0\right)^2 + \sum_i k_{\theta i} \left(\theta_i - \theta_i^0\right)^2 \\ & + \sum_i k_{\phi i} \left(1 + \cos\left(n\phi_i - \phi_i^0\right)\right) + \sum_i k_{\chi i} \left(1 + \cos\left(n\chi_i - \chi_i^0\right)\right) \\ & + \sum_{ij} \left(\left(\frac{A_{ij}}{r_{ij}}\right)^{12} - \left(\frac{B_{ij}}{r_{ij}}\right)^{6} \right) + \sum_{ij} \frac{q_i q_j}{4\pi\epsilon r_{ij}}, \end{aligned} \tag{5.2.23}$$

where b_i is a bond length, θ_i a bond angle, ϕ_i a torsion angle, χ_i an out-of-plane angle to correct for torsional bonds $\phi_i \approx \pi$ in the case of π-bonds (cis-conformation), and q_i the charge of an atom. The distance between atom i and j is denoted by r_{ij}. All other symbols denote constants depending on the kind of concerned atoms, which define the force field. The Lennard-Jones potential is calculated only to a cut-off radius $r_{ij} = 2.5$ nm, and the electrostatic contribution to a cut-off radius $r_{ij} = 0.95$ nm.

In our MD simulations we imply effectively no boundary conditions, allowing the polymer to move freely in vacuum. At the beginning, the system is arranged so that the centre of mass ($\mathbf{R}_{\text{cm}}$) of the PEO molecule is at a distance of 5 nm from the graphite sheet plane. We choose the origin of a Cartesian coordinate system to be in the graphite

plane and the z-direction perpendicular to it. To save computational time, the carbon atoms in the graphite layer are held fixed to their initial positions during all steps of the simulation. However, they will contribute to the non-bond terms of the potential energy in their interactions with the PEO.

Having situated the PEO molecule far from the surface we perform a potential energy minimisation to equilibrate the polymer structure. For this purpose we use a cascade of two minimisers, starting with the steepest-descent method, followed by the conjugate-gradient one. The steepest-descent algorithm is used to make sure that any severe strain within the polymer chain is removed. We apply this method until the gradient of the potential energy with respect to the atom coordinates $|\nabla_{\mathbf{r}}\mathcal{V}(\mathbf{r})| \leq 4.184 \times 10^{16}\ \mathrm{J\,mol^{-1}m^{-1}}$. We then proceed with the conjugate-gradient method until $|\nabla_{\mathbf{r}}\mathcal{V}(\mathbf{r})| \leq 4.184 \times 10^{10}\ \mathrm{J\,mol^{-1}m^{-1}}$. After this minimisation step the PEO molecule has adopted a structure close to a local potential energy minimum.

In the presence of a fully minimised configuration of PEO, we can start the molecular dynamics simulation with a target temperature $T = 298$ K in a NVT ensemble. To force the polymer towards the surface, we apply a constraint to the centre of mass of the PEO. So, in the potential energy an extra term

$$v_{\mathrm{cm}} = k(z_{\mathrm{cm}} - z_0)^2 \tag{5.2.24}$$

occurs, with $k = 2.092 \times 10^{27}\ \mathrm{J\,mol^{-1}m^{-1}}$ and $z_0 = 2.5$ nm. This quadratic potential is used during the first 10000 steps of 1 fs of our simulation. The polymer is than close enough to the surface to start our final step in the MD simulation.

Before the adsorption and spreading stage, we replace the previously introduced quadratic constrained by a flat-bottomed constraint

$$v_{\mathrm{cm}} = \begin{cases} k(z_{\mathrm{cm}} - z_0)^2 & \text{for } z_{\mathrm{cm}} < z_0, \\ 0 & \text{for } z_0 \leq z_{\mathrm{cm}} \leq z_1, \\ k(z_{\mathrm{cm}} - z_1)^2 & \text{for } z_{\mathrm{cm}} > z_1, \end{cases} \tag{5.2.25}$$

where $z_0 = 0$ nm, $z_1 = 2.5$ nm, and $k = 4.184 \times 10^{12}\ \mathrm{J\,mol^{-1}m^{-1}}$. This restraint prevents the PEO from moving too far from the graphite surface without influencing its behaviour in the vicinity of the surface. We run the MD simulation over 60000 time steps of 1 fs. Every 10 fs all atom coordinates are stored for post-processing.

In our simulations we varied the chain length ($n = 10, 30, 50$) and the interaction between PEO and the graphite sheet. The latter is achieved by scaling the Lennard-Jones potential between polymer atoms and graphite atoms by a factor γ.

From the stored atom positions of PEO, taken from $\mathbf{r}$ every 10 fs, we calculated a number of relevant quantities in order to visualise the adsorption and spreading process. The position of the polymer is reflected in the position of the centre of mass which is defined as

$$\mathbf{R}_{\mathrm{cm}} \equiv \frac{\sum_{i=1}^{N_{\mathrm{P}}} m_i \mathbf{r}_i}{\sum_{i=1}^{N_{\mathrm{P}}} m_i}, \tag{5.2.26}$$

where m_i is the mass of atom i and N_p is the number of atoms in the PEO molecule. This $\mathbf{R}_\mathrm{cm}$ can subsequently be used to calculate a mean distance of the PEO molecule to the surface

$$z_\mathrm{cm} = \mathbf{R}_\mathrm{cm} \cdot \mathbf{e}_z, \tag{5.2.27}$$

where $\mathbf{e}_z$ is the unit vector in the z-direction of the Cartesian coordinate system. The spreading process can be monitored by following the evolution of the parallel radius of gyration of PEO, defined as

$$R_{\mathrm{g}\|}^2 \equiv \frac{\sum_{i=1}^{N_\mathrm{p}} m_i \left((\mathbf{r}_i - \mathbf{R}_\mathrm{cm})^2 - ((\mathbf{r}_i - \mathbf{R}_\mathrm{cm}) \cdot \mathbf{e}_z)^2 \right)}{\sum_{i=1}^{N_\mathrm{p}} m_i}. \tag{5.2.28}$$

Furthermore, the distribution of the PEO atoms perpendicular to the surface is calculated. To this end, the number of atoms N_i in layer i of 0.5 nm in thickness, parallel to the surface, are counted for 5 layers. The fraction of atoms in layer i is then denoted by $x_i = N_i/N_\mathrm{p}$.

MD Results. As an example of the observed effects for the adsorption and spreading of PEO on a graphite surface, we will illustrate here the results obtained for EO_{30} with $\gamma = 3$. Similar results were also found for the other studied systems. At the start of the MD simulation the PEO is approximately 2.5 nm from the surface, and has to approach it, before a polymer segment will be in contact with the graphite. How this happens is depicted in fig. 5.3, where the fraction of the EO_{30} that is present in a layer at a certain distance from the surface is plotted as function of time. Clearly, the polymer starts from layer 5 (2.0–2.5 nm from the surface), and subsequently adsorbs and mainly ends up in layers 1 and 2. This implies a rather flat conformation of the molecule in the adsorbed state. This observation confirms the existence of a spreading process. The approach towards the surface can also be nicely monitored by the time dependence of the vertical position of the centre of mass as defined by eq. (5.2.27), which is shown in fig. 5.4. From this plot, however, we are not able to draw satisfying conclusions about the time constant of the spreading process. A more suitable quantity for this purpose is the radius of gyration of the PEO parallel to the surface.

Figure 5.5 shows the time evolution of $R_{\mathrm{g}\|}^2$ for EO_{30}. The fact that the parallel size of the PEO decreases in the beginning of the simulation is caused by the fact that at that point the polymer is pulled towards the surface after release of the constraint in the potential energy from eq. (5.2.24). The spreading of the polymer is clearly seen, and in order to compare it to our introduced spreading models in the previous section (eq. (5.2.18)) we fitted the data to the following equation:

$$R_{\mathrm{g}\|}^2 = R_{\mathrm{g}0}^2 + \sigma \left(1 - \exp\left(-\frac{t - t_0}{\tau} \right) \right), \tag{5.2.29}$$

with $R_{\mathrm{g}0}^2 = 0.316$ nm^2, $\sigma = 0.334$ nm^2, $t_0 = 2.82$ ps, and $\tau = 5.18$ ps. In this fit t_0 and $R_{\mathrm{g}0}^2$ are taken from the data by hand. Comparison of this fit with the data suggests that a simple exponential function is a good first approximation for the spreading of a flexible polymer near an interface. One should bear in mind that the presented

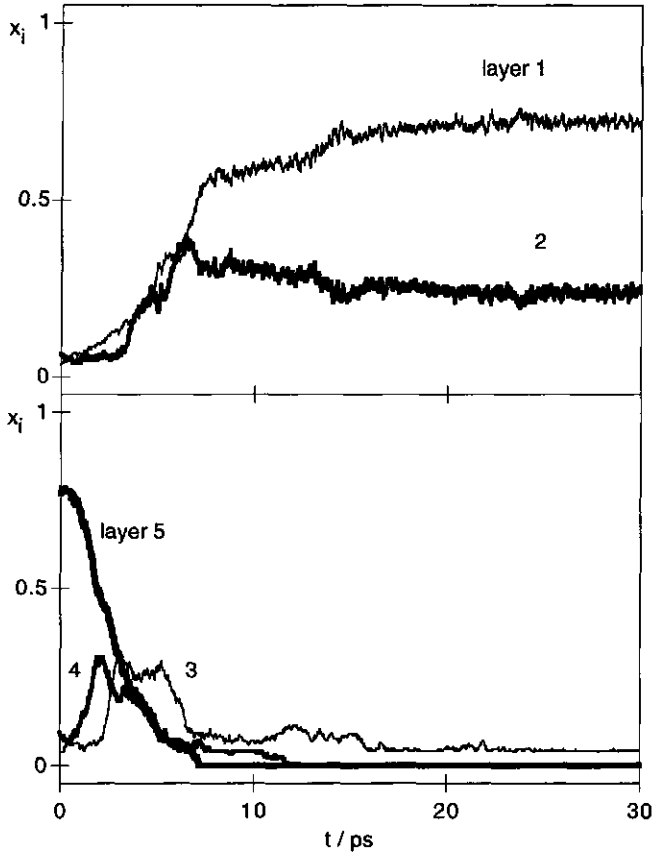

FIGURE 5.3. Fraction x_i of the atoms of EO_{30} in a 0.5 nm thick layer i ($i = 1, 2, 3, 4, 5$) parallel to the surface. The layers are numbered from the surface.

simulation only serves as an example, and that similar behaviour was observed for the other simulation runs. It should be evident that the presence of more polymers will complicate the situation. However, as long as the surface coverage is relatively low the single polymer approach serves as a good first approximation. For now we will use this crude model in our analytical calculations.

5.3. ANALYTICAL EXPRESSIONS FOR ADSORPTION KINETICS

In this section we will combine the above introduced transport equations and spreading models to arrive at analytical equations for the adsorption kinetics of macromolecules.

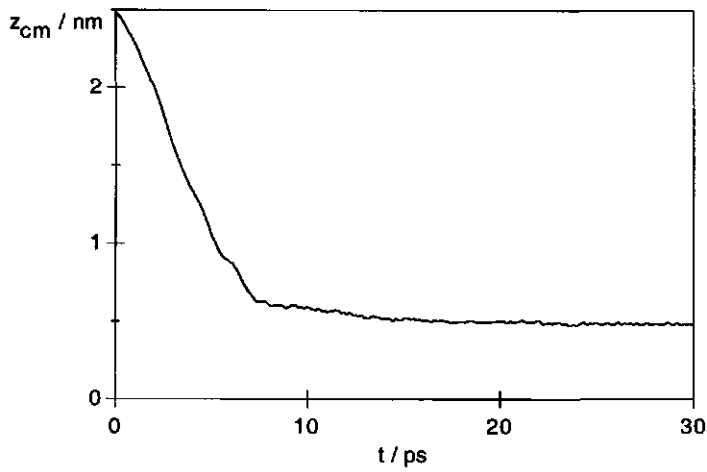

FIGURE 5.4. Approach of the centre of mass of EO_{30} to the graphite surface in the final stage of the MD simulation.

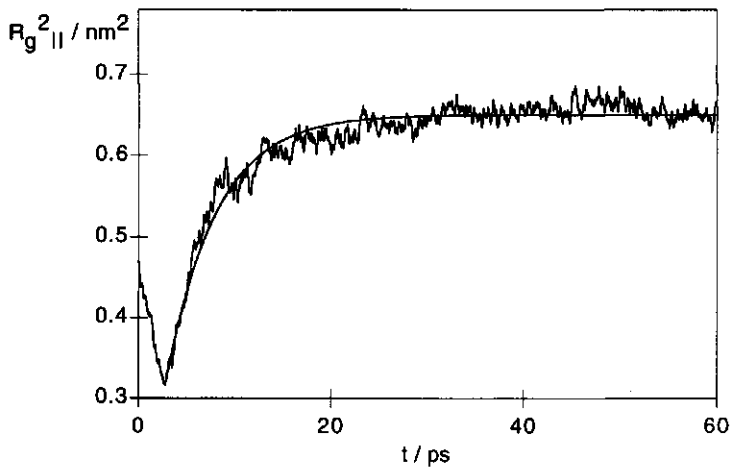

FIGURE 5.5. $R^2_{g||}$ as a measure for the occupied area of EO_{30} as a function of time. Also shown is a fit of the data to the function $R^2_{g||} = R^2_{g0} + \sigma\left(1 - \exp\left(-\frac{t-t_0}{\tau}\right)\right)$.

5.3.1. Adsorption at immobile interfaces

One of the most common interfaces for the adsorption of polymers is a solid–liquid one. In this case no convective polymer transport along the interface can occur. We will discuss the adsorption in a stagnation-point flow on such an immobile interface. If we assume that the attachment of polymer to the interface is fast as compared to the transport, then the adsorption rate is equal to the polymer flux J. So for the total

adsorbed amount we write

$$\frac{\mathrm{d}\Gamma}{\mathrm{d}t} = J = J_0 \frac{c^{\mathrm{b}} - c^0}{c^{\mathrm{b}}}. \tag{5.3.1}$$

The limiting flux J_0 is given by eq. (5.2.10), where we take $c_0 = 0$. Because the calculation of c_0 requires a non-trivial molecular model for the adsorption process, we will introduce a rather simplified model for the adsorption rate. We assume that the adsorption rate is proportional to the free surface area and the limiting polymer flux, giving

$$\frac{\mathrm{d}\Gamma}{\mathrm{d}t} = J_0 \beta, \tag{5.3.2}$$

where the relative free surface area is denoted as $\beta = 1 - \theta$. We realise that, using this assumption, we underestimate the adsorption rate, but it is a convenient first-order approximation which still allows us to predict the correct trends.

To take surface processes of the polymer into account, we will apply the two discussed spreading models to derive equations for the adsorbed amount.

Growing disk. When using the "growing disk" model it is most convenient the derive an equation for the relative free surface area β, which can be used to solve eq. (5.3.2). An amount $\mathrm{d}\Gamma$ adsorbed during a time interval $\mathrm{d}t'$ will occupy a fraction $\mathrm{d}\theta$ of the surface at time t given by

$$\mathrm{d}\theta = J_0 \beta(t') s(t - t') \mathrm{d}t'. \tag{5.3.3}$$

The occupied area $s(t-t')$ is taken from eq. (5.2.18). Before continuing it is convenient to non-dimensionalise all variables by the following rescaling:

$$J_0 s_{\mathrm{c}} \tau_{\mathrm{s}} \to J, \quad \Gamma s_{\mathrm{c}} \to \Gamma, \quad s_{\mathrm{s}}/s_{\mathrm{c}} \to \sigma, \quad t/\tau_{\mathrm{s}} \to t. \tag{5.3.4}$$

We obtain the relative free surface area by assuming an empty surface at $t = 0$, and calculating the fraction of occupied surface by integrating eq. (5.3.3). We then arrive at

$$\beta(t) = 1 - J \int_0^t \mathrm{d}t' \, \beta(t') \left(1 + (\sigma - 1)\left(1 - e^{t'-t}\right)\right). \tag{5.3.5}$$

This integral equation can be transformed to a differential equation by differentiating twice. After some rewriting we arrive at

$$\frac{\mathrm{d}^2\beta}{\mathrm{d}t} + (1 + J)\frac{\mathrm{d}\beta}{\mathrm{d}t} + J\sigma\beta = 0. \tag{5.3.6}$$

The solution of this linear, homogeneous differential equation is easily derived. Appendix 5.A.1 shows how it is done. The relevant boundary conditions of this equation are already contained in eq. (5.3.5), they are

$$\beta(0) = 1, \quad \left.\frac{\mathrm{d}\beta}{\mathrm{d}t}\right|_{t=0} = -J. \tag{5.3.7}$$

Equation (5.3.6) has three different solutions, depending on the roots of its characteristic equation. The discriminant of this equation is given by $D = (1 + J)^2 - 4J\sigma$.

The relative free surface area is calculated from eq. (5.A.2) by insertion of the boundary conditions. This leads to

$$\beta = -\frac{1-J-\sqrt{D}}{2\sqrt{D}} e^{-\frac{1+J+\sqrt{D}}{2}t} + \frac{1-J+\sqrt{D}}{2\sqrt{D}} e^{-\frac{1+J-\sqrt{D}}{2}t} \qquad \text{for } D > 0, \tag{5.3.8a}$$

$$\beta = \left(1 + \frac{1-J}{2}t\right) e^{-\frac{1+J}{2}t} \qquad \text{for } D = 0, \tag{5.3.8b}$$

$$\beta = \left(\cos\frac{\sqrt{-D}}{2}t + \frac{1-J}{\sqrt{-D}}\sin\frac{\sqrt{-D}}{2}t\right) e^{-\frac{1+J}{2}t} \qquad \text{for } D < 0. \tag{5.3.8c}$$

By noting that $\sqrt{-D} = i\sqrt{D}$, $\cos x = \cosh ix$, and $\sin x = -i\sinh ix$, it is easily seen that eq. (5.3.8a) is equivalent to eq. (5.3.8c). The adsorbed amount is now calculated by substitution of the previously obtained constants in eq. (5.A.3):

$$\frac{\Gamma}{J} = \frac{1}{J\sigma} + \frac{1-J-\sqrt{D}}{(1+J+\sqrt{D})\sqrt{D}} e^{-\frac{1+J+\sqrt{D}}{2}t} - \frac{1-J+\sqrt{D}}{(1+J-\sqrt{D})\sqrt{D}} e^{-\frac{1+J-\sqrt{D}}{2}t} \qquad \text{for } D > 0, \tag{5.3.9a}$$

$$\frac{\Gamma}{J} = \frac{1}{J\sigma} - \frac{4+(1-J^2)t}{(1+J)^2} e^{-\frac{1+J}{2}t} \qquad \text{for } D = 0, \tag{5.3.9b}$$

$$\frac{\Gamma}{J} = \frac{1}{J\sigma}\left[1 - \left(\cos\frac{\sqrt{-D}}{2}t + \frac{1-J^2+D}{2\sqrt{-D}}\sin\frac{\sqrt{-D}}{2}t\right) e^{-\frac{1+J}{2}t}\right] \qquad \text{for } D < 0. \tag{5.3.9c}$$

One-step model. Instead of finding an equation for the relative free surface area, it is also possible to obtain a set of differential equations directly, where we assume that a polymer can be present at the interface in two different states. We can then treat the adsorbed amount of the polymer in the different states separately. To this end, eq. (5.3.2) is replaced by

$$\frac{\mathrm{d}\Gamma_\mathrm{c}}{\mathrm{d}t} = J_0(1 - \Gamma_\mathrm{c}s_\mathrm{c} - \Gamma_\mathrm{s}s_\mathrm{s}) - k_\mathrm{f}\Gamma_\mathrm{c} + k_\mathrm{b}\Gamma_\mathrm{s}, \tag{5.3.10a}$$

$$\frac{\mathrm{d}\Gamma_\mathrm{s}}{\mathrm{d}t} = k_\mathrm{f}\Gamma_\mathrm{c} - k_\mathrm{b}\Gamma_\mathrm{s}, \tag{5.3.10b}$$

where the subscripts "c" and "s" refer to the coiled and spread states, respectively. The reaction constants for the forward (spreading) and backward (coiling) reaction are denoted by k_f and k_b. Again, we non-dimensionalise the equations by the rescaling

$$\frac{J_0 s_\mathrm{c}}{k_\mathrm{f}} \to J, \quad \Gamma_i s_\mathrm{c} \to \Gamma_i, \quad \frac{s_\mathrm{s}}{s_\mathrm{c}} \to \sigma, \quad \frac{k_\mathrm{b}}{k_\mathrm{f}} \to \kappa, \quad tk_\mathrm{f} \to t. \tag{5.3.11}$$

We write eq. (5.3.10) in a dimensionless Einstein matrix notation

$$\dot{\Gamma}_j = A_{jk}\Gamma_k + J_j \tag{5.3.12}$$

with the boundary condition $\Gamma_j(0) = 0$. Appendix 5.A.2 gives the general solutions of a set of m linear, nonhomogeneous first order differential equations. Our interest is in $m = 2$, for which the adsorbed amounts for the two states are given by

$$\Gamma_c = \frac{\kappa}{\kappa+\sigma} - J\frac{1+J-\kappa+\sqrt{D}}{\sqrt{D}(1+J+\kappa+\sqrt{D})}e^{-\frac{1+J+\kappa+\sqrt{D}}{2}t} + J\frac{1+J-\kappa-\sqrt{D}}{\sqrt{D}(1+J+\kappa-\sqrt{D})}e^{-\frac{1+J+\kappa-\sqrt{D}}{2}t}, \tag{5.3.13a}$$

$$\Gamma_s = \frac{1}{\kappa+\sigma} + \frac{2J}{\sqrt{D}(1+J+\kappa+\sqrt{D})}e^{-\frac{1+J+\kappa+\sqrt{D}}{2}t} - \frac{2J}{\sqrt{D}(1+J+\kappa-\sqrt{D})}e^{-\frac{1+J+\kappa-\sqrt{D}}{2}t}, \tag{5.3.13b}$$

where

$$D = (1+J+\kappa)^2 - 4J(\kappa+\sigma). \tag{5.3.14}$$

These equations are valid only if $D \neq 0$, i.e. the eigenvalues of A_{jk} are distinct. We will not give the equations for $D = 0$ here, because they are only limits of the general solution, and are therefore physically of little use. Finally, the surface coverage θ is easily calculated by substitution of eq. (5.3.13) in $\theta = \Gamma_c + \sigma\Gamma_s$.

Comparing the equation for the total adsorbed amount $\Gamma = \Gamma_c + \Gamma_s$ with eq. (5.3.9a) for the "growing disk" model, one observes that they are identical if we take $\kappa = 0$. This is what we expected, because the exponential function taken for the "growing disk" model is just the result of first order reaction kinetics without reverse reaction ($k_b = 0$).

5.3.2. Adsorption at expanding interfaces

Adsorption of polymers, and especially proteins, at expanding liquid–gas interfaces is of interest in, e.g. foaming processes. Again, we assume the adsorption rate to be proportional to the free surface area, but we also have to take into account the transport of polymer along the interface. Hence, the continuity equation reads

$$\frac{d\Gamma}{dt} = -\vartheta\Gamma + J_0\beta, \tag{5.3.15}$$

where it should be noted that the polymer flux J_0 is a function of the expansion rate of the interface (see eq. (5.2.16)). Unfortunately, it is in this case not possible to derive a simple equation for the free surface area β, because a polymer adsorbing at t' will be at another location at the interface at time t. Calculation of the occupied area therefore requires an Eulerian approach. So, in this case it is more convenient to use the one-step model.

One-step model. If we assume that a polymer is in a coiled state in solution, and can be in either a coiled or a spread state at the interface, we can rewrite eq. (5.3.15) for the adsorbed amounts of the two states as

$$\frac{\mathrm{d}\Gamma_\mathrm{c}}{\mathrm{d}t} = J_0(1 - \Gamma_\mathrm{c}s_\mathrm{c} - \Gamma_\mathrm{s}s_\mathrm{s}) - k_\mathrm{f}\Gamma_\mathrm{c} + k_\mathrm{b}\Gamma_\mathrm{s} - \vartheta\Gamma_\mathrm{c}, \tag{5.3.16a}$$

$$\frac{\mathrm{d}\Gamma_\mathrm{s}}{\mathrm{d}t} = k_\mathrm{f}\Gamma_\mathrm{c} - k_\mathrm{b}\Gamma_\mathrm{s} - \vartheta\Gamma_\mathrm{s}. \tag{5.3.16b}$$

We use the same rescaling as in eq. (5.3.11) with the addition of $\vartheta/k_\mathrm{f} \to \vartheta$. We use the same Einstein matrix notation as in the immobile interface case:

$$\dot{\Gamma}_j = A_{jk}\Gamma_k + J_j \tag{5.3.17}$$

with the boundary condition $\Gamma_j(0) = 0$. The solution can thus be taken from app. 5.A.2. The adsorbed amounts for the two states are given by

$$\begin{aligned}\Gamma_\mathrm{c} = {} & \frac{J(\kappa+\vartheta)}{J(\kappa+\sigma)+\vartheta(1+J+\kappa+\vartheta)} \\ & - J\frac{1+J-\kappa+\sqrt{D}}{\sqrt{D}(1+J+\kappa+2\vartheta+\sqrt{D})}e^{-\frac{1+J+\kappa+2\vartheta+\sqrt{D}}{2}t} \\ & + J\frac{1+J-\kappa-\sqrt{D}}{\sqrt{D}(1+J+\kappa+2\vartheta-\sqrt{D})}e^{-\frac{1+J+\kappa+2\vartheta-\sqrt{D}}{2}t},\end{aligned} \tag{5.3.18a}$$

$$\begin{aligned}\Gamma_\mathrm{s} = {} & \frac{J}{J(\kappa+\sigma)+\vartheta(1+J+\kappa+\vartheta)} \\ & + \frac{2J}{\sqrt{D}(1+J+\kappa+2\vartheta+\sqrt{D})}e^{-\frac{1+J+\kappa+2\vartheta+\sqrt{D}}{2}t} \\ & - \frac{2J}{\sqrt{D}(1+J+\kappa+2\vartheta-\sqrt{D})}e^{-\frac{1+J+\kappa+2\vartheta-\sqrt{D}}{2}t},\end{aligned} \tag{5.3.18b}$$

where

$$D = (1+J+\kappa)^2 - 4J(\kappa+\sigma). \tag{5.3.19}$$

As is the case for adsorption at immobile interfaces, these equations are also valid only if $D \neq 0$, i.e. the eigenvalues of A_{jk} have to be distinct. At this point it is also important to note that the fact that $J \propto c_\mathrm{p}\vartheta^{1/2}$ (see eq. (5.2.16)) limits the possibility of varying ϑ and J independently.

5.4. DISCUSSION AND CONCLUSION

In this section we will give some sample calculations with the presented models and discuss the validity of the models. We will especially focus on the restrictions of the models.

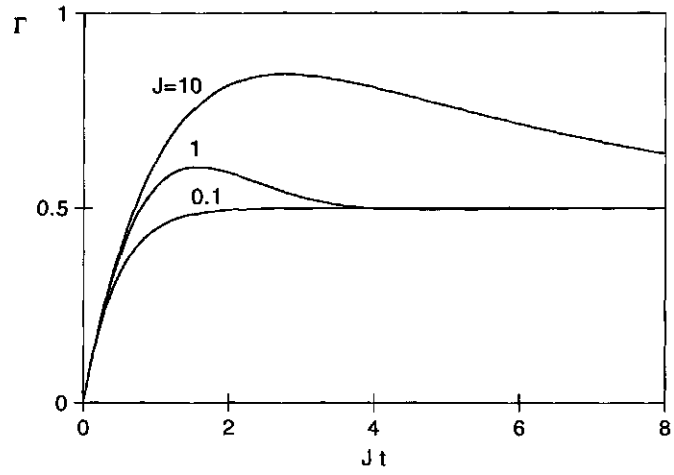

FIGURE 5.6. Dimensionless adsorbed amount $\Gamma(Jt)$ of a spreading polymer at an immobile interface as calculated by eq. (5.3.9) or (5.3.13) with $\sigma = 2$, and $\kappa = 0$. The polymer flux J is indicated in the plot.

5.4.1. Immobile interface

The adsorption of a spreading polymer at a solid–liquid interface is determined by two competing processes: the transport to the surface and the spreading. As an example we take the occupied area of a completely unfolded molecule to be twice that of a coiled polymer, i.e. $\sigma = 2$. Figure 5.6 shows the time dependence of the total adsorbed amount as calculated with the one-step model (see eq. (5.3.13)) for $\kappa = 0$ at different limiting polymer fluxes. The same plot is obtained by eq. (5.3.9) for the "growing disk" model. The adsorbed amount Γ is plotted against Jt to obtain an initial slope of unity in all cases. It is easy to show that there is a threshold for J beyond which the calculated adsorbed amount has a maximum value at a finite time $t_{\max}$. The desorption observed after this time is of a non-physical nature, because we allow polymers to spread on a fully occupied surface. Therefore, a negative free surface area β occurs, which can eventually even lead to a negative adsorbed amount of the coiled polymer as can be seen in fig. 5.7, where we plot the adsorbed amounts for each of the different states of the polymer, with $\kappa = 0$, $\sigma = 2$, and $J = 1$. This observation indicates that the equations used are only valid until t_{max} where $\beta = 0$ for the first time. The time t_{max} where this maximum is reached is calculated from $\theta = \Gamma_c + \sigma\Gamma_s = 1$:

$$t_{\max} = \begin{cases} \frac{1}{\sqrt{D}} \ln \frac{1-J+\kappa-\sqrt{D}}{1-J+\kappa+\sqrt{D}} & \text{for } J > \kappa + 2\sigma - 1, \\ \frac{1}{\sqrt{D}} \left(\ln \frac{1-J+\kappa-\sqrt{D}}{1-J+\kappa+\sqrt{D}} + 2\pi i \right) & \text{for } J < \kappa + 2\sigma - 1 \wedge D < 0, \\ \infty & \text{in other cases.} \end{cases} \tag{5.4.1}$$

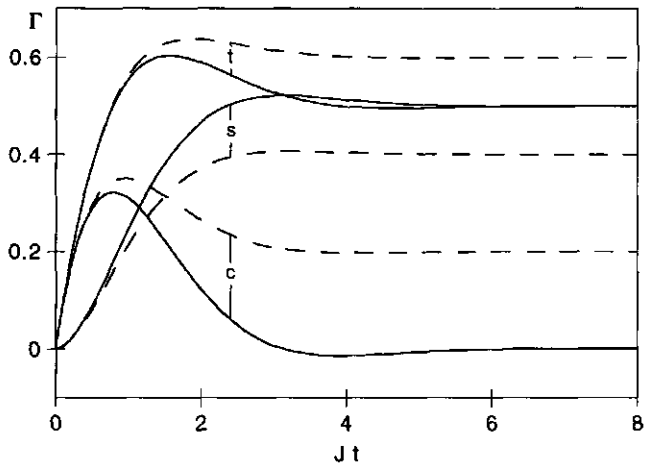

FIGURE 5.7. Adsorbed amount of the coiled (c) and spread (s) state of a polymer at an immobile surface with $\sigma = 2$ and $J = 1$. The total adsorbed amount (t) is also plotted. Solid lines: $\kappa = 0$; dashed lines: $\kappa = 0.5$.

Substituting eq. (5.4.1) in eq. (5.3.13) gives the maximum adsorbed amount for both the coiled and the spread state. Figure 5.8 gives two examples of these maximum adsorbed amounts as a function of J. It is obvious that by taking $\kappa > 0$, the final adsorbed amount of the coiled state will be larger, and therefore the occupied area smaller. This leads to an increase of the total adsorbed amount, as is seen in this figure.

From fig. 5.8 it is clear that the transport rate can be used to control the final mass and structure of an adsorbed polymer layer. One should however bear in mind that the experimental window may be well outside the interesting region, i.e. $0 \lesssim \ln(J) \lesssim 4$. This can for instance be the case for the adsorption of flexible polymers, because then the spreading process will be too fast.

5.4.2. Expanding interface

The only significant difference in the case that the interface is mobile, is that forced transport of adsorbed molecules along the interface will now occur. One of the consequences of this difference is that the *overshoot* of the surface coverage θ observed in the calculations for the immobile interface, is only present for small values of ϑ, and is relatively small, i.e. $1 - \theta \ll 1$. The adsorption of polymers and proteins at a liquid–air interface is often studied in a stationary state, such as obtained with the overflowing cylinder. Therefore, we will only discuss the maximum adsorbed amounts, which are independent of the boundary conditions of eq. (5.3.17) as long as we neglect the possible overshoot mentioned above.

The maximum adsorbed amounts are easily calculated by setting $\dot{\Gamma}_j = 0$ in eq. (5.3.17) or by taking $t \to \infty$ in eq. (5.3.18), and are thus given by the first terms in eqs. (5.3.18a)

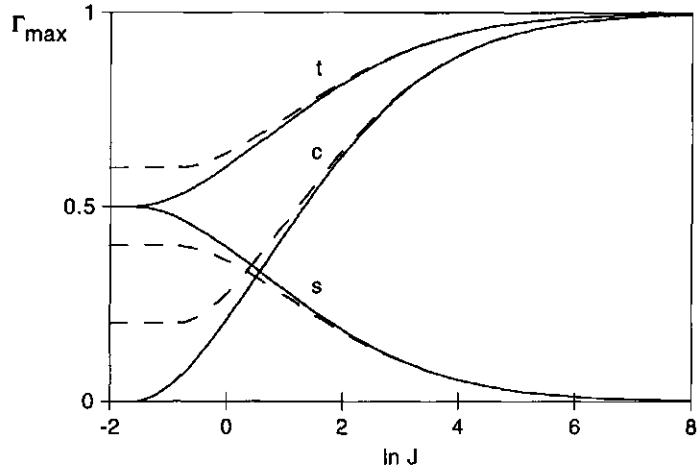

FIGURE 5.8. Adsorbed amount at t_{max} of a spreading polymer at an immobile interface, for $\sigma = 2$. Curves are shown for the coiled state (c), the spread state (s), and the total (t). Solid lines: $\kappa = 0$; dashed lines: $\kappa = 0.5$.

and (5.3.18b), respectively. The total adsorbed amount in the stationary state is thus found to be

$$\Gamma_{ss} = \frac{J(1+\kappa+\vartheta)}{J(\kappa+\sigma)+\vartheta(1+J+\kappa+\vartheta)}. \tag{5.4.2}$$

Figure 5.9 shows two examples of Γ_{ss} as a function of J and ϑ. Clearly, in an overflowing cylinder setup it is possible to control the amount of polymer adsorbed by changing either J (e.g. by way of changing the polymer concentration) or ϑ.

5.4.3. Final remarks

We have shown that with a straight forward analytical approach we are able to describe the adsorption and spreading of chain molecules. In a previous paper it was shown that the presented model is indeed capable of, at least qualitatively, describing the adsorption of the protein savinase on silica [5]. The use of intrinsically simple spreading models is justified by molecular dynamics simulations of poly(ethylene oxide) near a graphite surface. The major limitations of our model are the fact that we underestimate the polymer flux towards the surface by assuming a linear dependence of this flux with the free surface area (see eqs. (5.3.2) and (5.3.15)), and the fact that the spreading itself is independent of the surface coverage. This implies that the presented models should be used with care, and are bound to give qualitative, rather than exact quantitative, agreement with experiments.

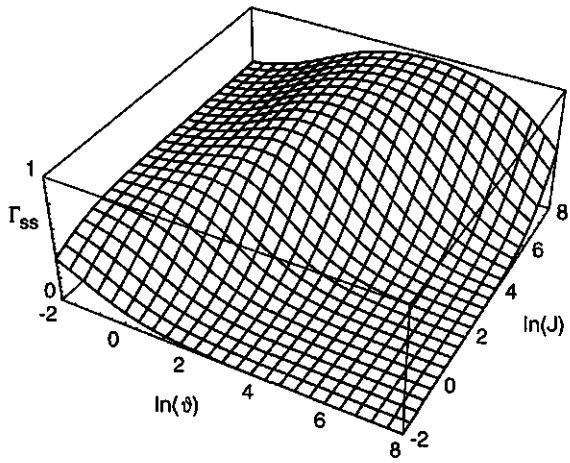

(a) Irreversible spreading ($\kappa = 0$) with $\sigma = 2$.

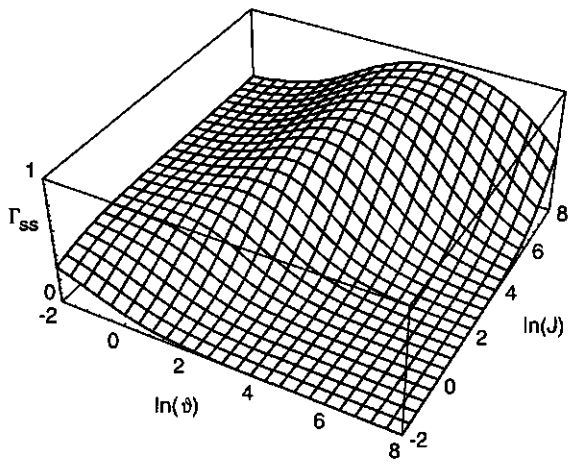

(b) Reversible spreading ($\kappa = 1$) with $\sigma = 4$.

FIGURE 5.9. Adsorbed amount in a stationary state for a polymer adsorbing at an expanding interface as a function of the surface expansion rate ϑ and the limiting polymer transport J.

ACKNOWLEDGEMENTS

We thank Herman van Leeuwen and Marcel Minor for useful comments and discussions. This research is also sponsored by the EC Human and Capital Mobility programme CHRX-CT94-0448-3.

APPENDIX 5.A. DIFFERENTIAL EQUATIONS IN ADSORPTION KINETICS

The analysis of the adsorption kinetics of polymers involves the solution of differential equations. Here, we will give a general approach in solving such equations for two kind of spreading models for the polymer at the interface.

5.A.1. Growing disk

If we assume that an adsorbing polymer will change its conformation at the interface by some simple exponential function, the relative free surface area β will be given by a linear, homogeneous second-order differential equation of the following form:

$$\frac{\mathrm{d}^2\beta}{\mathrm{d}t^2} + b\frac{\mathrm{d}\beta}{\mathrm{d}t} + c\beta = 0. \tag{5.A.1}$$

Let m_1 and m_2 be the roots of the characteristic equation $m^2 + bm + c = 0$, and let $D = b^2 - 4c$. Then there are three cases:

$$\beta = c_1 e^{m_1 t} + c_2 e^{m_2 t} \qquad \text{for } D > 0, \tag{5.A.2a}$$

$$\beta = c_1 e^{m_1 t} + c_2 t e^{m_1 t} \qquad \text{for } D = 0, \tag{5.A.2b}$$

$$\beta = (c_1 \cos qt + c_2 \sin qt) e^{pt} \qquad \text{for } D < 0, \tag{5.A.2c}$$

where $p = -b/2$ and $q = \sqrt{4c - b^2}/2$. The calculation of the adsorbed amount Γ involves the solution of the linear, first-order differential equation $\mathrm{d}\Gamma/\mathrm{d}t = J\beta$ (see eq. (5.3.2)). The adsorbed amount is simply given by $\Gamma = J\int_0^t \mathrm{d}t'\,\beta$, where we assumed $\Gamma(0) = 0$, so

$$\frac{\Gamma}{J} = \frac{c_1}{m_1} e^{m_1 t} + \frac{c_2}{m_2} e^{m_2 t} - \frac{c_1}{m_1} - \frac{c_2}{m_2} \qquad \text{for } D > 0, \tag{5.A.3a}$$

$$\frac{\Gamma}{J} = \frac{c_1 m_1 - c_2 + c_2 m_1 t}{m_1^2} e^{m_1 t} - \frac{c_1 m_1 - c_2}{m_1^2} \qquad \text{for } D = 0, \tag{5.A.3b}$$

$$\frac{\Gamma}{J} = \frac{c_1 p - c_2 q}{p^2 + q^2}(e^{pt}\cos qt - 1) + \frac{c_1 q + c_2 p}{p^2 + q^2} e^{pt} \sin qt \qquad \text{for } D < 0, \tag{5.A.3c}$$

where the constants are the same as in eq.(5.A.2).

5.A.2. n-Step model

The adsorption of polymers, but of course also of other molecules, can be addressed by assuming that the molecule can exist in $n + 1$ different states, either in solution or at the interface. It is then possible to use first order reaction kinetics to describe the adsorption process. The differential equations for the adsorbed amounts of the different states take the following general form:

$$\dot{\Gamma}_j = A_{jk}\Gamma_k + J_j. \tag{5.A.4}$$

We denote the eigenvalues and eigenvectors of the $m \times m$ matrix A_{jk} by λ_j and v_{jk}, respectively. In the case all eigenvalues are distinct, solution of the homogeneous equation $\dot{\Gamma}_j^{\mathrm{h}} = A_{jk}\Gamma_k^{\mathrm{h}}$ gives

$$\Gamma_{jk}^{\mathrm{h}} = v_{jk} e^{\lambda_j t}, \tag{5.A.5}$$

arriving at the general solution $\Gamma_j^{\mathrm{h}} = C_k \Gamma_{kj}^{\mathrm{h}}$, where C_k is a constant vector. To find a particular solution we apply the technique of variation of constants, i.e. we put

$$\Gamma_j^{\mathrm{p}} = B_k(t)\Gamma_{kj}^{\mathrm{h}}, \tag{5.A.6}$$

after which it is easy to show that

$$\dot{B}_k \Gamma_{kj}^{\mathrm{h}} = J_j. \tag{5.A.7}$$

Taking a single exponential function for B_j meets the set requirements. We take $B_j = \frac{b_j}{\lambda_j} e^{-\lambda_j t}$. The full solution of eq. (5.A.4) then is

$$\begin{aligned} \Gamma_j &= \Gamma_j^{\mathrm{h}} + \Gamma_j^{\mathrm{p}} \\ &= (C_k + B_k)\Gamma_{kj}^{\mathrm{h}}. \end{aligned} \tag{5.A.8}$$

Using the boundary condition $\Gamma_j(0) = \Gamma_j^0$ and eq. (5.A.7) we are able to calculate the introduced constants b_j and c_j. In the case we have a set of two differential equations, as is the case throughout this paper, then

$$b_1 = \frac{j_1 v_{22} - j_2 v_{21}}{v_{12}v_{21} - v_{11}v_{22}}, \tag{5.A.9a}$$

$$b_2 = \frac{j_2 v_{11} - j_1 v_{12}}{v_{12}v_{21} - v_{11}v_{22}}, \tag{5.A.9b}$$

$$c_1 = -\frac{b_1}{\lambda_1} - \frac{\Gamma_1^0 v_{22} - \Gamma_2^0 v_{21}}{v_{12}v_{21} - v_{11}v_{22}}, \tag{5.A.9c}$$

$$c_2 = -\frac{b_2}{\lambda_2} - \frac{\Gamma_2^0 v_{11} - \Gamma_1^0 v_{12}}{v_{12}v_{21} - v_{11}v_{22}}, \tag{5.A.9d}$$

where $\lambda_1 \neq \lambda_2$.

REFERENCES

[1] G. J. Fleer, M. A. Cohen Stuart, J. M. H. M. Scheutjens, T. Cosgrove, and B. Vincent. *Polymers at interfaces.* Chapman & Hall, London, 1993.

[2] E. Pefferkorn and A. Elaissari. Adsorption-desorption processes in charged polymer/colloid systems; structural relaxation of adsorbed macromolecules. *J Colloid Interface Sci*, 138:187–194, 1990.

[3] A. Elaissari and E. Pefferkorn. Polyelectrolyte adsorption at solid/liquid interfaces: a simple model for structural relaxation and excluded area effects. *J Colloid Interface Sci*, 143:85–91, 1991.

[4] H. M. Schneider, P. Frantz, and S. Granick. The bimodal energy landscape when polymers adsorb. *Langmuir*, 12:994–996, 1996.

[5] M. C. P. van Eijk and M. A. Cohen Stuart. Polymer adsorption kinetics: effects of supply rate. *Langmuir*, 13:5447–5450, 1997.

[6] J. Buijs, P. A. W. van den Berg, J. W. Th. Lichtenbelt, W. Norde, and J. Lyklema. Adsorption dynamics of IgG and its $F(ab')_2$ and Fc fragments studied by reflectometry. *J Colloid Interface Sci*, 178:594–605, 1996.

[7] J. C. Dijt, M. A. Cohen Stuart, and G. J. Fleer. Competitive adsorption kinetics of polymers differing in length only. *Macromolecules*, 27:3219–3228, 1994.

[8] A. N. Semenov and J.-F. Joanny. Kinetics of adsorption of linear homopolymers onto flat surfaces: Rouse dynamics. *J Phys II France*, 5:859–876, 1995.

[9] T. Dąbroś and T. G. M. van de Ven. A direct method for studying particle deposition onto solid surfaces. *Colloid Polym Sci*, 261:694–707, 1983.

[10] J. C. Dijt, M. A. Cohen Stuart, J. E. Hofman, and G. J. Fleer. Kinetics of polymer adsorption in stagnation point flow. *Colloids Surfaces*, 51:141–158, 1990.

[11] J. C. Dijt, M. A. Cohen Stuart, and G. J. Fleer. Reflectometry as a tool for adsorption studies. *Adv Colloid Interface Sci*, 50:79–101, 1994.

[12] D. J. M. Bergink-Martens, H. J. Bos, A. Prins, and B. C. Schulte. Surface dilatation and fluid–dynamical behavior of Newtonian liquids in an overflowing cylinder. *J Colloid Interface Sci*, 138:1–9, 1990.

[13] T. Dąbroś and Z. Adamczyk. Noninertial particle transfer to the rotating disc under an external force field (laminar flow). *Chem Eng Sci*, 34:1041–1049, 1979.

Samenvatting

In dit proefschrift komen verschillende aspekten van het gedrag van semi-flexibele polymeren, en in mindere mate van flexibele, in de buurt van een grensvlak aan de orde. Na een korte inleiding in de benodigde basisbegrippen worden in het eerste deel vooral de evenwichtseigenschappen belicht, terwijl in het tweede deel meer aandacht wordt besteed aan de adsorptiekinetiek.

Er bestaat een groot aantal manieren om polymeren te modelleren. De keuze voor een bepaald model wordt zowel bepaald door de akademische achtergrond van de individuele onderzoeker als door het specifieke polymeersysteem zelf. In ons onderzoek naar het globale gedrag van polymeren nabij een grensvlak is het voldoende om een polymeer te zien als een keten van segmenten zonder aandacht te besteden aan de molekulaire details. Een dergelijke keten wordt gekarakteriseerd door de segmentlengte b, het aantal segmenten N, de persistentielengte q en de gyratiestraal R_g. De persistentielengte kan gezien worden als de afstand langs de keten tot het punt waarop er nog net richtingskorrelatie met de eerste binding waarneembaar is. Met andere woorden: een stijver polymeer wordt gekarakteriseerd door een grotere waarde van q.

Ophoping van een stof aan een grensvlak wordt aangeduid als adsorptie. Deze ophoping kan uiteindelijk leiden tot de vorming van een nieuwe fase; dit proces wordt bevochtiging genoemd. Polymeeradsorptie speelt een belangrijke rol in een breed skala aan natuurlijke en industriële processen. Mede daardoor is het een populair onderwerp van zowel toegepast als fundamenteel onderzoek. Dat hierbij de nadruk veelal op evenwichtseigenschappen ligt is op zijn minst jammer te noemen. De doorgronding van een groot aantal adsorptieprocessen is vaak slechts mogelijk als de kinetiek ervan ook onderzocht wordt. Het onderzoek op dat gebied bevindt zich pas in zijn vlegeljaren, maar ontwikkelt zich snel. Met name de adsorptiekinetiek van niet-flexibele polymeren is een interessant fenomeen vanwege de grotere tijdschalen die daar een rol spelen.

De evenwichtseigenschappen van polymeren in de buurt van een grensvlak kunnen worden berekend met behulp van een gemiddeld-veldtheorie, waarbij de wisselwerkingen tussen de verschillende komponenten worden bepaald aan de hand van hun gemiddelde omgeving. In dit proefschrift maken we gebruik van zowel een dichtheidsfunktionaaltheorie als van de door Scheutjens en Fleer speciaal voor polymeren ontwikkelde zelfkonsistente-veldtheorie (SF ZKV). De kinetische experimenten zijn uitgevoerd met behulp van reflektometrie, een methode gebaseerd op de verandering van de reflektiekoëfficiënten ten gevolge van adsorptie.

In hoofdstuk 1 staat de evenwichtsadsorptie van semi-flexibele polymeren aan een vloeistof–vloeistof grensvlak centraal. We beschouwen twee faseschеidende monomere

vloeistoffen, C en D, en een polymeer A_N dat in beide oplosmiddelen evengoed oplosbaar is. We gebruiken de SF ZKV theorie om de eigenschappen in het verdunde gebied te berekenen. De stijfheid van het polymeer wordt gekontroleerd door gebruik van een diskreet rotatie-isomeriemodel. We laten zien dat de grensvlakbreedte ξ (bepaald door de wisselwerkingsparameter tussen de twee oplosmiddelen), de persistentielengte q en de ketenlengte N relevante parameters zijn voor het adsorptiegedrag. Een opmerkelijke konstatering is dat bij een konstante verhouding $N^{1/2}/\xi$ de geadsorbeerde hoeveelheid door een minimum gaat als funktie van q/ξ. Een toename van q/ξ ($q/\xi \lesssim 1$) leidt aanvankelijk tot een grotere kluwenafmeting, resulterend in een afname van de geadsorbeerde hoeveelheid. Echter, in het geval dat $q/\xi \gg 1$ zal oplijning van delen van het polymeer in de buurt van het grensvlak optreden, omdat voor stijvere ketens het entropieverlies geringer wordt. Dit oplijnproces heeft een toename van de geadsorbeerde hoeveelheid tot gevolg. Deze resultaten hebben ook konsekwenties voor de kontroverse rond de preferentiële adsorptie in een mengsel van flexibele en stijve polymeren. Met name de eindige breedte van het grensvlak moet in deze diskussie meegenomen worden om uitsluitsel te kunnen geven over welk polymeer preferent zal adsorberen.

De uitbreiding naar bevochtiging door polymeren van een vloeistof–vloeistof grensvlak in een vergelijkbaar systeem wordt uitgebreid bediskussieerd in hoofdstuk 2. Hierin wordt zowel het bevochtigingsgedrag van flexibele als van semi-flexibele polymeren aan de orde gesteld. Het ternaire systeem is bestudeerd in de buurt van de overgang van partiële naar volledige bevochtiging. In een symmetrisch systeem, waarin $\chi_{AB} = \chi_{BC} = \chi$, kan deze bevochtigingsovergang geïnduceerd worden door een verandering van de wisselwerkingsparameter χ. De verhouding tussen de breedte van het grensvlak ξ van het binaire A/C-systeem en de kluwengrootte van het polymeer bepaalt de orde van de faseovergang. Boven een kritische ketenlengte N_c (bij vaste ξ) is de bevochtigingsovergang van eerste orde, terwijl die van tweede orde is voor $N < N_c$. De kenmerken van de voorbevochtigingslijn, inklusief het kritisch punt van voorbevochtiging, worden in detail besproken. De niet-triviale ketenlengte-afhankelijkheid van de plaats van dit kritisch punt is geanalyseerd met behulp van een ruw thermodynamisch model. Voor een semi-flexibel polymeer is een toename van de ketenstijfheid bij een bepaalde waarde van χ voldoende om een bevochtigingsovergang te bewerkstelligen.

De eerste kinetische experimenten in dit proefschrift staan beschreven in hoofdstuk 3. De adsorptiekinetiek van het polysaccharide xanthaan vanuit waterige oplossing op zirkoonoxide is bestudeerd als funktie van pH en van ionsterkte. Reflektometrie is gebruikt om het adsorptiegedrag in een stagnatiepuntstroming te onderzoeken. Voor niet te extreme waarden van pH en ionsterkte bevindt xanthaan zich in een helixkonformatie en kan onder deze omstandigheden als een semi-flexibel polymeer gezien worden. Een verlaging van de zoutkoncentratie of een verhoging van de pH induceert een helix–kluwen overgang. Deze overgang wordt veroorzaakt door wederzijdse elektrostatische afstoting van de korte zijketens van xanthaan. De kluwen waarin het xanthaan overgaat kan als een Gaussische keten met een grote gyratiestraal beschouwd worden. De konformatie van het polysaccharide wordt weerspiegeld in het adsorptiegedrag. We

laten ook zien dat de elektrostatische wisselwerking tussen het polymeer en het oppervlak de stabiliteit van de helix beïnvloedt. Het adsorptieproces kan in twee gebieden verdeeld worden. Bij lage oppervlaktebedekking is de adsorptiesnelheid aanvoergelimiteerd wat in een stagnatiepuntstroming leidt tot een lineaire tijdsafhankelijkheid van de geadsorbeerde hoeveelheid. De adsorptiesnelheid verandert in dit gebied nauwelijks als funktie van de ionsterkte of pH. Het tijdsinterval waarbinnen dit gebied ligt doet dat echter wel. Dit kan toegeschreven worden aan elektrostatische effekten. Bij hogere oppervlaktebedekking worden twee typen gedrag waargenomen. Bij lage ionsterkte en op een hooggeladen oppervlak vindt een vrij abrupte verzadiging van de geadsorbeerde hoeveelheid plaats. Iets dergelijks wordt ook waargenomen bij flexibele polymeren. Blijkbaar adsorbeert xanthaan in een kluwen-achtige konformatie, wat waarschijnlijk veroorzaakt wordt door de instabiliteit van de helix in de buurt van het oppervlak. Bij hogere ionsterkte en op een zwakgeladen oppervlak neemt de geadsorbeerde hoeveelheid langzaam toe gedurende langere tijd. Onder deze omstandigheden is de helixvorm stabieler en wordt de langzame toename waarschijnlijk veroorzaakt door herrangschikking en oplijning van het stijve polymeer.

In de meeste studies naar het adsorptiegedrag van polymeren op vaste oppervlakken wordt gevonden dat de verzadigde geadsorbeerde hoeveelheid onafhankelijk is van de aanvoersnelheid J van het polymeer naar het oppervlak. Meestal wordt dit veroorzaakt doordat de aanvoer van polymeer veel trager is dan de oppervlakteprocessen (zoals konformatieveranderingen). In hoofdstuk 4 bestuderen we een tweetal biopolymeren, waarbij oppervlakteprocessen juist relatief langzaam verlopen. We hebben gevonden dat in dat geval de aanvoersnelheid een belangrijke rol speelt voor de struktuur van de geadsorbeerde laag en voor de geadsorbeerde hoeveelheid van zowel immunoglobuline G als van savinase op SiO_2 vanuit waterige oplossing. Het adsorptieproces kan gezien worden als een aanhechtingsstap gevolgd door spreiding van het polymeermolekuul over het oppervlak. We vinden een sterke J-afhankelijkheid voor de geadsorbeerde hoeveelheid als de benodigde tijd voor aanvoer naar het oppervlak van de zelfde orde is als de tijd voor spreiding. Vervolgens gebruiken we het zogenaamde groeiende-schijf-model voor een fenomenologische beschrijving van de adsorptiekinetiek van spreidende polymeren. Dit analytische model wordt in hoofdstuk 5 nader belicht en verder uitgebreid.

De uitgebreide analyse van de adsorptiekinetiek van spreidende polymeren in dat hoofdstuk omvat zowel het genoemde analytische model als ook molekulaire-dynamikasimulaties. Uit de MD simulaties van een polyethyleenoxide-keten in vakuum vlakbij een grafietoppervlak konkluderen we dat het spreidingsproces in eerste benadering beschreven kan worden met een enkele exponentiële funktie voor de grootte van het molekuul parallel aan het oppervlak, of met eerste-orde reaktiekinetiek. De kombinatie van deze spreidingsmodellen met de transportvergelijkingen voor verschillende geometrieën (stagnatiepuntstroming en overstromende cilinder) leidt tot analytische uitdrukkingen voor de adsorptiekinetiek van polymeren aan vast–vloeistof en aan vloeistof–vloeistof oppervlakken.

Levensloop

Op maandagmiddag 28 november 1966 werd ik geboren in het Noord-Brabantse Geldrop. Tijdens het slijten van mijn jonge jaren, behaalde ik daar in 1985 het VWO-diploma aan het Strabrecht College. Datzelfde jaar begon ik aan de studie Scheikundige Technologie aan de Technische Hogeschool Eindhoven, waarvan de naam niet veel later werd veranderd in Technische Universiteit. Tijdens de afstudeerfase kwam ik uitgebreid in kontakt met de chemische industrie door het uitvoeren van Ramanspektroskopisch onderzoek aan polyetheen bij DSM in Geleen. In 1991 sloot ik mijn studie af en begon in november van dat jaar aan een tweejarige ontwerpersopleiding aan de Technische Universiteit Delft. Omdat mijn wetenschappelijke interesse meer in de richting van fysische chemie ging, veranderde ik in juli 1993 van werkgever en begon als onderzoeker in opleiding aan mijn promotie-onderzoek bij de vakgroep Fysische en Kolloïdchemie (nu omgedoopt tot laboratorium voor Fysische Chemie en Kolloïdkunde) aan de Landbouwuniversiteit Wageningen. De resultaten van dit onderzoek vormen de inhoud van dit proefschrift, maar zijn ook gepresenteerd tijdens konferenties in Ven (Zweden), Munster (Frankrijk), Turku (Finland) en Eibergen en uiteraard tijdens de jaarlijkse SON-bijeenkomsten in Lunteren. Daarnaast heb ik me zowel in Delft als in Wageningen ingezet voor de verbetering van onderwijs. Vanaf 1 maart 1998 werk ik als adjunkt in de chemie aan de Universiteit van Aalborg.